Volume 4
Number 8
21 April 2023
Pages 1787–2018

Materials Advances

rsc.li/materials-advances

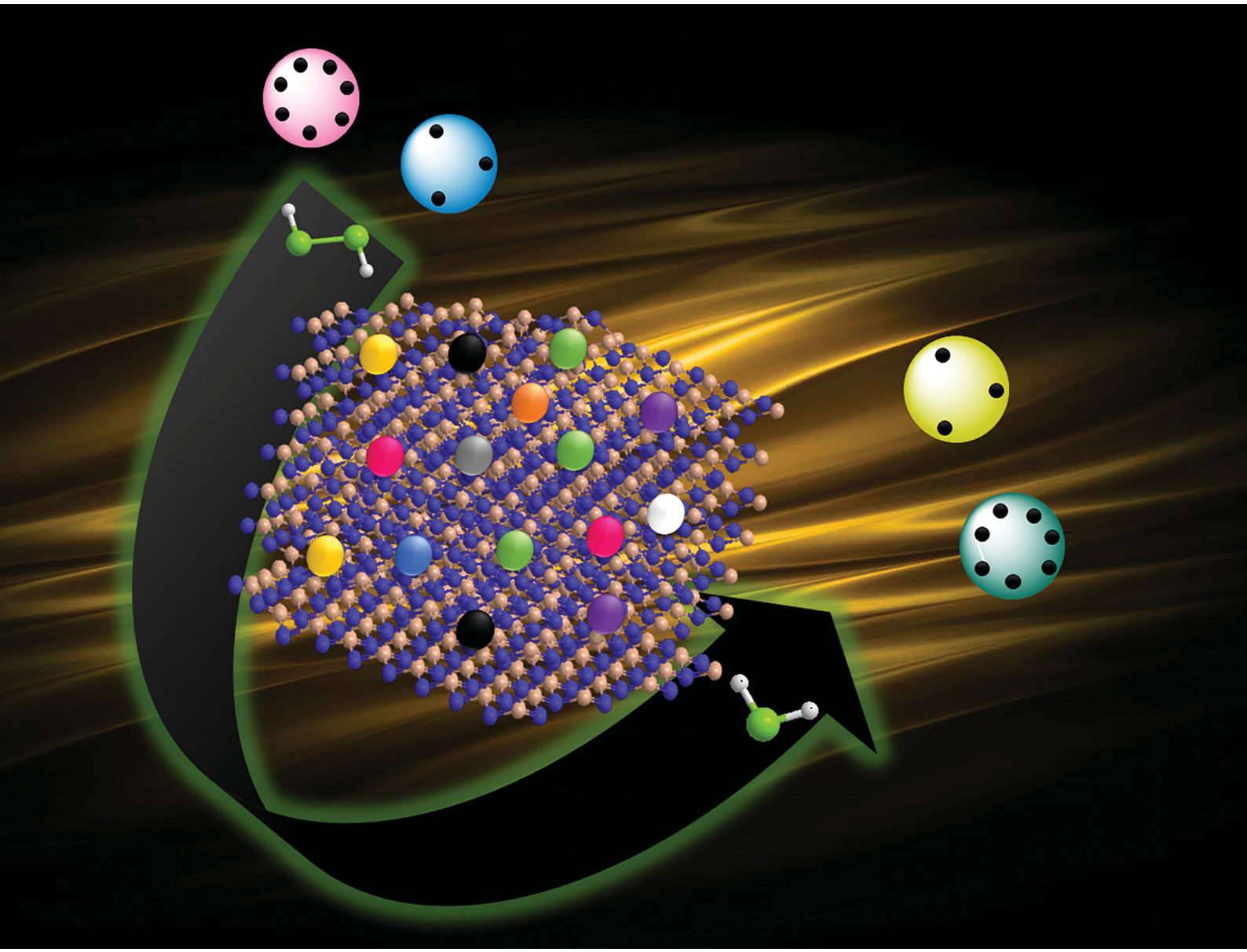

ISSN 2633-5409

ROYAL SOCIETY OF CHEMISTRY

REVIEW ARTICLE
Rakesh Kumar Sharma *et al.*
Advanced metal oxide-based nanocatalysts for the oxidative synthesis of fine chemicals

Materials Advances

ROYAL SOCIETY OF CHEMISTRY

REVIEW

View Article Online
View Journal | View Issue

Cite this: *Mater. Adv.*, 2023, 4, 1795

Advanced metal oxide-based nanocatalysts for the oxidative synthesis of fine chemicals

Rakesh Kumar Sharma, *[a] Rakeshwar Bandichhor,[b] Vishwesh Mishra,[c] Shivani Sharma,[d] Sneha Yadav,[a] Shilpa Mehta,[d] Bhavya Arora,[a] Pooja Rana,[a] Sriparna Dutta[a] and Kanika Solanki[a]

The development of nanocatalysis has ushered in a new era in chemistry by promoting the design of new catalytic production processes in organic synthesis with utmost level of waste minimization by conforming to green chemistry principles. Consequently, significant advancement has been made towards the generation of highly active and selective metal oxide-based materials with tunable properties that can be controlled at the nano-scale. A thorough literature survey revealed that these functional nano-architectures are endowed with exceptional potential to boost industrially significant oxidation processes in terms of activity, selectivity, product yield, atom economy, recoverability and reusability. This review aims to combine all the scattered literature pertaining to the applicability of diverse metal oxide nanocatalysts in the manufacturing of fine chemicals, which can serve as a guide for the scientific community working in this area. In the first section, we present an in-depth understanding on the fundamental concepts of metal oxide-based nanoarchitectures, emphasizing their role in expediting practically important oxidation processes. Subsequently, we present the state-of-art progress on various synthetic methodologies and functionalization strategies adopted by different research groups to acquire strategic vision of essential requisites for the design of nanoengineered metal oxides. Furthermore, an in-depth discussion on surface coating agents and functionalization strategies, which are key structural aspects for manufacturing nanohybrid catalysts with enhanced activity and selectivity, will also be covered. Finally, we summarize all the research work conducted on the utilization of surface-engineered metal oxide-based nanomaterials in accelerating oxidation reactions including alkane oxidation, alkene oxidation, arene oxidation, alcohol oxidation, amine oxidation and thiol oxidation. Further, it is envisioned that this review will give new directions to nanocatalysis research by providing clues for the judicious design of next-generation catalytic nanomaterials, which will not only improve industrial production but also protect the environment and human health.

Received 14th October 2022,
Accepted 18th February 2023

DOI: 10.1039/d2ma00977c

rsc.li/materials-advances

Introduction

Nanotechnology, a fast-evolving discipline, is often hailed as an innovative route for the design of next-generation raw materials, resulting in remarkable features useful in an array of scientific and industrial areas.[1,2] In fact, it has dramatically fostered the development of the manufacturing sector worldwide by opening new avenues towards cleaner and sustainable catalytic protocols for industrial chemical processes in an economically competitive manner. Considering this, the scientific community is focused on cutting-edge research to unlock the potential of engineered nanostructures in the field of catalysis, originating from the precise control of the design of materials owing to their tunable physico-chemical properties.[3] Indeed, the integration of nanoscience and catalysis is considered a versatile amalgamated stratagem that can bridge the gap between homogeneous and heterogeneous catalysts through the construction of nanometer-scale architectures having unprecedented catalytic efficacy due to the blend of the prominent facets of both catalysts.[4,5] By exploiting the technological advances delivered by the heterogenization approach, there have been numerous breakthrough innovations in novel catalytic materials based on distinct metal oxides to address all the formidable challenges often encountered during the practical application of their bulk counterparts.[6] Driven by the astonishing progress, pioneering researchers and materials science

[a] Green Chemistry Network Centre, Department of Chemistry, University of Delhi, New Delhi-110007, India. E-mail: rksharmagreenchem@hotmail.com; Fax: +91-011-27666250; Tel: +91-011-276666250
[b] Dr. Reddy's Laboratories, Limited, Innovation Plaza, IPDO Bachupally, Hyderabad, 500090, India
[c] Department of Chemistry, University of Delhi, Delhi-110007, India
[d] Department of Chemistry, Ramjas College, University of Delhi, Delhi-110007, India

engineers have devoted their efforts to exploring green innovative synthetic strategies for the judicious design of several metal oxides nanocatalysts using iron oxide,[7] silica,[8,9] alumina,[10] halloysite,[11] copper oxide,[12] zinc oxide,[13] titania,[14] *etc.* as the support matrix. These engineered oxide based nanocatalytic systems significantly contribute to shaping the sustainable future of modern society given that they provide a myriad of opportunities such as low energy consumption, economic viability, little environmental impact, enhanced activity and selectivity together with facile recovery.[15] Several studies proved that designed nano-scale metal oxide-based catalytic materials show remarkable potential to speed up previous and current oxidative transformations, which are the core of modern organic synthesis, given that they significantly contribute to the large-scale production of fine chemicals, intermediates and monomers for various polymers.[16–19] Our literature survey revealed that these oxidation reactions are often achieved by adding stoichiometric amounts of strong oxidants such as chromium(IV) reagents, permanganate, *tert*-butyl hydroperoxide, selenium oxide, ruthenium(VIII) oxide, nitric acid, and oxygen.[20–22] Unfortunately, the scope of the aforementioned oxidant-mediated protocols is limited given that these oxidizing agents are either toxic or unstable under atmospheric conditions, nonspecific in action, and produce undesirable side products. Thus, to improve the environmental footprint of chemical production processes, many research groups have developed another complementary pathway involving the utilization of hydrogen peroxide as a green oxidant, which is gradually replacing some well-established processes due to its excellent oxygen atom efficiency, low cost and production of water as the only by-product.[23–27] However, despite these exciting opportunities, there are still several challenges ranging from the scaling up to final commercialization of these new-generation nanocatalysts, which need to be addressed. Hence, to overcome the predominant obstacles, we attempt to combine all the scattered literature reports pertaining to nanoscale catalysts in a single reference, which will serve as a guide for material chemists and researchers in the field of oxidative organic synthesis.

The prime objective of this review is to shed light on the studies related to the fabrication of heterogeneous nanocatalysts based on different oxides nanostructures for boosting industrially significant oxidation processes. This review provides comprehensive coverage of the state-of-art progress on various synthetic methodologies adopted by different research groups together with an in-depth discussion on surface coating agents and functionalization strategies to acquire strategic vision on key structural aspects for manufacturing nanohybrid catalysts with enhanced activity and selectivity. Subsequently, we present a detailed discussion on the application of surface-engineered metal oxide-based nanomaterials in accelerating various oxidation reactions such as alkane oxidation, alkene oxidation, arene oxidation, alcohol oxidation, amine oxidation and thiol oxidation (Fig. 1). Also, we critically discuss the opportunities and challenges associated with emerging H_2O_2-based oxidation processes. Finally, we conclude with a summary and future perspective on new innovative directions towards the development of selective oxidation catalysts, highlighting the points needs to be addressed for their practical implications at the pilot and industrial scale.

It is worth mentioning that no review has been published to date that presents a compilation of the vast and scattered literature of heterogeneous nanocatalysts based on different oxide nanostructures for boosting industrially significant oxidation processes in a comprehensible manner. Finally, it is anticipated that this review will give new directions to nanocatalysis research by providing clues for the judicious design of next-generation benign catalytic technologies, which will not only improve industrial manufacturing but also assist in alleviating environmental challenges for sustainability in the near future.

Synthetic strategies for the development of various metal oxide nanostructures

The choice of the synthetic route utilized for the formulation of nanoscience-inspired metal oxide-based materials plays a key role in achieving desired features including size, dispersity, morphology and crystal structure. The tuning of physicochemical

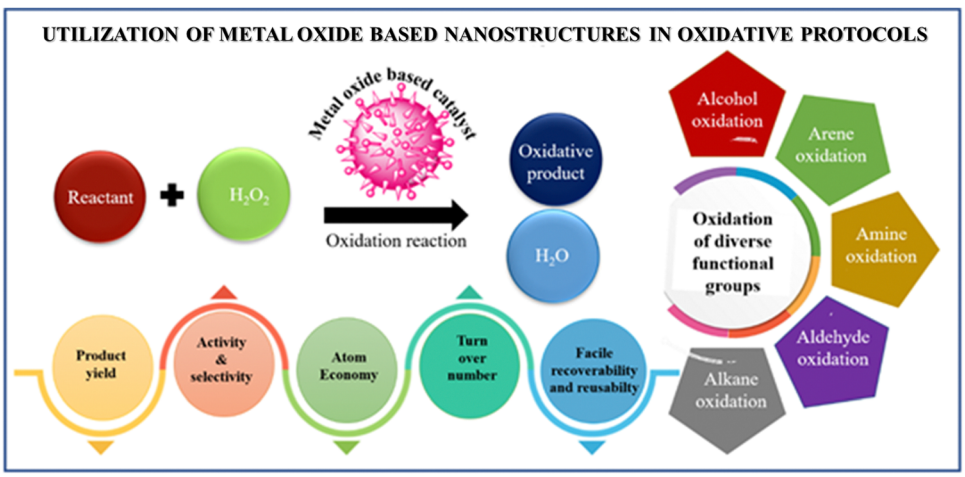

Fig. 1 Schematic representation of the application of metal oxide-based nanostructures in catalytic protocols.

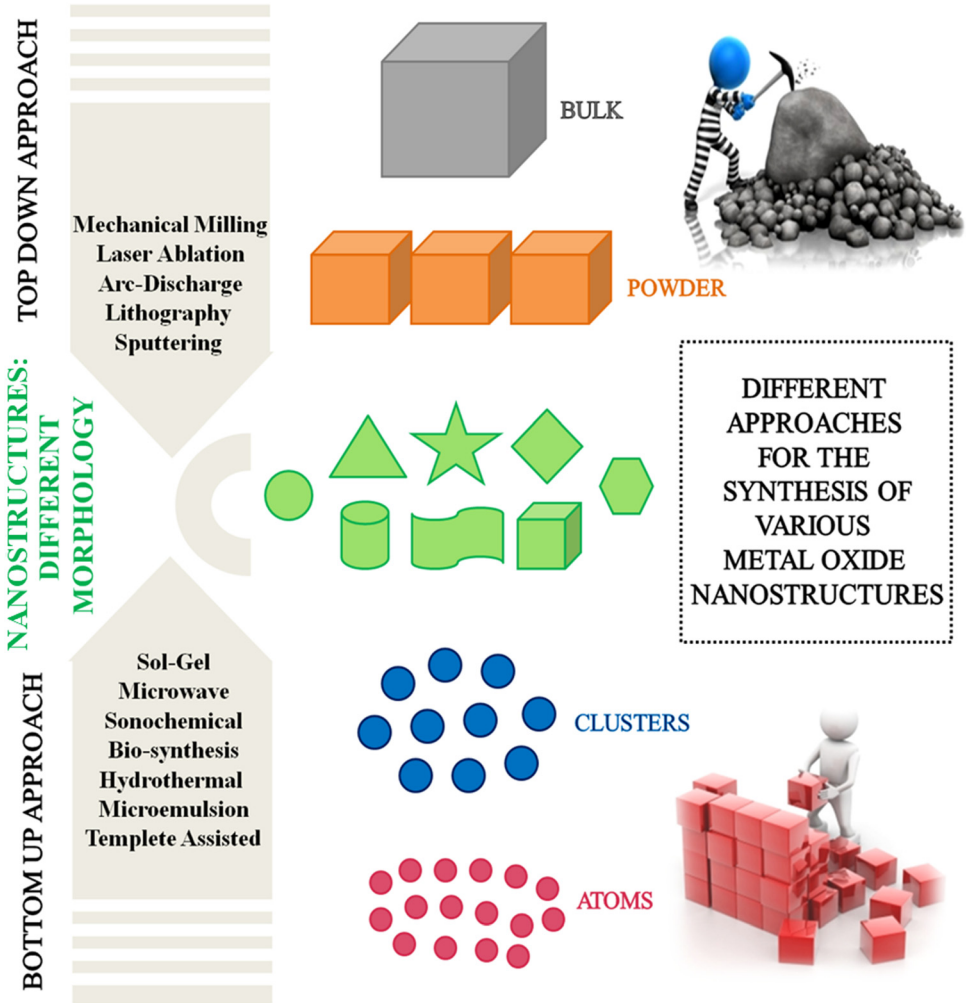

Fig. 2 Different approaches for the synthesis of various metal oxide nanostructures.

properties at the nanometer level imparts distinct characteristics to the developed material according to a particular application. A comprehensive literature survey revealed that a myriad of different studies has been carried out on the synthesis of metal oxides, which can be mainly categorized as top-down and bottom-up methods (Fig. 2). The former includes mechanochemical synthesis, spray pyrolysis, laser-assisted deposition, atomic-layer deposition, ion implantation, sputtering and etching. For instance, Zhang and Dai and their research group utilized a different solid-state mechanochemical nanocasting approach for the synthesis of a series of highly porous metal oxides such as ZrO_2, Fe_2O_3, CeO_2, CuO, La_2O_3, CuO_x–CeO_y and CuO_x–CoO_y–CeO_z, manifesting record-breaking surface areas.[28] To obtain the desired nanoporous metal oxides, a ball-milling process utilizing commercial porous silica as the template precursor was employed, followed by calcination and subsequent removal of silica with NaOH. Likewise, Botta and co-workers synthesized iron oxide nanoparticles using three different reactive systems involving different oxidation states of precursor iron salts and mean sizes in the range of 8–10 nm.[29] Flame spray pyrolysis is an advanced technique for the preparation of thermally stable and high surface area nanoparticles, and even their large-scale manufacture. In this case, Smirniotis *et al.* reported the fabrication of a series of MgO nanoparticles using a flame aerosol method, which were further utilized for CO_2 sorption at lower temperatures.[30] In another report, monodisperse and crystalline SnSe nanospheres were synthesized following a spray pyrolysis approach, which were subsequently transformed into SnO_2 nanospheres through a post-treatment oxidation process at 600 °C in air relying on Kirkendall diffusion.[31] CuO nanoparticles were also reported to be synthesized using the dc reactive magnetron sputtering technique at the low temperature of −194 °C. The synthesized nanoparticles were found to be highly pure with a narrow size distribution, average crystallite size ranging from 6–13 nm and high surface area.[32] Camacho-Lopez *et al.* delineated the preparation of molybdenum oxide (MoOx) nanoparticles through the laser ablation of solids in liquids technique. This technique employed an Nd:YAG (neodymium-doped yttrium aluminium garnet) laser for the fabrication of MoOx nanoparticles with nanosecond pulses in deionized water without the use of any additives or surfactants.[33] Likewise, Kupracz and co-workers synthesized a mixture of FeO, Fe_3O_4 and Fe_2O_3 nanoparticles *via* the pulsed laser ablation

technique and further decorated on anodized TiO_2 nanotubes, which subsequently exhibited enhanced activity towards the oxygen evolution reaction.[34] Recently, an ion implantation method was employed by Gentils and co-workers for the synthesis of highly pure Fe–Cr alloy nanoparticles. The developed protocol involved the consecutive implantation of Al and O ions in the Fe–Cr alloy nanoparticles at room temperature.[35] Alternatively, the bottom-up route includes sol–gel, sonochemical, photochemical solvothermal synthesis and thermal decomposition as the most commonly employed techniques for the synthesis of metal oxide nanoparticles. Kim and co-workers reported a template-free sonochemical reduction route for the transformation of potassium permanganate into α- and δ-MnO_2 phase with two different reaction times (15 min and 30 min) using polyethylene glycol as the reducing agent.[36] It was concluded that the spherical α-MnO_2 nanoparticles synthesized after 30 min reaction and having uniformly distributed mesopores played a significant role as an electrode material for supercapacitor applications. In another report, a sol–gel method assisted with ultrasonic irradiation was utilized by Torres-Martínez *et al.* for the fabrication of ZnO nanoparticles with high surface area and low particle size, which were found to have a profound impact on the photocatalytic H_2 production reaction without the use of any sacrificial agents.[37] A prolific attempt in this direction was made by Lee and co-workers, wherein they synthesized hydrophilic superparamagnetic Fe_3O_4 nanoclusters *via* a one-pot solvothermal strategy.[38] The gram-scale synthesis of spherical Fe_3O_4 nanoparticles having a uniform size of 200 nm was carried out through the reduction of $FeCl_3$ with ethylene glycol at 200 °C in the presence of sodium acetate and trisodium citrate as the alkali source and stabilizing agent, respectively. Recently, a thermal decomposition technique was employed for the preparation of size- and shape-selective Co_3O_4 nanoparticles through the decomposition of $[Co(acac)_2]$ or $[Co(NO_3)_2]$ in different solvents (ethanol and water) and capping agents (oleylamine or hexamethylenediamine), followed by calcination in air.[39] The developed methodology led to the production of spherical, cubic, octahedral and plate-like spinel nanoparticles of Co_3O_4 with a size in the range of 8 to 90 nm. The sol–gel process, which converts molecular precursors into a polymeric oxide network through hydrolysis and subsequent condensation reaction, is a versatile methodology for the one-pot synthesis of size- and shape-controlled porous nanostructures. In this context, a method for the cost-effective and well-controlled sol–gel synthesis of thorn-like ZnO nanoparticles was reported by Aliev *et al.*[40] The synthetic methodology involved the mechanical stirring of zinc acetate, NaOH and CTAB as the capping agent in bi-distilled water, which after a few minutes of agitation turned milky, indicating the generation of ZnO nanoparticles, and their antimicrobial activity was further evaluated against Gram-positive, Gram-negative bacteria and fungi. Along this line, a base-catalyzed sol–gel methodology accompanied with solvent-driven self-assembly process was employed for the fabrication of Mn_3O_4 and CuO nanoparticles.[41] The employed synthesis route facilely generated hexagonal, ribbon- or irregular-shaped Mn_3O_4 nanoparticles having an average diameter of 100–200 nm using different solvent systems such as water, water/ethanol and water/toluene. On the contrary, the same sol–gel process produced nanoporous thin sheets, nanoparticles, rods and ribbon-shaped CuO nanostructures in different solvents. In another publication, Joshi *et al.* delineated a photochemical process for the preparation of ZnO nanoparticles having a size of around 12 nm in an aqueous solvent mixture of alkaline alcohol-acetone under UV light and devoid of any capping agent.[42] Similarly, Mukasyan and research group developed a template-assisted combustion route for the fabrication of ultra-small α-Fe_2O_3 nanoparticles (size below 5 nm) and narrow particle size distribution within a very short reaction duration.[43] In this protocol, SBA-15 was employed as the template together with iron ($Fe(NO_3)_3$) and ammonium nitrate as oxidizers and glycine as fuel.

Recent advancements in the synthesis of nanoparticles have raised huge concern over chemical and physical methods given that they are not only exorbitant and labour intensive but also pose high risks to the environment due to the usage of toxic chemicals. Accordingly, greener biogenic approaches for the synthesis of nanoparticles have gained immense recognition in the past few years owing to their cost-effectiveness and environmentally benign routes. Wide arrays of biological entities are readily available such as extract from plants, plant products and microorganisms such as fungi, yeast, and bacteria, which are most commonly employed for the efficient production of non-toxic nano-sized metal oxide nanoparticles. Significant research has been conducted in this arena. A prolific attempt in this direction was made by Kim and co-workers, wherein they synthesized CuO nanoparticles from leaf extract of *Psidium guajava*, functioning as a reducing agent and stabilizing agent.[44] The employed protocol led to the production of spherical mono-dispersed nanoparticles with an average size in the range of 2–6 nm, whose efficacy was further tested in the photocatalytic degradation of Nile blue and reactive yellow dyes. Another report highlighted an eco-friendly route, wherein a biogenic source such as marine brown algae *Sargassum wightii* was employed as a reducing agent for the preparation of magnesium oxide nanoparticles.[45] The synthesized crystalline MgO NPs having an FCC structure and average size of 68.06 nm demonstrated potent antibacterial and antifungal activity towards pathogens together with good photodegradation efficacy towards methylene blue. Along similar lines, Stella *et al.* judiciously utilized immature fruit extract of *Cocos nucifera* as a reducing and stabilizing agent for the synthesis of three metal oxide nanoparticles, namely, CuO, NiO and Fe_2O_3, whose catalytic efficiency was further evaluated in the catalytic reduction of aromatic aldehydes using ammonium formate as the hydrogen donor.[46] The catalytic studies revealed the superiority of NiO nanoparticles given that they led to the formation of the corresponding alcohols in excellent yields under mild reaction conditions compared to the other synthesized nanoparticles. A comparative analysis of all the synthetic approaches is provided in Table 1.

Distinct morphologies of metal oxide architectures for tailoring nanoscale physico-chemical features

In the past few years, rapid advancements in materials science have enabled the development of novel structural and

Table 1 Comparative analysis of synthetic approaches for the fabrication of metal oxides

Methodology	Conditions	Advantages	Limitations	Ref.
Sol–gel	• Wet chemical method • Use of Molecular precursor • Hydrolysis/alcoholysis	• Narrow particle size distribution • Uniform nanostructures	• Requires costly precursors • Sometimes necessitates high temperature	47
Microwave	• Metal salt/precursor • Microwave heating • Ostwald ripening	• Rapid formation • High Repetition rate	• Extreme conditions	48
Sono-chemical	• Requires ultrasonic wave source • Comparatively low temperature ≈ 60 °C	• Very quick synthesis • Precise control over shape and size	• Sometimes surfactants require • Costly and toxic precursors	49
Hydrothermal	• Use of autoclave • High temperature and inorganic metal salts	• Uniform size and shape • Ease of tenability	• High temperature and pressure	50
Microemulsion	• Utilizes surfactants • Room temperature • Organic solvents or auxiliaries	• Narrow size distribution • Regular shape and morphology	• Use of harmful substances	51
Template assisted	• Inorganic precursor • A template • Self-assembly of template precursor • Condensation and removal of template	• High reproducibility • Controllable structure, size and morphology	• Needs a template • High temperature	52
Bio-synthesis	• Use of plant extracts • Varying temperature (100–250 °C)	• Environmentally benign synthesis	• Longer time duration • Poor control over size and shape	53
Mechano-chemical synthesis	• Pulverisation of precursors by ball milling • Does not require organic solvents and high temperature	• Simple operation • Ease of scaling up	• High purity is questionable • Low crystallinity	54
Laser ablation	• Use of laser beam in liquid • Self-standing and remote control	• High purity • Ease of manipulation	• Expensive • Needs specific set up and arrangements	55
Arc discharge	• Generation of NPs in both gas and liquid medium • Generation of arc between the electrodes (dielectric medium)	• Higher generation rate • Tunable morphology • Economical	• Requires special reactors and other arrangements	56
Lithography	• Preparation of colloidal crystal mask • Disposition of desired material through mask • Removal of mask	• Homogenous NPs • Precisely controlled morphology	• Multistep process • Expensive	57
Sputtering	• Bombardment of energetic particles on the target • Atoms from target are driven off • Deposition on a substrate	• Versatile approach • NPs formed have same composition as target source	• Severe conditions • Costly	58

morphological metal oxide-based nanostructures with more exposed reactive crystal planes. Metal oxide nanomaterials of diverse shapes and dimensions have been reported to date (Fig. 3).[8,59–65] For instance, metal oxide nanomaterials possessing a spherical shape are categorized as 0D nanomaterials. 1D nanomaterials are comprised of nanotubes, nanorods, nanowires and nanobelts, while nanosheets and nanofilms are characterized as 2D nanomaterials. 3D nanomaterials including core–shell and multi-nanolayers are advanced high-performance architectures. It has been perceived that the size and morphological features of these nanomaterials significantly affect their physico-chemical properties. Diverse crystal facets are accompanied with a difference in geometric structure and electronic state, which ultimately play a vital role in enhancing the catalytic performance of metal oxide nanomaterials.[66–68] Extensive studies by various research groups demonstrated the critical role of anisotropic morphology in determining the activity and selectivity of the catalysts at the nanometer scale through the selective exposure of a large fraction of reactive facets or active sites.[69,70] Thus, it is anticipated that the idea of morphology/plane-dependent nanocatalysis can bridge the gap between surface science and materials science by rendering potential routes for tuning the rate of reactions, extent of reactivity and formation of major products. It is worth highlighting here that Pathak *et al.* fabricated CuO nanostructures with different morphologies *via* the chemical precipitation technique, wherein Cu^{2+} was effectively stabilized after complexation with various organic acids including acetic acid, citric acid and tartaric acid.[71] CuO nanostructures possessing various morphologies such as rod, spherical, star and flower were facilely obtained through this route and further successfully characterized using XRD, HRTEM, FTIR, DLS and zeta potential measurements. The catalytic performance of the resulting nanomaterials was investigated in the $NaBH_4$-assisted reduction of 4-nitrophenol. Among the various morphologies, the star-shaped CuO exhibited the highest catalytic activity, which was further ascribed to its high specific surface area, positive surface charge and high indexed facet. Metal oxide nanoparticles as support materials have also been found to regulate the catalytic performance of the resulting nanocomposites. The great relevance of morphology-modulated properties stimulated Zhou and co-workers to synthesize Pd nanoparticle-loaded {100}-faceted CeO_2 nanocubes, {111}-faceted CeO_2 nanooctahedrons and [{100}{111}]-faceted CeO_2 nanorods for

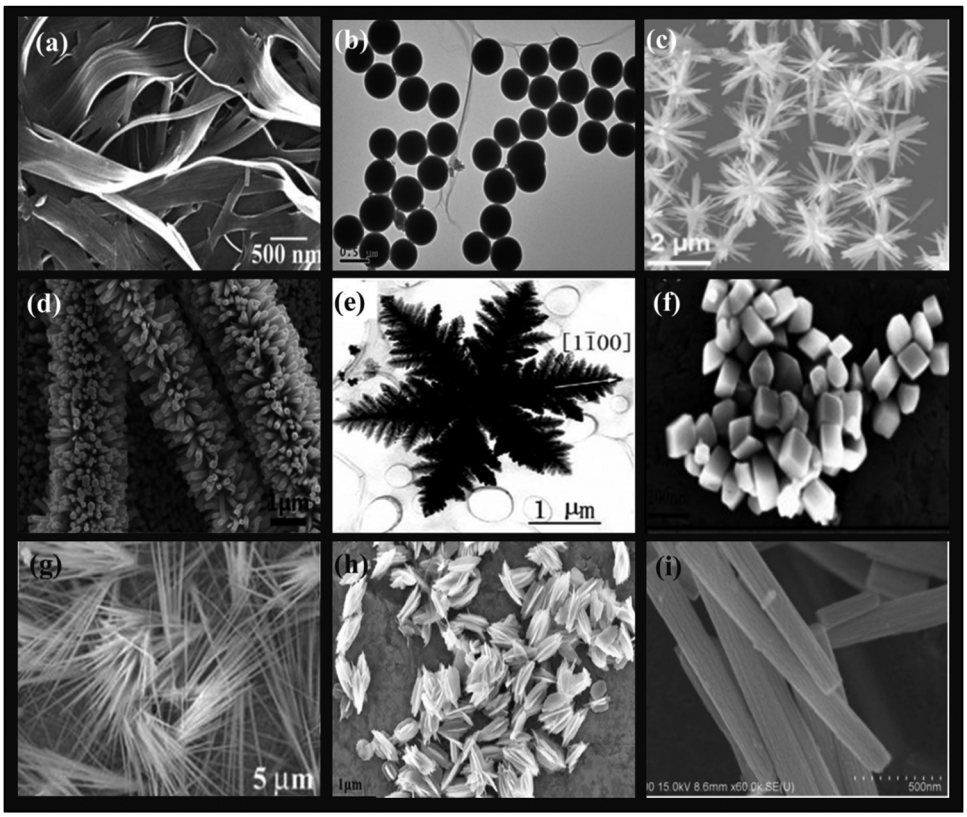

Fig. 3 Diverse morphologies of metal oxide nanomaterials: (a) Nanobelts. Reproduced with permission from ref. 59, Copyright 2007, the American Chemical Society. (b) Nanospheres. Reproduced with permission from ref. 8, Copyright 2014, The Royal Society of Chemistry. (c) Nanoflowers. Reproduced with permission from ref. 60, Copyright 2017, the American Chemical Society. (d) Nanorods. Reproduced with permission from ref. 61, Copyright 2014, the American Chemical Society. (e) Snowflakes. Reproduced with permission from ref. 62, Copyright 2006, Elsevier, B.V. (f) Distorted cubes. Reproduced with permission from ref. 63, Copyright 2015, Springer Nature. (g) Nanowires. Reproduced with permission from ref. 64, Copyright 2002, the American Chemical Society. (h) Nanohusks. Reproduced with permission from ref. 63, Copyright 2015, Springer Nature. (i) Nanotubes. Reproduced with permission from ref. 65, Copyright 2013, The Royal Society of Chemistry.

HCHO oxidation to CO_2.[72] Besides exhibiting immense potential in catalysis, these metal oxide nanoarchitectures possessing varying morphologies have also demonstrated considerable applicability in diverse fields. For instance, Boada and co-workers recently reported the fabrication of superparamagnetic iron oxide nanoparticles *in situ* co-precipitated in commercial cellulose sponge and further utilized them as an adsorbent for As(III).[73] Another research group explored the photocatalytic efficiency of NiO nanobelts in the degradation of organic pollutants such as rhodamine B (RhB), methyl orange (MO), methylene blue (MB) and crystal violet (CV).[74] The few micrometer-long cubic crystalline NiO nanobelts possessing bandgap of 4.07 eV resulted in good degradation of 79.1%, 82.75%, 76.7% and 89% of MO, MB, CV and RhB after 140 min under a xenon lamp. Likewise, various morphologies of ZnO such as nanorods, nanosheets and nanoparticles were coupled with polyaniline (PANI) to yield ZnO/PANI nanocomposites whose potential was further investigated towards NH_3 sensing at room temperature.[75] The morphology exhibited a significant effect on the sensing application and amongst them, the ZnO nanosheets with vapor-phase polymerized aniline showed a good sensing performance, high response, excellent selectivity and appreciable repeatability.

Recent reports have highlighted that metal oxide nanowires possessing good electrical properties, high dielectric constant and wide bandgaps have emerged as appealing materials towards sensing applications.[76] It is worth mentioning here that Pinna and research group demonstrated the gas-sensing response of one-dimensional SnO_2/NiO core–shell nanowires towards hydrogen at various temperatures.[77] The overall composite was prepared through a two-step process, wherein single-crystalline SnO_2 nanowires were first formed *via* the vapor–liquid–solid deposition method, and thereafter decorated with a polycrystalline NiO shell through atomic-layer deposition. The high surface to volume ratio of the SnO_2 nanowires together with the optimized and conformal NiO shell layer resulted in a remarkable performance towards hydrogen sensing. Xia *et al.* reported a hydrothermal method for the synthesis of δ-MnO_2 nanosheets, which exhibited an excellent supercapacitor performance with high specific capacitance of 411 F g^{-1} at a scan rate of 5 mV s^{-1} and 332.7 F g^{-1} at a current density of 0.5 A g^{-1}.[78] The remarkable performance of the developed δ-MnO_2 was attributed to its porous nanosheets structure, which further enhanced the specific surface area, increased the number of active sites and shortened the ion

diffusion distance in the δ-MnO_2 electrodes. In recent years, metal oxide nanoparticles have become a popular choice for developing antibacterial active materials owing to their unique electronic configuration and physicochemical properties.[79] In this case, Sundrarajan M. and co-workers fabricated titanium dioxide (TiO_2) nanoparticles using *Morinda citrifolia* extract and studied their inhibitory activities against human pathogens including *Staphylococcus aureus*, *Escherichia coli*, *Bacillus subtilis*, *Pseudomonas aeruginosa*, *Candida albicans* and *Aspergillus niger*.[80] The results revealed that the TiO_2 nanoparticles demonstrated good antimicrobial activity against a broad spectrum of Gram-positive bacteria.

Surface modification of metal oxide nanostructures: way towards smart design of advanced nanocatalytic systems

The synthesis of metal oxide nanostructure is often followed by further surface modification to support the active metal species, which can effectively enable recyclability, whilst retaining the metal catalytic efficacy. However, some studies also report the coating of the developed oxide nanomaterials to prevent them from agglomeration using different polymers prior to their functionalization, as shown in Fig. 4. Considering the substantial benefits of coating agents, it is evident from our literature survey that these agents not only prevent the aggregation of metal oxides but also impart active sites to a large extent for further tethering with functionalizing moieties, which actively participate in enhancing the catalytic efficacy of the resultant nanostructured matrices.[81] For instance, the synergistic effect of sulfamic acid and amino-functionalized ferrite nanoparticles in catalyzing the one-pot synthesis of α-amino nitriles (up to 98%) was revealed by Kassaee *et al.*[82] The reusability test showed that the catalyst could sustain its efficacy for at least four runs. In another report, Chen and co-workers investigated the catalytic potency of sulfonic acid-functionalized Fe_3O_4@C magnetic nanoparticles with a size of about 190 nm in the condensation of benzaldehyde and ethylene glycol under ambient reaction conditions.[83] Likewise, sulfonated-mercaptopropionic acid-immobilized magnetic nanoparticles (Fe_3O_4/SMPA) manifested stupendous catalytic performance to yield 97% of 3,4-dihydropyrimidin-2(1*H*)-ones in a solvent-free environment.[84] The optimization studies revealed that both the Lewis acidity (SO_3H) and Brönsted acidity (Fe^{3+}) of Fe_3O_4/SMPA effectively contributed to facilitating the formation of the desired product. Recently, Awasthi *et al.* outlined the fabrication of magnetically retrievable amine-functionalized silica-coated ferrite nanoparticles (NH_2@SiO_2@Fe_3O_4 NPs) and their catalytic efficacy in the multicomponent synthesis of bioactive 2-amino-4*H*-benzo[*b*]pyrans in good to excellent yields.[85]

To make nano-oxides suitable candidates for catalytic applications, modification through certain specific functional groups can be achieved by physical or covalent tethering of existing homogeneous active sites on diverse solid support nanostructured matrices such as ferrite, nano-silica, and alumina.[86–92]

The physical modification strategy involves two ways, where one is the inclusion of a modifier in the pores of a solid support matrix and the other is the electrostatic interaction between them. However, surfactant molecules or macromolecules are mainly incorporated in metal oxide nanostructures by electrostatic interactions.[93] For example, Zhu and group developed a nanofiller for polylactide matrices by modifying the surface of silica with oleic acid.[94] Alternatively, a poly(L-lactic acid)/TiO_2 nanocomposite film was fabricated by incorporating carboxylic acid and long-chain alkyl amine-modified TiO_2 nanoparticles in a poly(L-lactic acid) matrix by Nakayama *et al.*[95] Besides, the concept of physical adsorption of metal nanoparticles on the surface of metal oxides was illustrated in the work presented by Saire-Saire *et al.*, which demonstrated the fabrication of a nanoengineered material composed of gold nanoparticles decorated on the surface of magnetic cobalt ferrite (Scheme 1).[96] Their study revealed that the developed nanocatalyst exhibited an excellent performance not only in the reduction of 4-nitrophenol but also in the selective oxidation

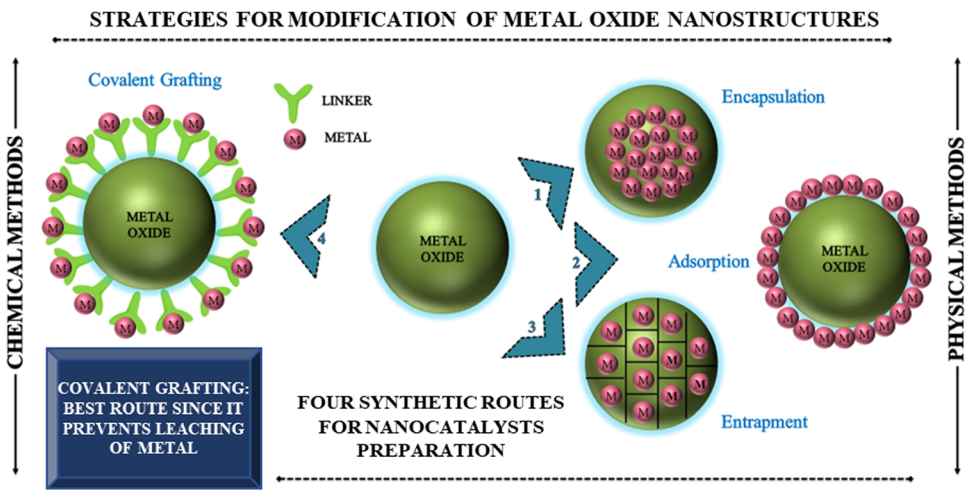

Fig. 4 Strategies for modification of metal oxide nanostructures.

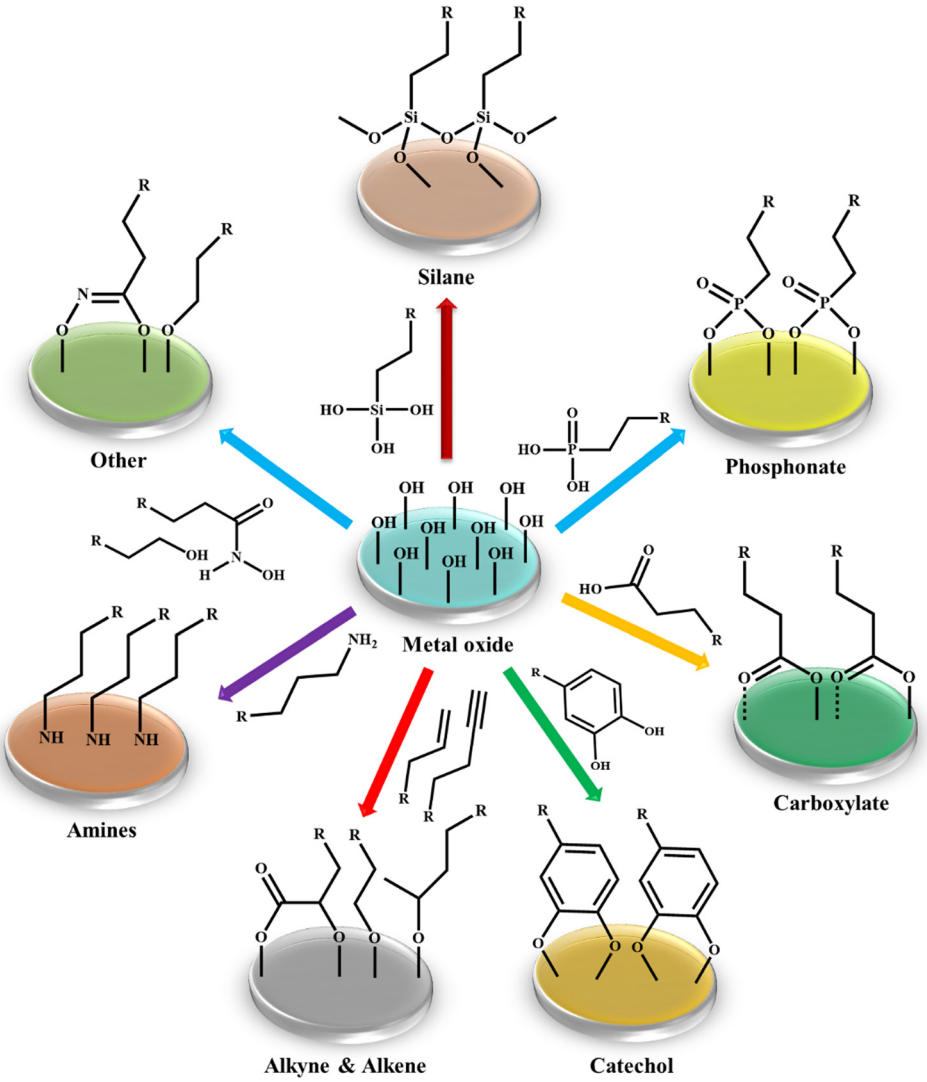

Scheme 1 Most frequently employed functionalizing agents for modifying the surface of metal oxide nanoparticles.

of dimethylphenylsilane to dimethylphenylsilanol. To date, several reports have been published involving hybrid catalyst preparation using a similar synthetic route. Although this strategy is an important advancement, it is not considered to be suitable from an industrial perspective due to the associated metal leaching problem given that the anchoring of the active species on the oxide support is based on weak physical forces. This serious metal contamination issue prompted the scientific community to direct their effort towards alternative approaches, *i.e.*, covalent modification of metal oxide surfaces, which can effectively prevent leaching as a result of the much stronger interactions between the modifiers and support matrix.[97] In this context, there are reports in the literature on the utilization of different modifying agents and grafting polymers to chemically modify the surface of diverse metal oxide nanostructures. Some of the reported modifiers include silane coupling agents, phosphonates, carboxylates, catechols, alkenes/alkynes, and amines.[98] However, the functionalizing agents most often used for the surface modification of metal oxides are silanes and phosphonates, prompting us to provide a detailed discussion on these modifiers (Table 2).

Silane coupling agents

The most common functionalizing entities preferentially chosen by several researchers working in this area are silane coupling agents, which are endowed with hydrolyzable and organo-functional end groups, further allowing the surface immobilization of the desired molecules.[123,124] One of the main advantages of silanes is that they can bear numerous functionalities, for example, amino, cyano, carboxylic acid, and epoxy groups. This method is applicable to numerous metal oxides such as SiO_2, Al_2O_3, TiO_2, SnO_2, ZrO_2, and V_2O_5.[125] The general representation of these linkers is $RSiX_3$, where X is any organo-functional end group including chloro, ethoxy or methoxy groups, which react with the hydroxyl groups of oxide nanostructures, and R is an alkyl chain having a variety of functionalities and is chosen to meet the requirements of the polymer (Fig. 5a).[126] Several research groups reported functionalization

Table 2 Modifiers frequently employed for the surface functionalization of metal oxide nanostructures

S. no	Name of modifiers	Abbrev.	Structure	Ref.
	Silane Coupling Agents			
1.	3-Methacryloxypropyltrimethoxysilane	MPS	$CH_2{=}C(CH_3)COO(CH_2)_3Si(OCH_3)_3$	99–101
2.	Triethoxyvinylsilane	TVS	$CH_2{=}CHSi(OCH_2CH_3)_3$	102–106
3.	Tris(2-methoxyethoxy)(vinyl)silane	TMEVS	$CH_2{=}CHSi(OCH_2CH_2OCH_3)_3$	107 and 108
4.	3-Aminopropyltrimethoxysilane	APTMS	$NH_2(CH_2)_3Si(OCH_3)_3$	109
5.	3-Aminopropyltriethoxysilane	APTES	$NH_2(CH_2)_3Si(OCH_2CH_3)_3$	110
6.	3-Mercaptopropyltrimethoxysilane	MPTMS	$HS(CH_2)_3Si(OCH_3)_3$	101
7.	Hexadecyltrimethoxysilane	HDTMS	$CH_3(CH_2)_{15}Si(OCH_3)_3$	101
8.	Bis[3-(triethoxysilyl)propyl]tetrasulfide	BTESPT	$(CH_3CH_2O)_3Si(CH_2)_3(S)_4(CH_2)_3Si\ (OCH_2CH_3)_3$	108
	Phosphonates			
9.	Aminotris(methylene phosphonic acid)	ATMP	$N(CH_2PO_3H_2)_3$	111
10.	Bis(hexamethylene-triamine)-penta(methylene phosphonic acid)	BHMTPMPA	$H_2PO_3CH_2\text{-}N\text{-}[(CH_2)_6\text{-}N(CH_2PO_3H_2)_2]_2$	111
11.	Phenyl phosphonic acid	PPA	$C_6H_5{-}PO_3H_2$	112
12.	Ethylenediamine tetrakis(methylene phosphonic acid)	EDTMP	$(CH_2)_2\text{-}[N(CH_2PO_3H_2)_2]_2$	113
13.	1-Hydroxyethane-1,1-diphosphonic acid	HEDP	$OHCH_3C{-}(PO_3H_2)_2$	113
14.	Benzene-1,3,5-triphosphonic acid	BTP	$C_6H_3(PO_3H_2)_3$	114
15.	3,5-Diphosphonobenzoic acid	BDP	$HOOC{-}C_6H_3{-}(PO_3H_2)_2$	115
16.	5-Phosphonoisophthalic acid		$C_6H_3(COOH)_2(PO_3H_2)$	115
17.	1,4-Phenylenediphosphonic acid	BDPA	$C_6H_4(PO_3H_2)_2$	116
18.	Phosphorous acid		H_3PO_3	117
	Carboxylates			
19.	Lauric acid	LAU	$CH_3{-}(CH_2)_{10}COOH$	118
20.	Succinic acid	SA	$HOOC{-}CH_2{-}CH_2{-}COOH$	119
21.	Stearic acid	SA	$CH_3{-}(CH_2)_{16}{-}COOH$	120
22.	Photopolymerisable 10-undecynylphosphonic acid	10UCYPA	$H_2PO_3{-}(CH_2)_9{-}C{=}CH$	121
23.	Citric acid	CA	$HOC(CH_2{-}COOH)_2$	122

using different silylating agents as a facile route to construct hybrid nano design catalytic systems.

Phosphonates

Surface modification of a distinct metal oxide nanostructures by phosphonate groups from either by P–OH, P–OR (R1/4 alkyl) or P–O^--containing precursors leads to the formation of M–O–P bonds. For example, if phosphonic acid is used as the precursor for the surface modification of TiO_2 nanoparticles, then it will form Ti–O–P covalent bonds.[126,127] Alternatively, the functionalization of titania through silane coupling agents will create Ti–O–Si bonds, which are very unstable toward hydrolysis. Another important difference from silanes is that phosphonates only undergo reactions with surface OH groups without undergoing homocondensation, and hence P–O–P bonds will not form. Various metal oxides nanostructures can easily be functionalized with phosphonates, which include alumina, stannia, zirconia, and magnetite, and also easily functionalized with phosphonate groups.[128–130] The different modes of anchoring of a phosphonate group on a metal oxide surface, *i.e.*, mono-, bi-, and tridentate, are well illustrated in Fig. 5b. A recent investigation of the binding of (11-hydroxyundecyl)phosphonic acid or (12-carboxydodecyl)phosphonic acid on an SnO_2 surface by solid-state ^{31}P NMR showed the bi- and tridentate attachment of the phosphonate ligands.[131] Besides, multidentate attachment is another stabilizing factor for modified nanoparticles.[132] In the case of the bifunctional (11-hydroxyundecyl)phosphonic acid, it is interesting to note that the phosphonate group and not the carboxylate group was bonded to the stannia surface.

Carboxylates

Carboxylate ligands, in particular fatty acids, have also been utilized for the surface modification of metal oxide nanostructures (Fig. 5c). For instance, Zhang *et al.* employed all-trans-retinoic acid as a carboxylate modifier for the surface modification of titania nanoparticles with various controlled sizes.[133] This study unveiled the size-dependent surface binding forms, indicating that adsorption decreases with a decrease in the size of the developed nanoparticle, while the percentage of chemisorption forms increases. Recently, Jia and co-workers designed chemoselective catalysts by modifying the surface of manganese oxide nanoparticles with carboxylate materials to tune their ammoxidation selectivity during the reaction of hydroxyaldehyde.[134] The results of their study showed that the developed catalyst enhanced the selectivity for hydroxynitrile from 0 to 92%. Further, it was also reported that the product distribution of dinitrile and hydroxynitrile could be altered by simply varying the amount of carboxylate modifier.

Nature of active sites of metal oxide-based catalysts

Metal oxide nanostructures invariably find applications in nanocatalysis owing to their array of fascinating properties and tunable structure, boosting numerous chemical conversions.[16] The surface of metal oxides is generally terminated by oxide O^{2-} because of its larger size compared to M^{n+} cations, eventually leading to the loss of symmetry and coordination of M^{n+} cations at the surface.[135,136] Overall, the surface of metal oxides possesses oxide ions, coordinatively unsaturated cations (M^{n+}) as Lewis acid sites and cations terminated by –OH groups, which act as Brønsted acid sites (Scheme 2).

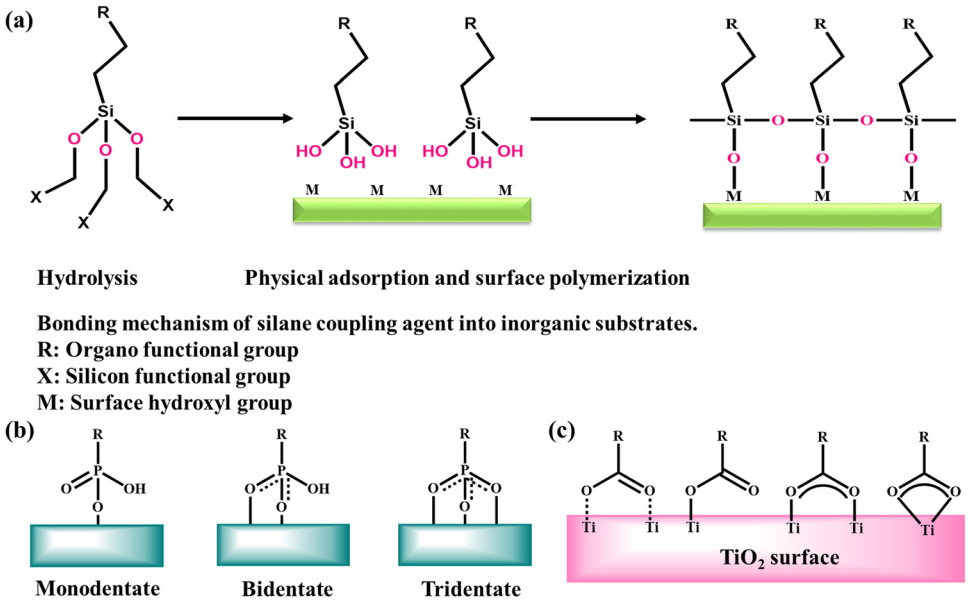

Fig. 5 (a) Bonding mechanism of silanes on inorganic substrates. (b) Different binding forms of phosphonates and (c) adsorption and chemisorption forms of carboxylate ligands on titania nanoparticles. Left to right physical adsorption, monodentate coordination, bridging chemisorption, and chelating chemisorption.

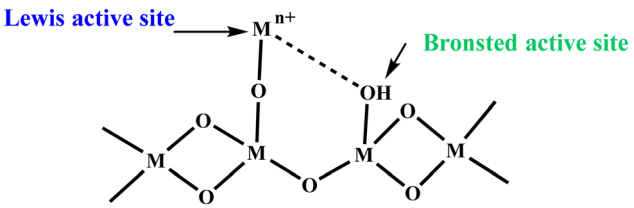

Scheme 2 Surface of metal oxides with Brønsted acid and Lewis acid sites.

Besides, at the nanoscale level, the surface of metal oxides may have different defect sites such as corners, edges and other crystalline discontinuities, which also play key role in expediting the catalytic performance in particular organic transformations.

For instance, Pandian Manjunathan *et al.* utilized tin oxide with Brønsted acidic –OH sites and Lewis acidic Sn^{4+} sites (Scheme 3) in ring-opening reactions.[137] Further, it was established that the developed catalyst showed an excellent performance with high activity and selectivity for different epoxides with alcohols and amines. Besides, studies with 2,6-lutidine were conducted to identify the active sites, which revealed that both the Lewis and Brønsted acid sites accelerate the reaction but the major input is from the Brønsted sites. Similarly, Liu *et al.* reported the preparation of a $CoFe_2O_4$@hollow@mesoporous TiO_2 catalyst for the selective oxidation of styrene.[138] It was observed that styrene oxide and benzoic acid were selectively obtained upon the use of oxygen and hydrogen peroxide as the oxidant, respectively.

Indeed, it is evident from the literature that surface-engineered metal oxide nanocomposites having Brønsted acid

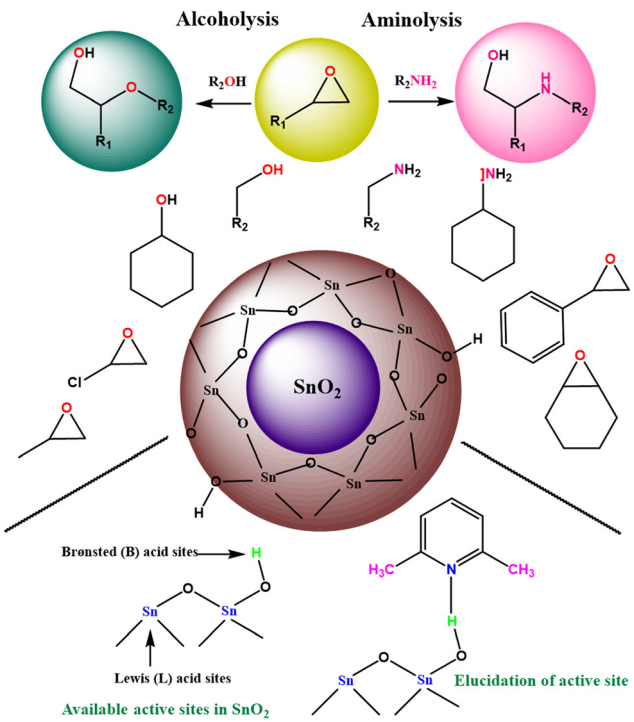

Scheme 3 Alcoholysis and aminolysis of epoxides using tin oxide as the catalyst.

(proton donating) and Lewis acid (electron withdrawing) sites are nowadays more often employed in industrial catalysis. In this context, Mirfakhraei and co-workers demonstrated the facile synthesis of sulfonated-polyethylene glycol-coated Fe_3O_4 (Fe_3O_4/PEG-SO_3H), followed by its utilization as an effective

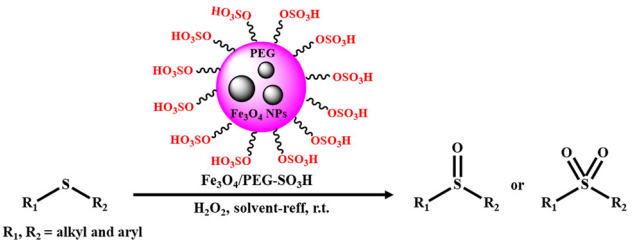

Scheme 4 Fe_3O_4/PEG-SO_3H-catalyzed oxidation sulphides or sulfones.

nanocatalyst for the selective oxidation of sulfides to sulfoxides or sulfones using hydrogen peroxide as a green oxidant (Scheme 4).[139]

Ghorbani-Choghamarani *et al.* fabricated Lewis acid nanocatalytic materials by immobilizing Ni, Co, Cr, Zn or Cd complexes on Fe_3O_4 magnetic nanoparticles for the oxidation of sulfides and oxidative coupling of thiols (Scheme 5).[140] The developed nanostructured catalytic system successfully afforded a wide range of aromatic and aliphatic sulfides and thiols with diverse functional groups.

These nanoengineered metal oxide materials represent model well-defined catalysts for fundamental studies and investigation of the structure–activity relationship in oxidation reactions.[141] This can be attributed to the following facts: (1) the total number of active centres can be controlled during the development of these catalytic systems, (2) the determination of the number of exposed catalytic active sites allows quantitative calculation of the turnover frequencies for oxidation studies, (3) the influence of different metal oxide supports and distinct ligands on the reaction kinetics can be examined and (4) the molecular and electronic structures of surface-modified metal oxides can be studied in detail under all environmental conditions with the help of several physico-chemical characterization techniques. Subsequently, this information is very fruitful in the establishment of structure–activity relationships, which further facilitate the judicious design of advanced nanostructured catalytic architectures. In this context, a study by Kouotou and group revealed the synthesis of a series of cobalt ferrite thin films, which were then comprehensively characterized to gain insight into their structure, surface and morphological properties.[142] It was further observed that Fe substitution by Co in the mixed oxide systems strongly influenced their catalytic performance towards CO oxidation. Besides, the catalytic activity of the Co–Fe oxides with bare α-Fe_2O_3 was also compared, which proved that Co–Fe oxides are better catalytic systems than the latter.

Improvising catalytic conversions utilizing nanoscale-engineered metal oxide-based materials

Oxidation of alcohols. The oxidation of alcohols to carbonyl compounds represents one of the central transformations in synthetic organic chemistry given that it generates countless moieties, which are a core skeleton in a variety of drugs, vitamins, polymers, fine chemicals, *etc.*[143] Owing to their pivotal significance in industrial settings, numerous stoichiometric oxidants have been widely investigated for carrying out oxidation, but they generate huge quantities of toxic

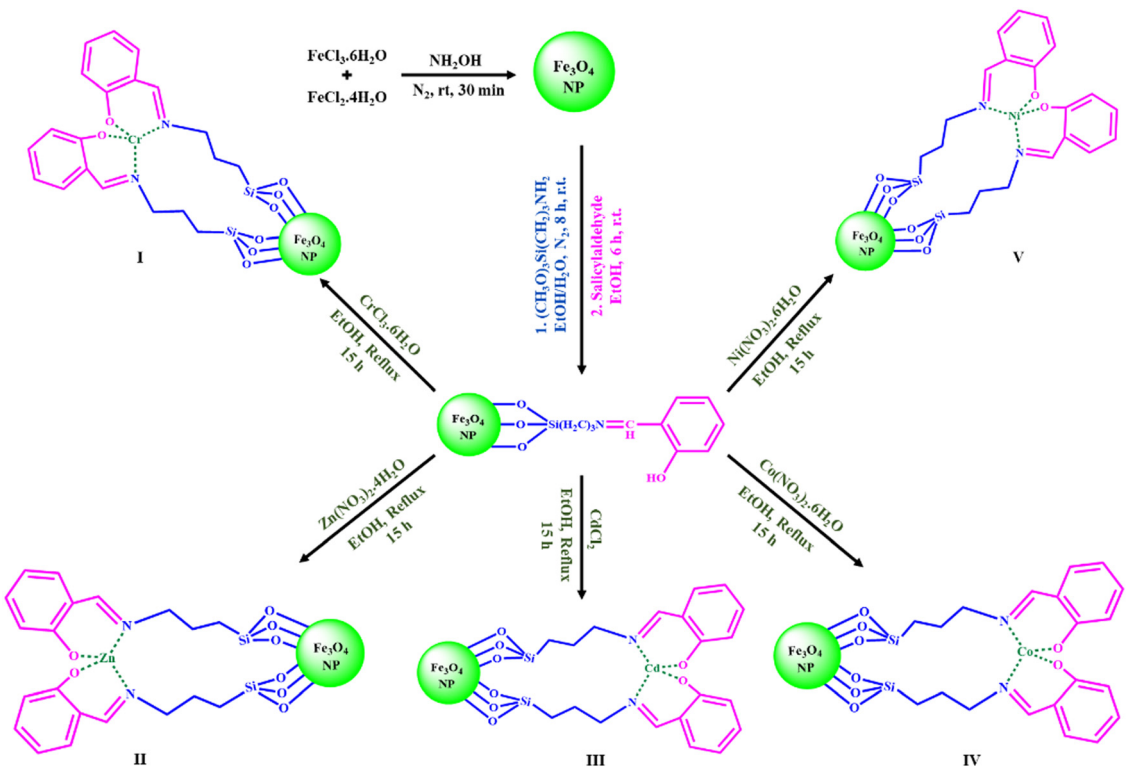

Scheme 5 Synthesis of ferrite based salen complexes.

waste.[144–146] While shedding light on the processes involving oxidation, catalytic selective oxidation using hydrogen peroxide (H_2O_2) as the oxidant has emerged as a forerunner in the area of catalysis owing to the unmatched benefits offered by H_2O_2 such as availability in great abundance, economic viability and tendency to generate only water as the by-product. Thus, the research fraternity has devoted significant efforts to developing catalytic processes that incorporate environmentally benign oxidants in conjunction with metal oxide-based nanocatalysts. Significant work has been carried out in this direction by various research groups.[147]

For instance, Cavaleiro *et al.* reported the fabrication of silica NP-supported iron(III)-containing polyoxometalates (POMs), *i.e.*, Keggin-type α-$[PW_{11}Fe^{III}(H_2O)O_{39}]^{4-}$ and sandwich-type tungstophosphate B-α-$[(PW_9O_{34})_2Fe^{III}{}_4(H_2O)_2]^{6-}$ through the alkaline hydrolysis of TEOS using a reverse micelle and sol–gel approach involving Triton X-100 as the surfactant, 1-octanol as the co-surfactant and cyclohexane as the organic phase.[148] The catalytic activity of the synthesized nanocomposites was investigated in the epoxidation of geraniol using H_2O_2 as the oxidizing agent. The experimental studies revealed the preferential epoxidation of geraniol at the 2,3-position to produce 2,3-epoxygeraniol in major amounts together with the formation of minor products such as 6,7-epoxide and diepoxide. Between the two fabricated nanomaterials, the α-$[PW_{11}Fe^{III}(H_2O)O_{39}]^{4-}$ demonstrated high geraniol conversion (96%) and good regioselectivity (88–91%) towards 2,3-epoxygeraniol after 3 h of reaction in comparison to the B-α-$[(PW_9O_{34})_2Fe^{III}{}_4(H_2O)_2]^{6-}$, which exhibited 81% conversion even after 5 h.

In continuation of work focused on the development of immobilized catalysts for oxidation reactions, Karimi and co-workers delineated the synthesis of tungstate ions immobilized on periodic mesoporous organosilica (PMO) with an imidazolium ionic liquid framework (WO_4^-@PMO-IL) as an effective catalytic system for the H_2O_2-mediated selective oxidation of alcohols.[149] To accomplish the desired goal, the catalyst was fabricated *via* step-by-step assembly, wherein the first step involved the preparation of the ionic liquid BTMSPI precursor by the addition of CPTMS to a suspension of sodium imidazolide and refluxing until a biphasic mixture of toluene and ionic liquid was obtained, and the former was removed to yield pure BTMSPI. The next step involved the hydrolysis and co-condensation of ionic liquid-based imidazolium cations (BTMSPI) and tetramethoxyorthosilicate (TMOS) in Pluronic P123 under acidic conditions in dry methanol with hydrothermal treatment at 100 °C for 72 h to generate PMO-IL. The final step involved the successive functionalization of PMO-IL by the replacement of the chloride ions with tungstate ions *via* a facile ion exchange approach. The resulting material was successfully utilized for the transformation of primary aromatic or aliphatic alcohols to aldehydes and secondary aromatic or aliphatic alcohols to ketones (Table 3). However, despite the fact that secondary aliphatic alcohols exhibit lower reactivity, even open chain and cyclic aliphatic substrates were converted into ketones with good yields under the optimized reaction conditions. Further, the catalyst was easily recovered from the reaction media and reused for six consecutive runs without showing any significant decrease in catalytic activity and selectivity.

Table 3 WO_4^-@PMO-IL-catalysed oxidation of alcohols

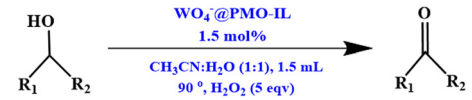

Entry	Acohol	Time (h)	Conversion (%)	Selectivity (%)
1.	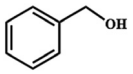	12	75	100
2.	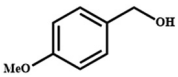	7.5	76	100
3.	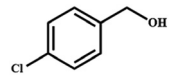	11	82	100
4.	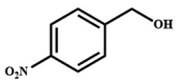	24	65	93
5.	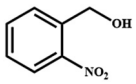	33	77	97

Recently, Pineda *et al.* synthesized metal nanoparticles (Cu, W, Mo and Nb) supported on a silica matrix through a one-pot microwave-aided approach, which were denoted as M-MINT (M = metal supported and MINT = microwave-induced nanotubes), and subsequently utilized in the H_2O_2-assisted wet chemical oxidation of isoeugenol to vanillin.[150] The size of the metal nanoparticles was found to be in the range of 2 to 52 nm and the overall material revealed a high surface area together with a pore size in the mesopore range. Catalytic studies were performed in a parallel reaction station Carrousel Reaction Station TM using acetonitrile as the solvent for 6 h at 80 °C. Amongst the various metal nanoparticles supported on silica, Cu-MINT demonstrated superior selectivity (88%) towards vanillin formation with isoeugenol conversion of 58 mol%.

Another publication reported the synthesis of iron oxide nanoparticles supported on two different aluminosilicates, namely, Al-MCM-41 and Al-SBA-15, *via* the microwave-assisted route.[151] The catalytic performance of the resulting composites was evaluated in the H_2O_2-mediated aqueous selective oxidation of alcohols to the corresponding carbonyl motifs under both conventional and microwave heating. Quite astonishingly, the use of Fe/Al-SBA-15 resulted in slightly superior conversion towards the targeted products in comparison to Fe/Al-MCM-41, which was further attributed to the difference in the acidity or the difference in interactions between Fe and Al in both materials. Using Fe/Al-SBA-15 as the catalytic entity, the protocol was further explored for a range of aromatic and cyclic alcohols, furnishing the desired products in good to excellent yields. Besides, the magnetic characteristics arising due to the presence of iron oxide nanoparticles in the catalyst facilitated its easy removal from the reaction media *via* an external

magnet, which was reused for multiple cycles and maintained 90% of its initial activity even after five cycles.

Nanostructured spinel oxide materials have gained significant attention not only in the field of materials science but also as heterogeneous catalysts because of their intriguing magnetic and optical properties.[152–156] It is worth mentioning here that Vijaya and co-workers synthesized a $CoAl_2O_4$ normal spinel structure in which Co^{2+} is accommodated in the tetrahedral sites, while Al^{3+} occupies the octahedral positions.[157] For comparative analysis, $CoAl_2O_4$ nanoparticles were prepared using both conventional hydrothermal treatment and microwave-assisted technique utilizing *Sesamum* (*S. indicum L.*) plant extract as the reducing and stabilizing agent. Spectroscopic and microscopic techniques revealed that $CoAl_2O_4$ synthesized through the microwave technique had a large surface area and fine crystallites with a narrow size distribution, ultimately paving the way towards improved catalytic performance in the selective oxidation of benzyl alcohol to benzaldehyde (up to 94% yield) using H_2O_2 as the oxidizing agent. The catalytic studies divulged the selective formation of benzaldehyde from benzyl alcohol when acetonitrile was employed as the solvent together with H_2O_2. The authors proposed a plausible mechanism for this observation, wherein acetonitrile activates H_2O_2 by forming a perhydroxyl anion (OOH^-), and it nucleophilically attacks nitrile to form a peroxycarboximidic acid intermediate, which is an O_2 transfer agent. The introduction of O_2 produces coordinated perhydroxyl anion (Co–OOH*) species, which confirms the interaction of the phenyl ring and OH groups of benzyl alcohol with the Co metal of $CoAl_2O_4$. The subsequent regeneration of the active sites through the action of the oxidant with the catalyst leads to the desorption of the product molecule.

In fact, nowadays, the interesting feature of ferrite has transformed the creative outlook of researchers and motivated them towards crafting magnetically responsive catalysts. Working in this direction, Beller reported the use of unsupported or free nano-γ-Fe_2O_3 as an efficient and recyclable catalyst for the selective oxidation of alcohols and olefins to the corresponding carbonyl compounds in the presence of H_2O_2 as the oxidant of choice.[158] High selectivity together with good conversion of the desired products was obtained with these nano-sized iron oxide particles with a size in the range of 20–50 nm. Furthermore, the presence of a thin carbon layer on the iron oxide nanoparticles resulted in the high stability of the catalyst during the course of the organic transformations. Likewise, another research group reported the synthesis of magnetic Fe_3O_4 nanoparticles using a co-precipitation method as a catalytic material for the oxidation of primary and secondary benzylic alcohols and aliphatic alcohols to corresponding carbonyl compounds.[159] The reaction was carried out using Fe_3O_4 as the catalytic entity in a greener solvent-water using H_2O_2 as the oxidant at 50 °C for a specific period to produce the desired products in good to excellent yields. Continuing on the path of utilizing the benefits of the magnetic field-assisted catalyst separation strategy *via* the incorporation of magnetic nanoparticles (MNPs) as the core component, Bhat and co-workers prepared a nickel hydroxide-coated Fe_3O_4 nanocatalyst for the selective liquid-phase-assisted oxidation of alcohols utilizing H_2O_2 as the oxidant.[160] The microscopy studies revealed that Fe_3O_4@APTES@$Ni(OH)_2$ is a combination of spherical and rod-shaped nanoparticles having a smooth surface with a crystallite size of around 40 nm and 130 nm, respectively. The synthesized nanocatalyst exhibited a remarkable catalytic performance in the oxidation of alcohols, *i.e.*, conversion rate of up to 98% in the case of phenylethanol. This enhanced catalytic efficacy was further attributed to the large surface area of the nanoparticles, which delivered abundant coordination sites and surface vacancies during the course of the transformation. Further, the adsorbed nickel hydroxide acted as a Bronsted base and worked synergistically with the Lewis acidic (Fe) center of the nanocatalyst, thereby promoting the quick deprotonation of the alcohols to yield the corresponding carbonyls in good yields.

With the aim to design a magnetically retrievable nanocatalyst, the same research group fabricated a nickel hydroxide-functionalized spinel AFe_2O_4 (A = Mn and Ni) nanocatalyst for the oxidation of aromatic alcohols to carbonyl motifs in the presence of H_2O_2 as the oxidizing agent.[161] The motive to devote attention towards soft ferromagnetic spinel ferrites is associated with their inherent features including high dispersion, low toxicity, excellent stability, and low oxidation potential values. For accomplishing the desired goal, firstly, $MnFe_2O_4$ and $NiFe_2O_4$ nanoparticles were synthesized *via* the co-precipitation method, and further functionalized with APTES in toluene with continuous stirring at 80 °C for 6 h to form aminosilane-modified magnetic nanoparticles. Subsequently, the prepared aminosilane-modified magnetic nanoparticles were stirred with $NiCl_2$ under basic conditions at r.t. for 24 h to produce nickel hydroxide-functionalized $MnFe_2O_4$ (10–20 nm) and $NiFe_2O_4$ (20–60 nm) nanoparticles. Between the two fabricated nanomaterials, the superior rate of alcohol conversion was observed in the case of nickel hydroxide-functionalized $NiFe_2O_4$ nanoparticles. The substrate scope of the developed nanocatalysts was explored for a diverse range of aromatic and aliphatic alcohols under the optimized reaction conditions. Furthermore, the recycling studies divulged that the nanomagnetic catalysts could be efficiently reused for five consecutive runs without showing any significant loss in their catalytic activity.

Pourjavadi and research group fabricated a magnetically retrievable catalyst, wherein Fe_3O_4 nanoparticles were entrapped in a tungstate-functionalized multi-layered cross-linked poly(ionic liquid) matrix.[162] The catalyst was fabricated in a stepwise manner, wherein the synthesis of Fe_3O_4 nanoparticles *via* the co-precipitation method represents the first step towards achieving the desired goal. Subsequently, the resulting magnetic Fe_3O_4 nanoparticles were coated with silica and surface-modified using 3-(trimethoxysilyl)propylmethacrylate (MPS) to generate MNP@MPS. Then, MNP@MPS was covalently attached on the highly cross-linked poly(ionic liquid) possessing tungstate ions through the free radical initiation polymerization of the ionic liquid monomer to form the desired MNP@PILW. The catalytic potential of the resulting material

was evaluated in the oxidation of a broad array of organic substrates ranging from alcohols and olefins to sulfides in the presence of H_2O_2 as the oxidizing agent. Furthermore, the high stability and durability of the catalyst was also evident from the recycling studies, which showed reusability up to ten cycles without any significant deterioration in catalytic efficacy.

Another research group led by Zamani *et al.* delineated the preparation of Cr(III)-containing Fe_3O_4/polyacrylonitrile-ethylenediamine nanocomposite as an effective catalyst for the selective oxidation of aromatic and aliphatic alcohols using H_2O_2 as the oxidant under mild reaction conditions.[163] The catalyst was fabricated through a series of steps, wherein the synthesis of polyacrylonitrile (PAN)-coated Fe_3O_4 nanoparticles through *in situ* polymerization using benzoyl peroxide as the initiator was the key step. The prime idea behind the use of iron oxide as the core material was in view of its phenomenal capability to undergo ready separation from the reaction mixture using only an external magnet. The next step involved the functionalization of Fe_3O_4-PAN with ethylenediamine, onto which chromium was finally immobilized by stirring under an inert atmosphere at room temperature. The synthesized catalyst led to the generation of a library of corresponding aldehyde moieties in high yields together with good selectivity within a short reaction time.

Similarly, another report by Maleki *et al.* highlighted the use of a hybrid chromium(VI) magnetic nanocomposite, *i.e.*, Fe_3O_4@SiO_2@PPh_3@$Cr_2O_7^{2-}$, for the oxidation of benzyl alcohol to benzaldehyde, cyclohexanol to cyclohexanone and epoxidation of cyclohexene using H_2O_2 under ultrasonic conditions at room temperature.[164]

Chattopadhyay and co-workers synthesized and characterized water-soluble Fe(III) and Mn(III) Schiff base complexes immobilized on dopamine-functionalized Fe_3O_4 nanoparticles possessing a CTAB micelle structure, *i.e.*, CTAB/Fe_3O_4@dopa@ML (M = Fe or Mn, L = cyclohexane-1,2-diylbis(azanylylidene)bis(methanylylidene)bis(2,4-diXphenol, where X = Cl, Br, and I) (Scheme 6).[165] The synthesized nanomaterials served as efficient catalysts for the oxidation of a diverse range of alcohols using H_2O_2 as a green oxidant at room temperature. Density functional theory and spectroscopic studies revealed the crucial role of the generated hydroperoxo intermediates in the reaction. Besides, the magnetic characteristics of the synthesized nanocatalyst permitted its facile removal from the reaction media *via* an external magnet and it could be reused for five successive runs.

In recent years, owing to their unique catalytic properties, supported gold nanomaterials have been widely explored for executing a broad array of organic transformations. In this case, Cao *et al.* investigated the catalytic potential of supported Au nanomaterials such as Au/C, Au/Fe_2O_3, Au/Al_2O_3, Au/TiO_2 (World Gold Council), Au/CeO_2 and Au/TiO_2 (Mintek) for the oxidation of various activated and non-activated alcohols using H_2O_2 as the oxidizing agent.[166] Amongst the aforementioned catalysts, the H_2O_2–Au/TiO_2 system demonstrated the highest conversion rate of 99% for 1-phenylethanol in aqueous media at 90 °C. The scope of the H_2O_2–Au/TiO_2 system was also scrutinized for structurally diverse alcohols, which revealed that primary alcohols were oxidized to the corresponding carboxylic acids, while secondary alcohols to ketones. It is worthy to note that the H_2O_2–Au/TiO_2 system was also capable of oxidizing even primary aliphatic alcohols, which are considered to be the most inactive alcohol species in the absence of a base. Another remarkable aspect of this report was the heterogram-scale clean oxidation of alcohols to the corresponding carboxylic acids. The authors further highlighted the role of H_2O_2 as the hydrogen scavenger, wherein H_2O_2 abstracts the α-hydrogen of the substrate to generate an Au–alcoholate complex, which is further attacked by another molecule of H_2O_2 to produce Au-hydroperoxide, ultimately forming the desired carbonyl products through the β-elimination pathway. Another publication by Jain and co-workers reported the use of nano zinc oxide particles as catalysts for the oxidation of aromatic alcohols to carbonyl motifs using H_2O_2 as an environmentally benign oxidant and dimethyl carbonate as the reaction medium.[167] ZnO_2 nanocrystals with a size ranging from 50–150 nm were synthesized *via* a facile hydrothermal route. The synthesized nanocatalyst successfully afforded a broad range of carbonyl compounds through the oxidation of alcohols in excellent yields. Furthermore, the spent zinc oxide (ZnO) was readily recovered from reaction media through filtration and treated with aq. H_2O_2 at 150 °C to yield ZnO_2, which was used for further recycling studies. Jérôme *et al.*

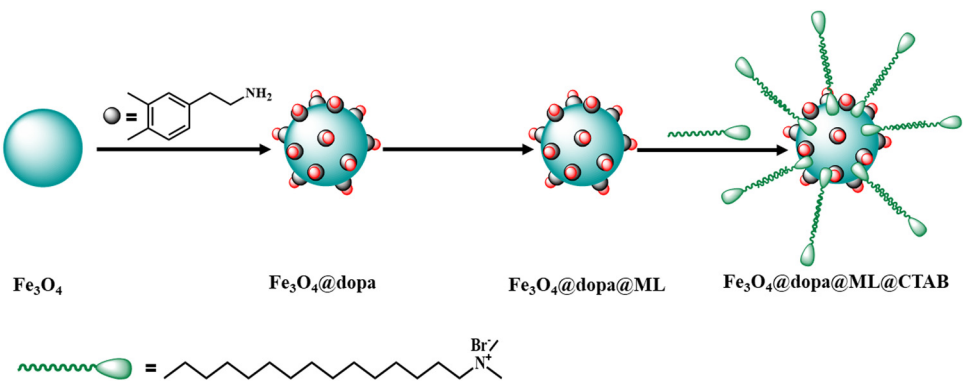

Scheme 6 Schematic representation of the synthesis of bilayer CTAB/Fe_3O_4@dopa@FeL (CHCAT-1) and CTAB/Fe_3O_4@dopa@MnL (CHCAT-2).

reported the fabrication of CuO nanoleaves through an unconventional sonochemical route, and subsequently evaluated their catalytic efficacy in the base-free aq. oxidation of glycerol to dicarboxylic acids.[168] This protocol was surfactant and template free, involved an *in situ* pseudo-calcination step, and also credibly reduced the reaction time (synthesis time of 5 min). It is worth mentioning here that copper was chosen as the active metal of choice due to its abundance, low cost, low toxicity and exceptional performance. The microscopy analysis revealed that the CuO nanoleaves were comprised of numerous small particles, whose assembly resulted in the formation of the overall leaf-like morphology (Fig. 6). Further, using H_2O_2 as the oxidant of choice, glycerol selectively produced oxalic acid (56%) and tartronic acid (22%) in an overall yield of 78%. Besides, the DFT studies highlighted the synergistic role of CuO and H_2O_2 in achieving this high conversion rate, and also in maintaining the high stability of the catalyst.

Continuing the trend of developing supported catalysts for the oxidation of alcohols, Naeimi and his competent team of researchers came up with the idea of designing an MoO_3/copper Schiff base complex for the green oxidation of alcohols.[169] For the fabrication of the desired catalyst, MoO_3 nanoparticles were first synthesized using *Sesbania sesban* plant extract. Simultaneously, the Schiff base ligand was prepared through the condensation of vanillin with 9-aminoacridine and its complexation with copper generated a copper Schiff base complex, which was eventually mixed with the MoO_3 nanoparticles *via* ultrasonication to form the anticipated nanocomposite. The developed nanocatalyst successfully converted diverse alcohol substrates to the corresponding aldehydes or ketones with a high conversion rate and good selectivity. The same research group prepared a manganese oxide nanoparticle-supported copper complex nanocomposite (Mn_3O_4/CuL) *via* the sonochemical route and evaluated its catalytic potential in the oxidation of a broad array of primary and secondary alcohols using H_2O_2 as the oxidant under solvent-free conditions.[170]

Recently, Amini and co-workers reported the use of ultrasmall iron oxide hydroxide (FeOOH) having a size of <10 nm as the catalyst for the H_2O_2 assisted oxidation of a series of alcohols, sulfides and alkenes.[171]

The selective oxidation of vanillyl alcohol to vanillin is a key transformation for the production of a wide array of pharmaceuticals. Accordingly, Valange *et al.* prepared spinel Co_3O_4 nanoparticles *via* a controlled homogeneous co-precipitation approach, and further explored their potential in catalyzing the oxidation of vanillyl alcohol to vanillin using H_2O_2 as the oxidant and water as the reaction medium under ultrasonication.[172] In an attempt to study the influence of the reaction parameters on the concerned oxidation reaction, it was also performed under conventional heating conditions. The experimental results demonstrated the high efficiency of ultrasonication in comparison to traditional heating conditions (15 min in comparison to 60 min), conversion (38% *vs.* 32%) and selectivity (50% *vs.* 22%). The aforementioned results were further ascribed to the *in situ* generated chemical effects under ultrasonic conditions, *i.e.*, the formation of hydroxyl radicals together with the enhanced mass transfer phenomenon between the Co_3O_4 catalyst and the organic substrate. Similarly, Hamid and research group fabricated a mesoporous, highly crystalline Cu–Ti composite as a heterogeneous catalyst for the liquid-phase oxidation of vanillyl alcohol.[173] This composite was synthesized through a modified solution method-based approach, wherein copper acetate, titanium(IV) isopropoxide and trifluoroacetic acid were first mixed in methanol for 4 h. In the next step, the solvent was extracted by applying pressure under vacuum and the obtained solid was ground and calcined in air at 500 °C for 6 h to yield the desired composite catalyst. The synthesized catalyst exhibited a conversion rate of 66% together with 71% selectivity towards vanillin formation from vanillyl alcohol, which was further attributed to the synergistic effect between Cu and Ti of the Cu_3TiO_4–TiO_2 mixed metal oxide catalyst.

Rabbani and co-workers synthesized a magnetically recyclable TCPP/Zn–Fe_2O_4@ZnO catalyst for the H_2O_2-mediated oxidation of primary and secondary alcohols.[174] To synthesize the desired catalyst, Zn–Fe_2O_4 nanoparticles were first prepared through the hydrothermal route. In the next step,

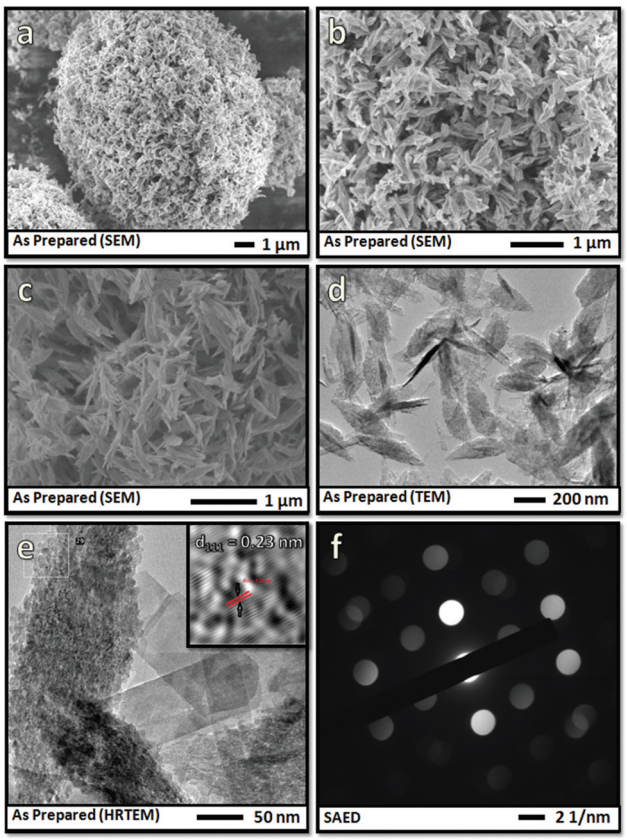

Fig. 6 (a) Low- and (b) high-magnification SEM images of CuO nanoleaves synthesized by low-frequency ultrasound and (c) SEM images of CuO nanoleaves synthesized by the conventional method. (d) Low-magnification TEM image, (e) high-magnification TEM image, and (f) SAED pattern of CuO nanoleaves. Reproduced with permission from ref. 168. Copyright 2018, The Royal Society of Chemistry.

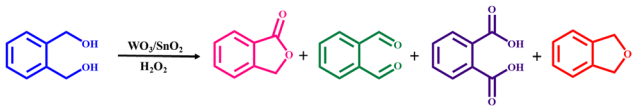

Scheme 7 Schematic representation of the oxidation product distribution of 1,2-benzenedimethanol by WO_3/SnO_2.

Zn–Fe_2O_4@ZnO was synthesized by dispersing the as-synthesized Zn–Fe_2O_4 nanoparticles in water together with zinc acetate and ammonia, and finally stirring at 120 °C for 3 h. In the final step, 5,10,15,20-*meso*-tetrakis(4-carboxyphenyl) porphyrin was immobilized on Zn-Fe_2O_4@ZnO *via* the co-precipitation approach. The resulting catalyst demonstrated high activity and selectivity (up to 100%) in the concerned oxidation reaction. Besides, the catalyst was magnetic in nature and could be facilely recovered from the reaction medium and reused for four consecutive runs without showing any appreciable loss in its catalytic performance.

The selective oxidation of 1,2-benzenedimethanol to generate phthalides is an important transformation for the production of dyes, pharmaceuticals, *etc.* A prolific attempt in this direction was made by Dai and co-workers, wherein a series of WO_3/SnO_2 composites was synthesized through the co-precipitation-impregnation approach, followed by calcination at varying temperatures, and subsequently utilized in the preparation of phthalides from 1,2-benzenedimethanol using H_2O_2 as the oxidizing agent (Scheme 7).[175] The experimental studies revealed that the optimized calcination temperature for the support and catalyst, which resulted in an enhanced catalytic performance, was 1023 K and 823 K, respectively. The authors further highlighted that the high dispersion of tungsten species together with the existence of a few W^{6+} ions in the SnO_2 lattice was beneficial for achieving the optimal catalytic activity in the oxidation reaction. Thus, the calcination temperature was found to have a profound influence on the overall catalytic activity of WO_3/SnO_2.

Thiol oxidation

The oxidation of thiols to disulphides or sulphoxides is a key preparative step in organic synthesis, which renders the production of several other significant sulphur-based moieties and related cyclic analogues such as disulphide S-oxides, disulphide S-dioxides and sulfonic acids possessing remarkable biological activities. Considerable work has been done by various research groups in this arena. It is worth mentioning here that Rajabi and co-workers fabricated a magnetically retrievable catalyst comprised of iron oxide nanoparticles stabilized on SBA-15 for carrying out the aqueous oxidation of sulfides to sulfoxides.[176] The catalytic activity of the synthesized composite was investigated using methylphenyl sulfide as the model substrate in the presence of H_2O_2. Further, different experimental parameters such as amount of catalyst, polarity of solvent, oxidant dosage, temperature and time were studied to achieve the best reaction conditions. Interestingly, it was found that by using 1 mol% of catalyst, 0.5 mmol H_2O_2 and water as the solvent, high product yield was attained in just 120 min at room temperature. The other fascinating attributes of the developed protocol include broader substrate scope, high stability of composite with negligible leaching of active species, facile magnetic separation, and excellent reusability for ten successive runs.

Rostami and Atashkar were the first to synthesize a chiral oxo-vanadium (+)-pseudoephedrine complex supported on Fe_3O_4 magnetic nanoparticles (VO(pseudoephedrine)@MNPs), and further utilized it as a catalyst in the chemoselective oxidation of sulfides to sulfoxides.[177] The synthesized nanocomposite was systematically characterized *via* UV-Vis spectroscopy, SEM, XRD, TGA, FT-IR, VSM, EDX and AFM (Fig. 7). Further, experimental investigations revealed that VO (pseudoephedrine)@MNPs provided a high product yield (85–97%) with 20–27% enantiomeric excess under solvent-free conditions. Moreover, a diverse range of sulfides bearing different substituents were subjected to oxidation under the optimized conditions, furnishing good to excellent yields in shorter reaction times.

Another study by Kuwahara *et al.* reported the successful conversion of sulfides to sulfoxides in the presence of a newly designed yolk–shell nanostructured Pd@TSS catalyst and H_2O_2 as the oxidant.[178] A facile interfacial self-assembly approach

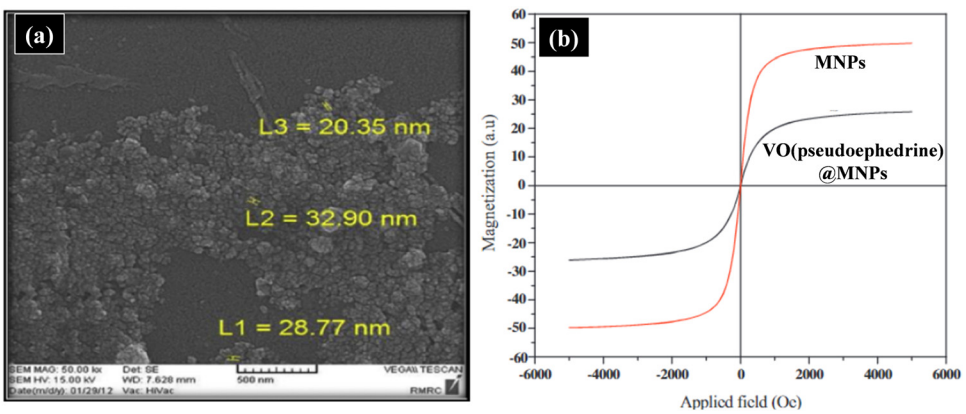

Fig. 7 (a) SEM image of VO(pseudoephedrine)@MNPs and (b) VSM analysis curve comparing the magnetization of MNPs and VO(pseudoephedrine)@MNPs. Reproduced with permission from ref. 177. Copyright 2015, Elsevier B.V.

was utilized for the fabrication of a titanosilicate (TSS) yolk–shell nanoarchitecture, which was composed of active Pd NPs inside a hollow cavity, while Ti sites were dispersed in a silica shell region. Compared to the traditional palladium homogenous catalyst, the designed Pd@TSS possessed higher catalytic efficacy and afforded excellent product yield. The impressive catalytic performance was accredited to the yolk–shell structure, which was responsible for the fast diffusion of H_2O_2 to the neighbouring active metal sites. Working along similar lines, Zhao and research group designed a greener route for the selective oxidation of sulfides *via* the design of a monoprotonated divanadium-substituted phosphotungstate ($[\gamma\text{-}HPV_2W_{10}O_{40}]^{4-}$)/$H_2O_2$ catalytic system.[179] Using this catalyst, a wide range of sulfoxides was obtained with high turnover number and excellent conversion percentage. Closer inspection of the catalytic mechanism revealed that initially H_2O_2 attacks $[\gamma\text{-}HPV_2W_{10}O_{40}]^{4-}$, leading to the formation of μ-hydroxo-μ-hydroperoxo species. In the next step, the hydroperoxo species reversibly dehydrates to produce active vanadium oxygen entities, which further react with sulfides and form the corresponding sulfoxides. Notably, the attractive feature of the aforementioned protocol is the utilization of water as the solvent, thereby eliminating the need for harsh organic solvents.

Among discrete sulphur containing compounds, disulphides have gained much prominence as a key intermediate in various industrial, pharmaceutical, food and drug delivery systems. The reason behind their high significance is their characteristic S–S bond, which plays an important role in stabilizing the protein structure and can be easily regulated during the reactions. Thus, considering the significant benefits of disulphides, Rajabi *et al.* successfully fabricated a heterogeneous catalyst by decorating/incorporating Fe NPs on the surface of SBA-15 and employed it for the chemo-selective synthesis of disulphides.[180] The reaction was performed using thiophenol as the reactant, which was dissolved in acetonitrile, and to initiate the reaction, an optimum amount of FeNPs@SBA-15 and H_2O_2 was added to the reaction mixture. It was then allowed to stir for 20 min at refluxing temperature, which eventually generated the desired disulphides. The special features of this protocol such as simple work-up procedure, mild reaction conditions, high selectivity, greater functional group tolerance, facile recoverability, excellent reusability, and shorter reaction time make a better alternative for conducting the reaction in contrast to the reported methodologies. Similarly, Sabet and co-workers described the fabrication of magnetically separable sulfonic acid-coated γ-Fe_2O_3 NPs.[181] The synthesis of the nanocomposite was carried out in a stepwise manner. Initially, a simple co-precipitation method was employed to synthesize the γ-Fe_2O_3 NPs, and in the next step, chlorosulfonic acid reacted with the prepared magnetic NPs, which ultimately afforded the γ-Fe_2O_3–SO_3H nanocomposites. Further, the catalytic performance of the γ-Fe_2O_3–SO_3H nanocomposite was explored in the H_2O_2-mediated oxidation of thiols. Through a deeper analysis of the experimental results, it was found that the γ-Fe_2O_3–SO_3H nanocomposite showed superior catalytic activity with promising product yield only in the short time of 60 s.

Kulkarni *et al.* delineated the fabrication of a novel, durable and recyclable $NiFe_2O_4$ nanocatalyst, which exhibited a splendid catalytic performance in the conversion of thiols and sulphides using H_2O_2 as the oxidant.[182] The newly fabricated nanocomposite was well characterized *via* XRD, TEM, SEM, EDX and AAS and it was found that $NiFe_2O_4$ possessed a cubic morphology with an average size ranging from 14 to 20 nm. Further, the authors shed light on the reaction mechanism, revealing the formation of a redox couple between the two metal centres (Ni and Fe), which activates H_2O_2 to generate active $^{\bullet}OH$ species. Further, the $^{\bullet}OH$ species attacks the thiols and sulphides, ultimately forming the corresponding disulphides and sulfoxides, respectively. Besides, due to its ferrimagnetic nature, $NiFe_2O_4$ could be easily separated from the reaction mixture and reused for five successive runs without showing any appreciable loss in its activity. Similarly, Ghorbani-Choghamarani *et al.* fabricated metal (Cr, Zn, Cd, Co, Ni)-salen complexes immobilized on APTES-functionalized Fe_3O_4 for the oxidation of thiols and sulphides using H_2O_2.[140] Among the synthesised catalysts, Co-salen-MNPs and Ni-salen-MNPs demonstrated the highest catalytic activity with excellent product yield at 35 °C under solvent-free conditions. Further, to broaden the scope of this protocol, the reaction was conducted using a variety of alkyl, aryl, dialkyl, cyclic sulfides and aromatic, aliphatic, benzylic or heteroaromatic thiols possessing different functionalities. The results indicated that the reaction proceeded satisfactorily without the formation of by-products, signifying the proficiency of adopted methodology. Nikoorazm *et al.* proposed the idea of designing a novel and reusable nickel Schiff base complex grafted on Fe_3O_4@MCM-41 nanocatalyst for the oxidation of sulfides to sulfoxides and thiols to disulfides (Scheme 8).[183] As indicated by the SEM and TEM analysis, Fe_3O_4@MCM-41@Ni-P2C consisted of uniform spherical particles with a size in the nanometre range. Moreover, to obtain the best reaction profile, various parameters such as amount of oxidant, catalyst dosage and nature of solvent were studied. Simple work-up procedure, mild reaction conditions, green oxidant, high product yield, short reaction times and broad substrate scope were some of its notable advantages, making this protocol economically viable for large-scale production.

Oxidation of amines

The oxidation of aromatic amine motifs to O-containing compounds such as nitroso, hydroxylamine, and oxime compounds and their reduction to azo/azoxy derivatives are two significant sustainable chemical processes that have been widely used for the generation of dyes, pigments, pharmaceuticals, food additives, analytical reagents, *etc.* Owing to the broad and versatile application of azo and azoxy derivatives, various researchers have successfully carried out their reduction using reducing agents. However, the developed processes involve harsh reaction conditions, and generally are accompanied with hazardous by-products. Thus, to avoid these environmental issues, it is

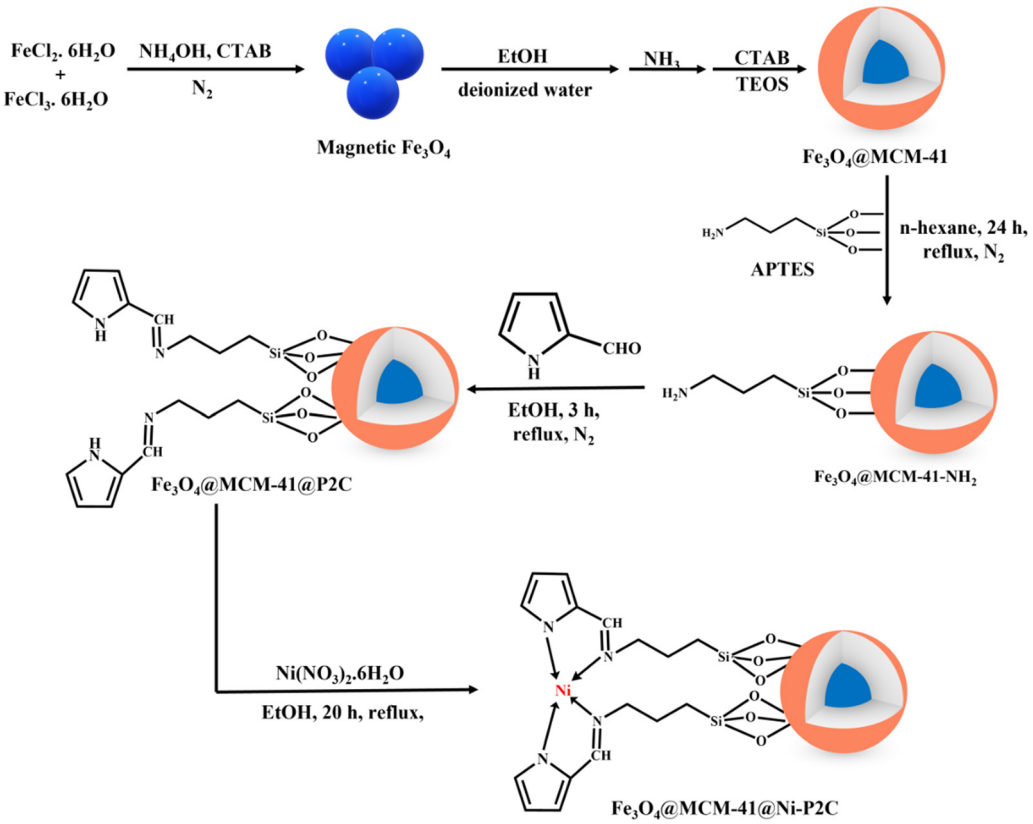

Scheme 8 Illustration depicting the fabrication of Fe_3O_4@MCM-41@Ni-P2C.

necessary to develop greener protocols. Based on this and in a quest to obtain promising results for the oxidation of aniline to azoxybenzene, Bal and co-workers employed the synergistic effect of two different metals (Cu and Cr) by fabricating copper chromite spinel nanoparticles (NPs).[184] The catalyst preparation route involved the use of the anionic surfactant cetyltrimethylammonium chloride (CTAC) as a templating agent, which was added to the solution of metal ion salts, and then kept under solvothermal conditions at 200 °C for 18 h. Further, the calcination of obtained green fluffy material in a tubular furnace at 700 °C resulted in the formation of the desired spinel catalyst. The prudently constructed material successfully yielded suitable azoxybenzenes with outstanding selectivity (92%) and excellent conversion (78%) at 70 °C compared to the conventional and commercial catalysts. The underlying reason for this marvellous catalytic potency was accredited to the high surface/volume ratio and large accessible surfaces of the catalyst toward the reactant molecules. Besides, high functional group tolerance, broad substrate scope, exceptional yields and mild reaction conditions were some of the intriguing features of the developed protocol. One year later, the same research group reported a method for the facile synthesis of Ag/WO_3 *via* the sequential anchoring of Ag NPs on the surface of WO_3 to produce azoxybenzenes from amino groups.[185] The determination of the morphological and structural attributes of the catalyst was carried out using various techniques such as SEM, TEM, XRD, BET, XPS and TGA. After a deeper analysis, it was found that 0.10 g catalyst, 10 mL acetonitrile and 2.15 g of H_2O_2 at 25 °C were best reaction conditions, which oxidized 1 g of aniline, thereby yielding 99% of azoxybenzene. Moreover, the authors shed light on the significant role played by Ag nanoparticles in generating highly reactive peroxide ($^{\bullet}OOH$) species, which initially attacked the N–H bond of aniline to form the phenyl hydroxyl amine intermediate (Scheme 9). In the next step, the intermediate further oxidized and ultimately produced azoxybenzene under similar conditions. Therefore, the findings led to the conclusion that due to the nanosize effect of the silver nanoparticles, Ag/WO_3 exhibited incredible catalytic potency in comparison to bare Ag and WO_3.

Similarly, a study aimed at the selective oxidation of aniline was conducted by Cheng *et al.*, wherein molybdenum oxide $[N(C_4H_9)_4]_2[Mo_6O_{19}]$ was utilized as the catalyst for the reaction in the presence of H_2O_2 as an environmentally benign oxidant.[186] Furthermore, to determine the best reaction conditions, various parameters such as influence of solvent, temperature, time, amount of catalyst and oxidant were investigated. The experimental investigations revealed that in the absence of catalyst, no desired product was formed, indicating the proficiency of the catalyst in the reaction system. Moreover, it was observed that the reaction failed to occur under an O_2 atmosphere given that it was not reactive enough to activate the $[N(C_4H_9)_4]_2[Mo_6O_{19}]$ composites, thereby signifying the importance of H_2O_2 in conducting the process. Under the optimized reaction conditions, the catalytic potency of the

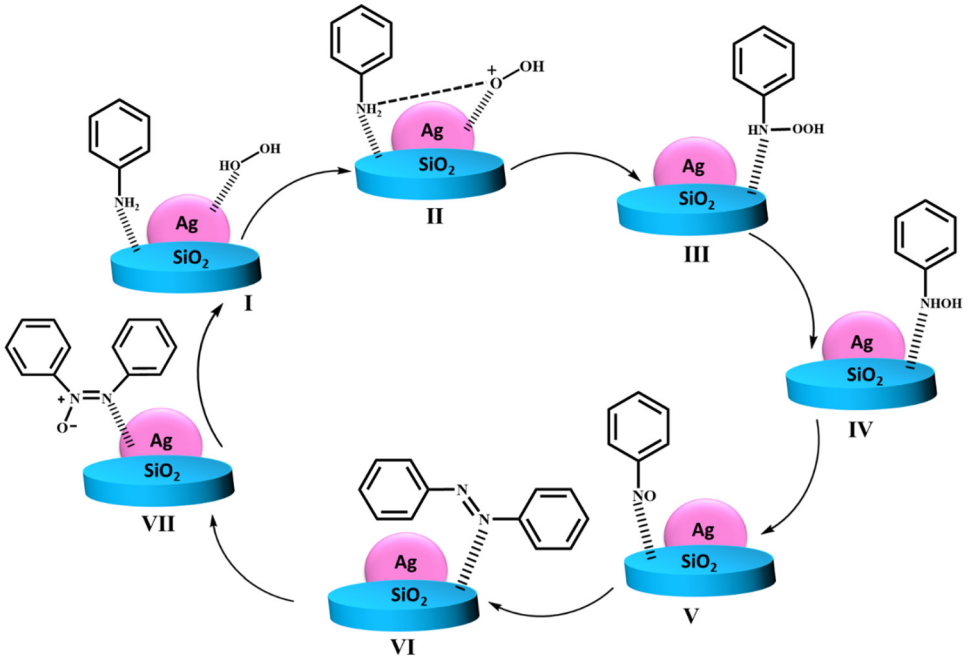

Scheme 9 Schematic illustration of the mechanism during the oxidation of aniline to azoxybenzene.

designed $[N(C_4H_9)_4]_2[Mo_6O_{19}]$ composite was found to be exceptionally remarkable with high selectivity and excellent yield.

Besides yielding azoxybenzenes, the oxidation of amines with hydrogen peroxide also leads to the formation of nitroso compounds, which occupy a significant place in the field of discrete biological metabolic processes and synthetic chemical transformations, for instance, nitroso aldol cycloadditions, ene reactions, synthesis of indoles and azoarenes. In this direction, considerable efforts have been made by Lykakis and research team, wherein they successfully fabricated a novel, stable and recyclable Au/TiO_2 nanocatalyst for the oxidation of amines.[187] For this, the authors employed a facile deposition–precipitation method, wherein the surface of TiO_2 was loaded with Au NPs. The synthesized Au/TiO_2 displayed astonishing catalytic activity, which is higher than that of P25 and Hombikat. Moreover, deep insight into the mechanistic studies revealed that Au played a pivotal role in activating H_2O_2, which *in situ* generated highly reactive $[Au–OH]^{\bullet+}$ species to trigger the concerned reaction (Scheme 10). Besides, the catalytic potency of Au/TiO_2 was exploited for executing the oxidation of diverse aromatic amines, revealing promising outcomes. Based on these encouraging findings, the designed catalytic system was found to be highly chemoselective for obtaining nitroso motifs even for large-scale industrial synthesis.

Pyridine *N*-oxide, which is considered an active biological heterocyclic compound, has also been gaining immense popularity in the pharmaceutical sector. The benefits offered by this moiety are not just limited to its biological significance but also as an auxiliary agent, protecting group, oxidant and ligand for metal complexes in various fields. Considering this, a prolific attempt was made by Rajagopal *et al.*, wherein the authors prepared an Ru(PVP)/c-Al_2O_3 composite by anchoring small-sized PVP-stabilised Ru NPs on the surface of Al_2O_3.[188] During the preparation of the catalyst, PVP served as a suitable capping and stabilizing agent, which controlled the size and shape of the particle and protected them from aggregating in the system. The microscopy studies revealed that the Ru NPs possessed a spherical shape and uniform in size with an average diameter of 5–6 nm. This Ru(PVP)/c-Al_2O_3 nanocomposite exhibited unprecedented catalytic efficiency towards amine oxidation, yielding 99% of the desired product. Further, the authors also explored the scope and generality of the designed catalytic system by performing the reaction with a wide variety of tertiary amines, resulting in the product in good to excellent yield. Amine-bearing electron-donating groups reacted rapidly and afforded good yields of the corresponding desired product. However, reactants containing electron-withdrawing groups (–COOH, –Br and –CN) deactivated the basicity and nucleophilicity of the amine groups and lower yields were obtained in these cases.

In a recent work, Kidwai and Bhardwaj highlighted the significance of a newly designed heterogeneous nanocrystalline TiO_2 catalyst in the transformation of amines into the corresponding oximes.[189] Notably, the experimental analysis revealed an interesting fact that with only 10 mol% of nano-TiO_2 and 1 mmol of benzylamine, 84% of the desired benzyloxime was produced in a short time of 6 h. The main reason for this marvellous efficacy is accredited to the higher surface area to volume ratio of nano-TiO_2, which offered a larger number of active accessible sites in contrast to the traditional bulk TiO_2. Over the past few decades, substantial progress has been made in designing efficient heterogeneous catalysts exhibiting tremendous potential for oxidation reactions. In this regard, Chu

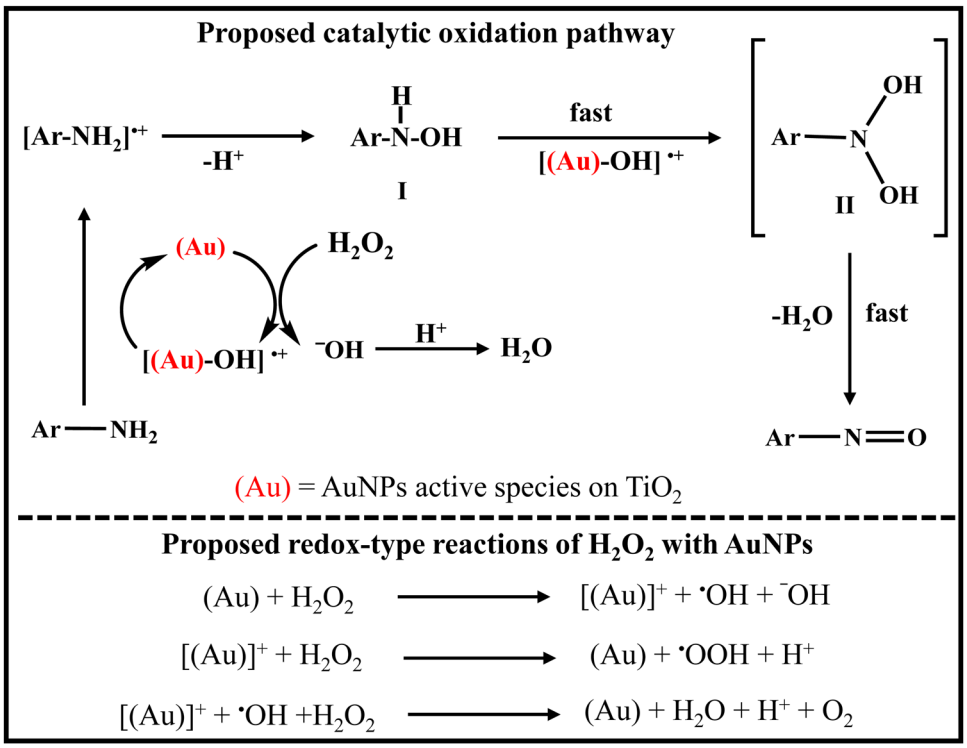

Scheme 10 Schematic description of amine oxidation-catalysed by Au/TiO_2.

and group succeeded in developing a competent catalytic system, wherein the synergistic benefits of V_2O_5 and H_2O_2 were exploited for the oxidation benzyl amine to imines.[190] For this, an adequate amount of V_2O_5 was initially added to a flask containing 1 equivalent of benzyl amine, followed by the addition of 3 equivalent of 30% of H_2O_2 to the above-mentioned reaction mixture and kept under constant stirring for 3.5 h. After completion of reaction, the yellow solid pure crystalline product was obtained, which required no further purification. It is worth mentioning that the nanometer size, smaller pores and abundant active sites were responsible for boosting the catalytic efficacy. One of the fascinating attributes of this protocol is that water was utilized as a green solvent, thereby eliminating the need for harsh organic solvents. Jain *et al.* proposed the idea of fabricating PEG@Fe_3O_4, which was eventually used for the oxidative cyanation of tertiary amines in the presence of H_2O_2.[191] The utilization of PEG proved to be beneficial in the synthesis of the catalyst given that it endowed Fe_3O_4 NPs with high dispersibility and stability. The characterization of the designed nanocomposite was conducted using various physicochemical techniques such as SEM, TEM, XRD, UV-vis-NIR, FTIR, TGA, EDX and BET analysis. The microscopy studies revealed that the catalyst was spherical in nature, having a mean size of 10–25 nm. Due to the unique structural and morphological attributes of the designed PEG@Fe_3O_4, it demonstrated splendid activity towards the oxidation reaction. Besides, due to its magnetic nature, the catalyst was easily retrieved using an external magnet and recyclable for up to six consecutive runs without showing any significant loss in its activity.

Recent advancements in the arena of discrete cubic ferrite spinels have attracted interest from various researchers as suitable support materials in heterogeneous catalytic systems. In this case, Moradi-Shoeili *et al.* delineated the fabrication of metal ferrite nanocrystallites, MFe_2O_4 (M = Mn, Co, Ni, and Zn) through a facile co-precipitation method and utilized them for the oxidation of *o*-phenylenediamine (OPD) to 2,3-diaminophenazine with H_2O_2.[192] Various physico-chemical studies revealed that the synthesized nanomaterials exhibited a spherical morphology with a size in the range of 20–40 nm. Moreover, a series of catalytic control experiments was carried out to obtain the best reaction conditions. According to the thorough assessment of the experimental results, it can be concluded that amongst the synthesized nanocomposites, $MnFe_2O_4$ demonstrated the highest catalytic activity.

Alkane oxidation

The selective conversion of alkanes to more valuable oxidized compounds is one of the most noteworthy transformations employed in industry, which generates countless motifs such as alcohols, aldehydes, and carboxylic acids of fundamental interest. However, the C–H bond is highly inert, and therefore these reactions are carried out under harsh temperature and pressure conditions. Thus, to overcome the problems associated with traditional protocols, chemists are relentlessly working towards developing greener and more sustainable approaches for these reactions. Diverse research groups are actively working in this direction. The idea of designing synergistically coupled tungsten–vanadia oxides (WO_3/V_2O_5) for the

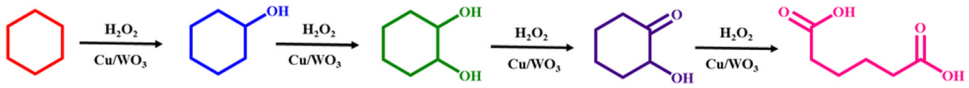

Scheme 11 Mechanistic pathway towards the synthesis of adipic acid catalyzed by Cu/WO_3.

liquid-phase oxidation of cyclohexane was executed well by Makgwane *et al.*[193] On comparing individual oxides, the enhanced catalytic performance of the WO_3/V_2O_5 composites was accredited to the redox and structural modifications. This protocol was found to be green and sustainable given that the reaction proceeded in H_2O_2 at room temperature. Additionally, the nanostructured WO_3/V_2O_5 catalyst exhibited tremendous potential in generating free-radical oxy-functionalization, which afforded 90% conversion in just 6 h. Moreover, the catalytic efficacy of the nanocomposites was efficient after their reused for four cycles. Likewise, Bal and group devoted significant efforts to the synthesis of W(VI) oxide-supported Cu(II) nanoclusters with a size in the range of 35–65 nm.[194] In this report, a promising hydrothermal approach was adopted for the preparation of Cu/WO_3 nanoparticles, which were employed for the oxidation of cyclohexane to form adipic acid under the influence of H_2O_2. A plausible mechanistic route for the concerned reaction is outlined in Scheme 11. Further, the synthesized Cu/WO_3 nanocatalyst presented 88% selectivity towards adipic acid at 70 °C. Besides, the catalyst possessed remarkable reusability for up to four consecutive runs without showing any appreciable loss in its activity.

Further, Bordoloi *et al.* developed a strategy for the facile synthesis of WO_x-SBA-15-based Ag nanoparticles for the direct oxidation of cyclohexane to adipic acid under ambient conditions.[195] In this methodology, both WO_3 and metallic Ag nanoparticles were incorporated in the mesoporous SBA-15 framework, as evidenced by the reduction in its pore size from 1.18 ccg^{-1} to 0.84–1.07 ccg^{-1}. DFT studies revealed that the activation energy decreased to 1.96 eV in the case of Ag–W complex, and thus highlighted the significance of Ag-WO_x-SBA-15 in promoting the selective oxidation of cyclohexanes. The catalyst showed high activity and selectivity in the presence of H_2O_2, which facilitated 89.6% conversion and ≥99% selectivity of adipic acid within a period of 16 h.

In another report, diverse silica-coated magnetite nanoparticle-supported catalysts [Fe_3O_4@SiO_2-M^{2+}, M = Mn^{2+}, Co^{2+}, Cu^{2+} and Zn^{2+}] were synthesized by Martins and co-workers, which were employed in the oxidation of cyclohexane to KA oil using hydrogen peroxide as an oxidant under solvent-free conditions (Scheme 12).[196] It was noteworthy that among the catalytic materials, Fe_3O_4@SiO_2-Mn^{2+} and Fe_3O_4@SiO_2-Cu^{2+} presented highest yield of oxygenated products (cyclohexanone and cyclohexanol, 24% and 21%, respectively) after 2 h of reaction at 80 °C. This protocol employed economically viable catalysts given that Fe_3O_4@SiO_2-M^{2+} could be isolated from the reaction media with the aid of a readily available external magnet and efficiently reused for five successive runs with no appreciable loss in activity. Simple work-up procedure, cost-effective metal precursors, solvent-free approach and use of microwave irradiation for heating the reaction mixture are the additional salient features of this methodology, making this protocol sustainable and worthwhile.

One year later, Crombie and co-workers adopted an economically favourable route for the production of cyclohexane and cyclohexanol (KA oil) catalyzed by bi-functional Pd-based catalyst *via* the *in situ* generation of H_2O_2 from molecular H_2 and O_2.[197] It was observed that the concentration of KA oil was improved by incorporating V in a Pd-supported catalyst. Besides, the *in situ*-produced H_2O_2 has immense benefits over the commercially utilized H_2O_2 given that it involves lower reaction temperatures.

To date, the oxidation of toluene is a challenge for researchers given that the available methods generate toxic chlorinated by-products, which are harmful to the environment. In this regard, Altaf *et al.* adopted an alternative greener and chlorine-free pathway to oxidize toluene to benzaldehyde and benzyl alcohol in the presence of $MnMoO_4$ as catalytic entity and H_2O_2 as the oxidant at 80 °C.[198] Here, the $MnMoO_4$ nanocatalyst was synthesized *via* the solvothermal approach (Scheme 13), which was then exploited in the oxidation of toluene *via* C–H activation and it was observed that 40.62% of toluene was converted to the desired products after 18 h of reaction using 0.06 g of catalyst. The high conversion percentage of toluene and efficient selectivity towards benzaldehyde and benzyl alcohol highlighted the remarkable catalytic performance of $MnMoO_4$ under mild reaction conditions. In addition, the catalyst could be efficiently reused for six cycles to transform toluene to the desired products with turnover frequencies in the range of 1.94–1.01 s^{-1}.

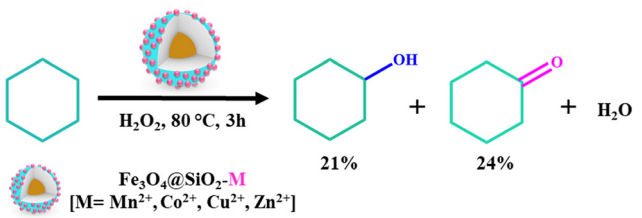

Scheme 12 Schematic representation of oxidation of cyclohexane.

Oxidation of alkenes

The oxidation of alkenes has acquired significance in the field of organic synthesis given that this oxidative transformation allows the conversion of carbon–carbon double (C=C) bonds into carbon oxygen (C–O) bonds, leading to the synthesis of valuable oxygen-containing chemicals (mostly alcohols or epoxides), which have widespread utility in the chemical sector. It is well known that oxidation can be used for versatile applications including epoxidation, dihydroxylation and carboxylation.

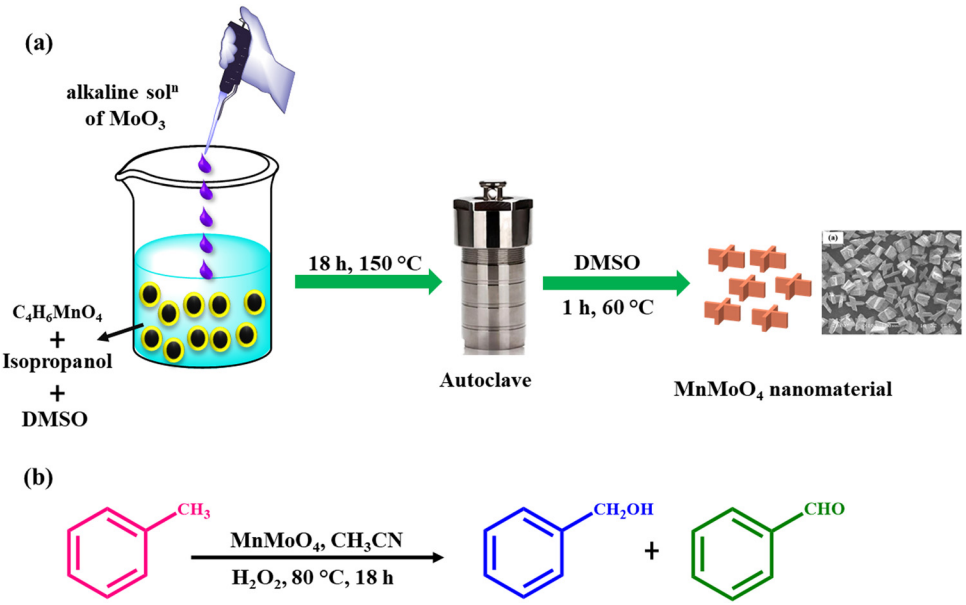

Scheme 13 (a) Illustration depicting the fabrication of $MnMoO_4$-based nanomaterial and (b) catalytic application of developed $MnMoO_4$-based nanomaterial in the oxidation of toluene.

However, traditional oxidation methods employ $KMnO_4$ or other oxidizing agents such as OsO_4–$NaIO_4$, which do not comply with the principles of green and sustainable synthesis given that they lead to the generation of toxic by-products. Thus, the search for highly active and selective catalysts that can help in fulfilling the desirable attributes of sustainable catalytic oxidation is ongoing.

Inspired by the prospects offered by H_2O_2-mediated oxidations, Tong and co-workers designed hollow spheres of Mg–Cu ferrite ($Mg_{0.5}Cu_{0.5}$ Fe_2O_4) using carbon spheres as the template with the aid of a combination of approaches including sol–gel autocombustion, hydrothermal synthesis and co-precipitation for achieving the oxidation of styrene in the presence of H_2O_2 as the oxidant.[199] For the preparation of the catalyst, the metal ions were first adsorbed on the surface of carbon spheres, and subsequently the carbon cores were eliminated *via* calcination in air, which resulted in the formation of the expected hollow spheres (Fig. 8). The hollow structure endowed the resultant material with a high surface area, as evidenced through BET analysis, and consequently enhanced catalytic activity (in terms of high turnover number and selectivity up to 75.2% for benzaldehyde). Additionally, the catalyst offered advantages of facile separation and remarkable reusability for up to six consecutive runs.

On similar grounds, Rayati and co-researchers developed metalloporphyrin-based magnetic nanocatalysts comprised of *meso*-tetrakis(4-carboxyphenyl) porphyrinatoiron(III) chloride (Fe(TCPP)Cl) and *meso*-tetrakis(4-carboxyphenyl) porphyrinatomanganese(III) acetate (Mn(TCPP)OAc) discretely immobilized on an amine-functionalized silica-coated magnetite support (ASMNPs), as depicted in Scheme 14.[200] The catalyst worked exceptionally well in oxidizing a wide range of alkenes with 100% conversion and 100% selectivity. The strategic design involved the basic principles of co-ordination chemistry, wherein metal–ligand complexes are usually tethered on the surface of a support material *via* co-ordinate/covalent linkages, which is named "covalent immobilization" and remains the preferred choice in the design of catalysts given that it avoids the problems associated with leaching typically encountered in the case of supports comprised of dispersed/physically adsorbed metal species. The durability of the catalyst was proven through a leaching test, and the results indicated that negligible leaching occurred, as evidenced through AAS. Thus, undeniably, the stability of the metalloporphyrins can be improved by immobilizing them on a support material.

Working along similar lines, Afshari *et al.* synthesized a cobalt salophen complex, which was supported on the surface of imidazole-functionalized magnetic nanoparticles (MNPs), and then utilized for the oxidation of alkenes (Scheme 15).[201] A cobalt-based complex was targeted as the transition metal active complex owing to the ability of Co(II) to act a good oxygen transfer reagent, while MNPs as the core material not only offered facile catalytic separation but also displayed the added benefits of a high specific surface area together with the ability to avoid pore diffusion by allowing the catalytically active species to be distributed on only their outer surface. In the typical list of MNPs, spinel ferrite $CoFe_2O_4$ NPs were chosen because of their high magnetic anisotropy, notable magnetic saturation and outstanding chemical stability. The cobalt ferrite NPs were imparted special stability *via* encapsulation in a silica shell, besides acting as a good coating agent, also offered further prospects of surface functionalization owing to the presence of surface silanol groups, which were covalently tethered with a functionalizing agent/linker. An illustration of the catalyst preparation is provided in Scheme 11. The TEM micrograph revealed that the NPs were spherical in shape and

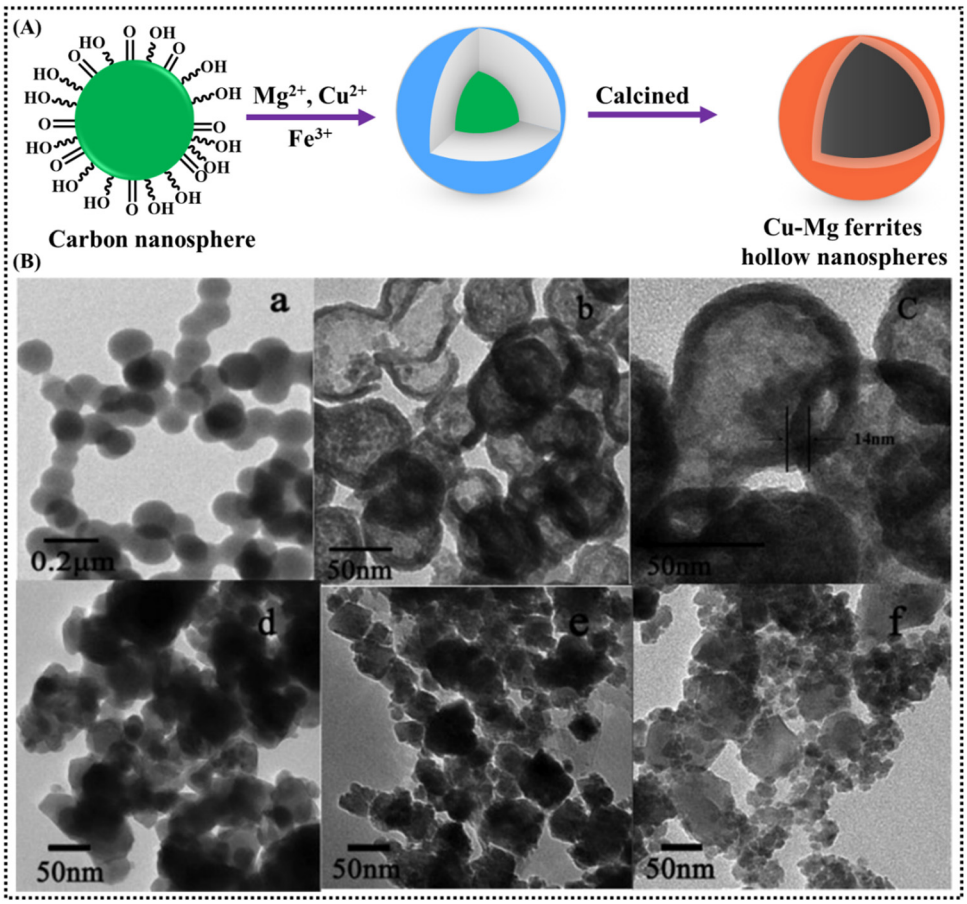

Fig. 8 (A) Schematic illustration of the preparation of Cu–Mg ferrite hollow nanospheres and (B) TEM images of (a) carbon spheres; (b and c) MCFO-1; (d) MCFO-2; (e) MCFO-3; and (f) MCFO-4 (MCFO-1 are $Mg_{0.5}Cu_{0.5}Fe_2O_4$ ferrite hollow spheres, while MCFO-2, MCFO-3 and MCFO-4 are $Mg_{0.5}Cu_{0.5}Fe_2O_4$ ferrite nanopowder synthesized *via* sol–gel auto-combustion, hydrothermal and co-precipitation route). Reproduced with permission from ref. 199. Copyright 2014, Elsevier B.V.

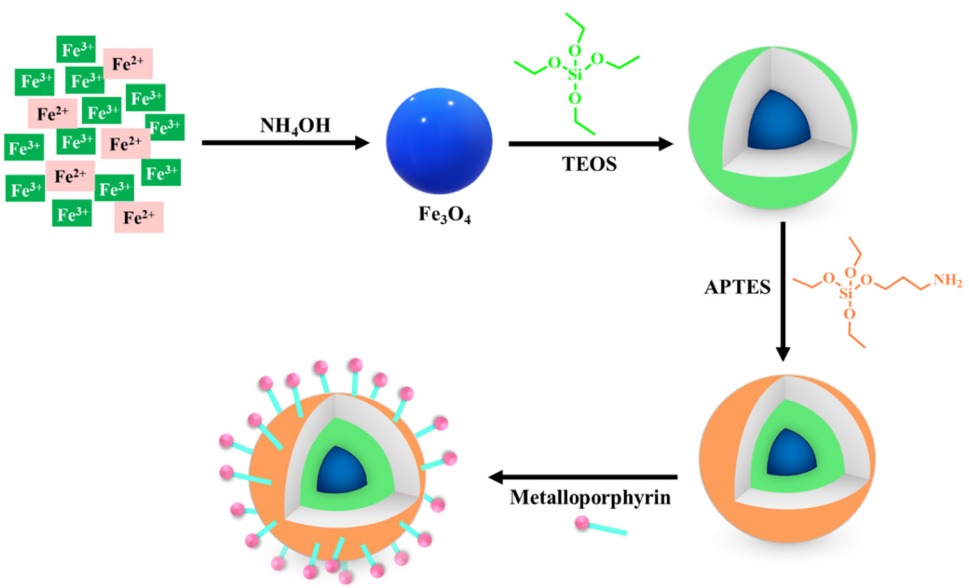

Scheme 14 Synthesis of magnetic nanocatalyst.

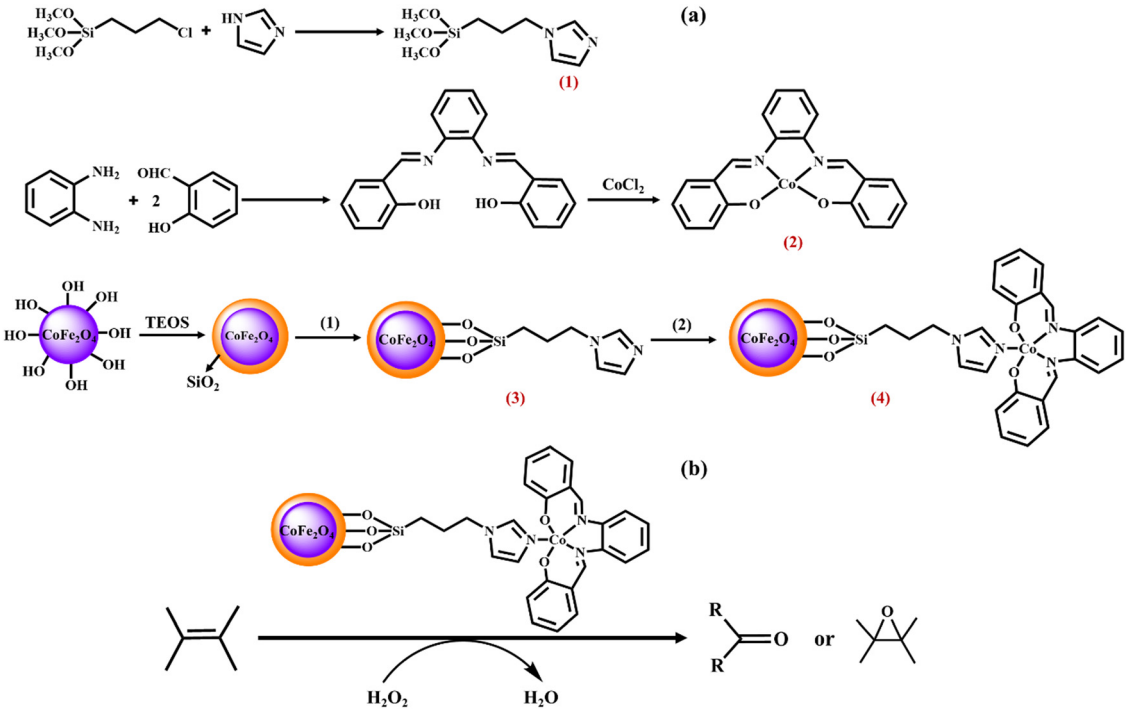

Scheme 15 (a) Schematic representation of the formation of Co(salophen)-imid-Si@Si-MNP catalyst and (b) its application in catalyzing the oxidation of alkenes.

possessed a size of less than 30 nm. The as-synthesized Co(salophen)-imid-Si@Si-MNPs (0.1 g) exhibited excellent efficiency in catalyzing the oxidation of alkenes (α-methylstyrene,4-methoxystyrene,4-methylstyrene,4-nitrostyrene,cyclohexene and 1-octene) using aqueous 30% H_2O_2, offering yields of up to 95% and recyclability in up to five continual runs.

Similarly, using the covalent immobilization approach, a transition metal complex (Mn Schiff base) was supported on different SiO_2 nanomatrices (MCM-41, SBA-15 and carbon nanomaterials, *i.e.*, CMK-3), leading to the formation of L@MCM-41-Mn_{II}, L@SBA-15-Mn_{II} and L@CMK-3-Mn_{II} for expediting the alkene epoxidation by Mavrogiorgou *et al.*[202] Two different strategies were adopted for the general synthesis of the catalysts, involving two steps (ligand grafting and metalation and single-step method (ligand grafting and metalation accomplished in one-pot in one step (Scheme 16).

As highlighted in Scheme 17, demonstrating the synthesis of a CMK-3-supported Schiff base complex, a one-step covalent grafting methodology was adopted to obtain the desired catalyst. The resulting single-site heterogeneous catalysts exhibited excellent activity and selectivity in the formation of epoxides with the aid of H_2O_2 as the oxidant source and CH_3COONH_4 as the additive. In fact, the highest turnover frequency (TOF) of 634 h^{-1} was achieved with L@MCM-41-Mn_{II} and Mn_{II}-L@CMK-3 (Fig. 9).

Lashanizadegan and team reported the preparation of a silica-coated magnetite (SiO_s@Fe_3O_4 NP)-supported Cu(II) Schiff base complex (Scheme 18), which showed excellent efficiency for catalyzing the oxidation of diverse olefins (especially styrene and norbornene with 100% and 79% conversion, respectively).[203] The average size of the nanoparticles, as evidenced through SEM and TEM, was found to be 27.35 nm. The striking attributes of this catalytic protocol included the use of a greener oxidant, shorter reaction time, good reusability of the catalyst, high conversion and decent selectivity.

Impressed by the high catalytic activity of surface-engineered $CoFe_2O_4$ NPs in the oxidation of alkenes, Liu *et al.* developed a magnetically separable yolk shell-structured $CoFe_2O_4$@hollow@mesoporous TiO_2, and subsequently utilized it for the selective oxidation of styrenes (Scheme 19).[138] The catalyst was prepared in a stepwise manner beginning from the synthesis of $CoFe_2O_4$ nanoparticles *via* a facile co-precipitation technique, followed by the coating of these NPs with silica using a modified Stober's method. The next step involved the introduction of a TiO_2 layer using titanium tetra-isopropanolate as the precursor, and finally etching of the intermediate silica layer.

Thus far, the spinel ferrites fabricated for the purpose of oxidizing alkenes saw a new interesting addition with the design and development of rare earth Ce and Nd''-doped spinel nickel ferrite (Ce–$NiFe_2O_4$ and Nd–$NiFe_2O_4$, respectively) *via* a sol–gel synthetic route.[204] The route for the preparation of the $NiFe_2O_4$ NPs involved the dissolution of stoichiometric amounts of iron nitrate and nickel nitrate hexahydrate in water, followed by stirring at r.t., to which specific amounts of tartaric acid and polyethylene glycol (PEG) were added and the obtained sol was subjected to heating at 70 °C. For the synthesis of the Ce- and Nd-doped NPs, a similar strategy was adopted with the addition of $Ce(NO_3)_3{\cdot}6H_2O$/$Nd(NO_3)_3{\cdot}6H_2O$, respectively. The size of the bare and doped NPs was found to

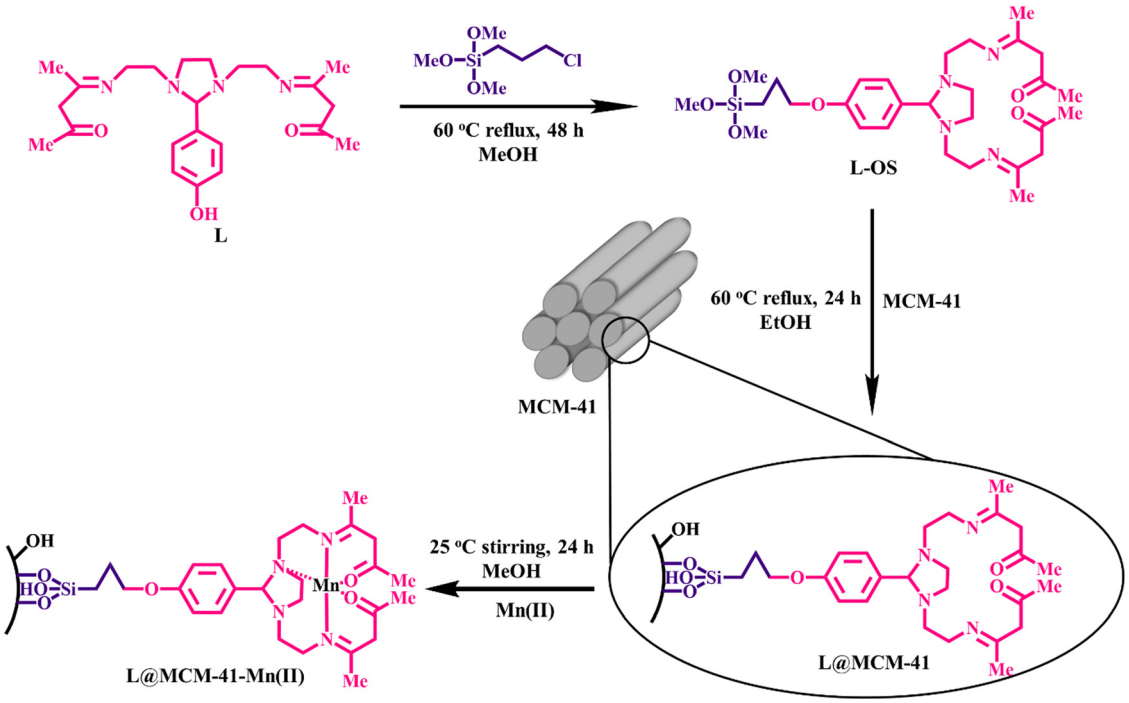

Scheme 16 Schematic representation of the L@MCM-41-MnII heterogeneous catalyst.

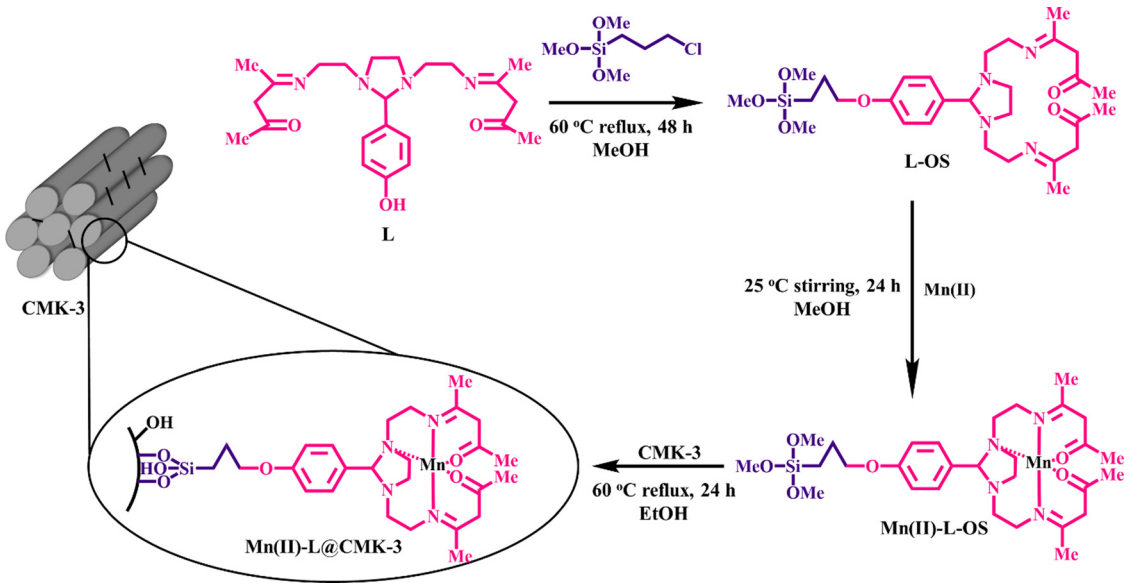

Scheme 17 Schematic representation of the preparation of the MnII-L@CMK-3 heterogeneous catalyst.

be in the range of 7–10 nm. Although the catalysts showed good conversion and selectivity in the presence of H_2O_2, TBHP could also be employed as the oxidant in the case of some of the substrates.

Lately, earth abundant metals have witnessed a radical revolution in the field of catalysis science and technology with their ability to replace the precious and toxic metals that were employed for catalyzing a number of important transformations for decades. Amongst the various earth abundant-based metal oxides synthesized thus far, MnO has seen expansive interest in its utility. One example was provided by Najafpour *et al.*, where they synthesized nano-sized MnO using an aqueous solution of manganese nitrate and stirring it, followed by heating at 100 °C, which could achieve the epoxidation of both aromatic and non-aromatic olefins, displaying both selectivity and conversion up to 100%.[205] Subsequently,

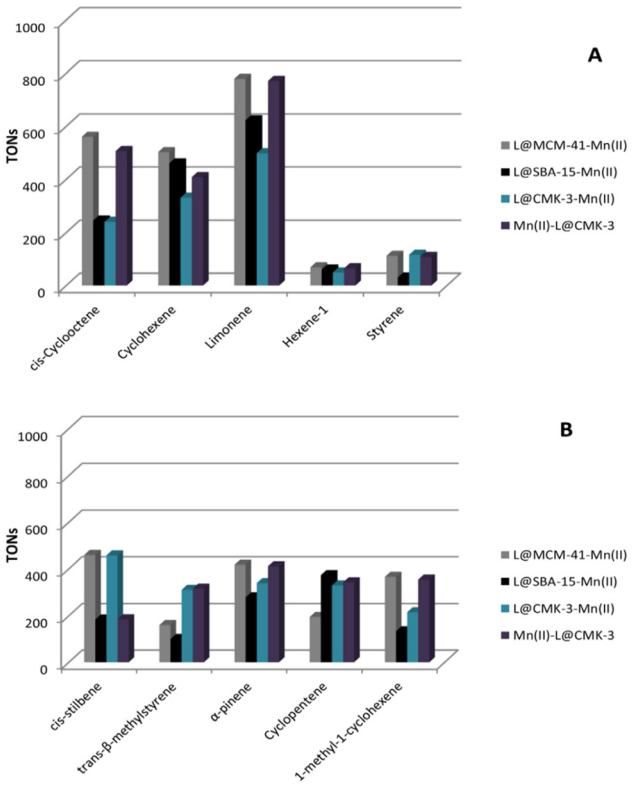

Fig. 9 (A and B) TOFs for alkene epoxidation catalyzed by L@MCM-41-MnII, L@SBA-15-MnII, L@CMK-3-MnII and MnII-L@CMK-3 in the presence of H_2O_2. Conditions: [catalyst : H_2O_2 : CH_3COONH_4 : substrate] = [1 : 2000 : 1000 : 1000]; catalyst = 1 mol in 0.85 mL CH_3COCH_3 : CH_3OH (0.45 : 0.40). Reproduced with permission from ref. 202. Copyright 2016, Elsevier B.V.

the same team of researchers deposited nano-sized gold and silver on the surface of the active MnO layer and succeeded in obtaining enhanced catalytic activity of MnO towards the epoxidation of olefins using H_2O_2 and $NaHCO_3$.[206] Mechanistically, the catalyst worked by co-ordination of HCO_4^- to Mn present on the surface of MnO, followed by the transfer of an oxygen atom from the intermediate to olefin, which generated the epoxide.

Ghosh *et al.* designed a nanostructured silver-supported tungsten oxide (WO_3) catalyst, which was comprised of metallic Ag NPs with a size of approx. 5 nm, which were supported on WO_3 nanorods possessing a diameter in the range of 40–60 nm.[207] The HR-TEM image of the catalyst demonstrated the one-dimensional rod-like morphology of WO_3, which possessed an average width of ~50 nm with uniformly dispersed silver particles having an average size of nearly ~5 nm. This supported nanocatalyst effectively catalyzed the oxidation of cyclohexene to form adipic acid with a conversion of >99%, approx. 94% selectivity and notable TOF value of 12 h^{-1}. The synthesis of adipic acid was attempted primarily considering its significance in the manufacture of a wide range of industrial products including nylon 6,6 plasticizers.

Tuning the morphology of a nanosized material using controlled synthetic pathways can result in tremendous boosting of its catalytic activity in oxidative transformations, which was proven by Sun and co-workers.[208] By making proficient use of the sol–gel methodology, this team of researchers smartly designed titanium–zirconium mixed oxide spheres and titanium oxide cubes, which worked exceptionally well in the oxidation of alkenes. The focus of the synthesis was to design a material that possesses a new texture, which was achieved *via* the doping of either zirconium or L(+) or (−) sodium tartarate in a sol–gel. The Kirkendall effect was exploited in this process, which brought about a different texture as a result in the difference in the rate of diffusion of zirconium and titanium. The alternative use of tartarate was to induce chirality and bring about modification in the structure. Consequently, the catalytic oxidation of R(+) limonene could be carried out with

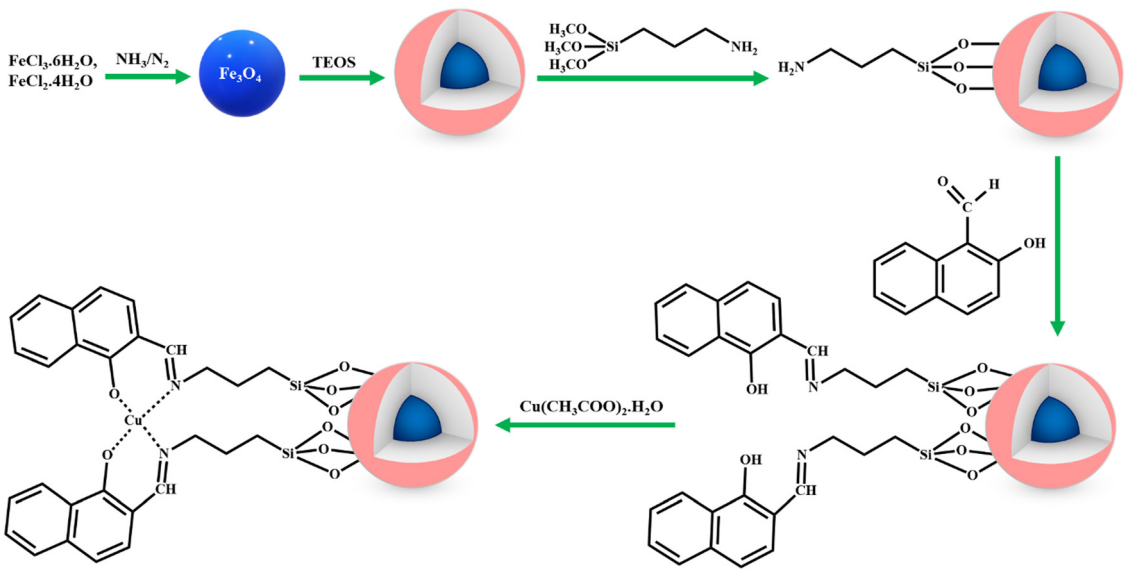

Scheme 18 Preparation of Fe_3O_4@SiO_2/Schiff base/Cu nanocatalyst.

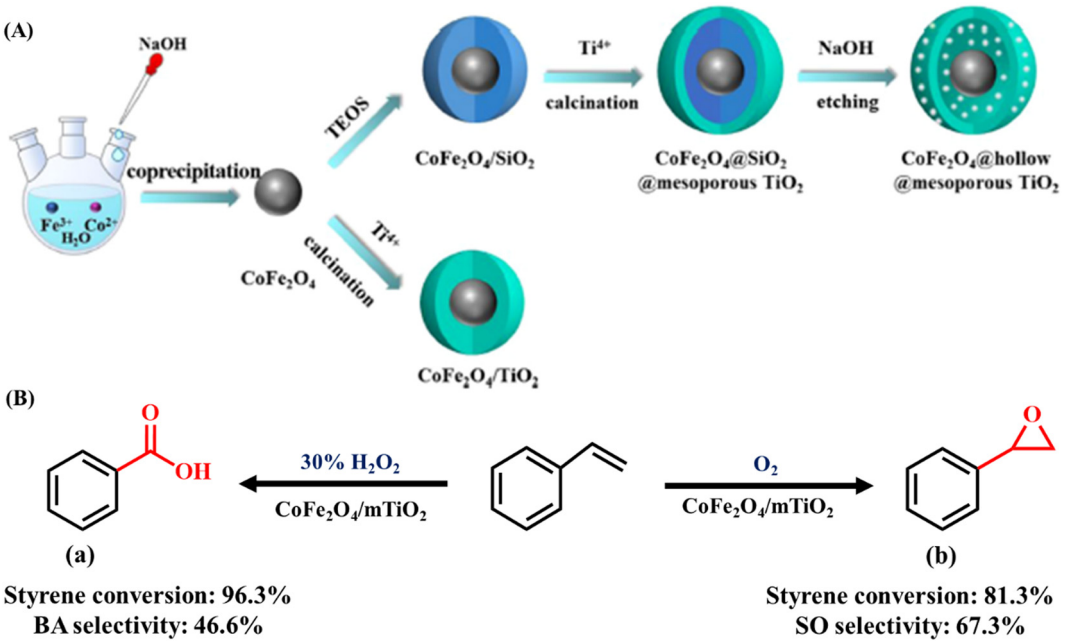

Scheme 19 (A) Procedure for the synthesis of $CoFe_2O_4$@hollow@mesoporous TiO_2 yolk–shell structure and $CoFe_2O_4/TiO_2$ core–shell structure and (B) application in styrene conversion. Reproduced with permission from ref. 138. Copyright 2020, the American Chemical Society.

good efficiency using H_2O_2 as the oxidant and 2 mol% of the Ti catalyst, showing up to 45% conversion, whereas the oxidative transformation of (−)-α-pinene could be accomplished with 100% conversion using a combination of the Ti catalyst (TIS) and H_2O_2 with higher diastereoselectivity of epoxide.

To achieve high selectivity of oxygenated products, tailoring the surface properties of catalysts by controlling their morphology has emerged as a rational solution, as already discussed in the example above. Likewise, Paul *et al.* also utilized a similar concept of structure-guided/morphology controlled catalytic activity and designed highly competent and robust 3-D octahedron $NiCo_2O_4$ spinel NPs using a one-pot poly(vinylpyrrolidone)-assisted hydrothermal route, which could successfully convert styrene into styrene oxide with 67% selectivity with the use of H_2O_2 as the oxidizing agent.[209] The nanoparticles possessed a truncated octahedron shape with uniform size in the range of 20–30 nm, as indicated by the SEM micrograph. Furthermore, evidence of the existence of the $NiCo_2O_4$ spinel NPs in a pure phase was attained by EXAFS analysis. Additionally, the true heterogeneous nature of the catalyst was experimentally examined and proven by Sheldon's hot filtration test.

Another interesting example of improving the catalytic performance in styrene oxidation through morphology control was provided by Wang *et al.*, where they designed supported cobalt oxide nanoparticles using a simple hydrothermal methodology.[210] The morphology of the catalysts could be tuned by changing the synthetic process parameters such as time and temperature and the catalytic activity showed a significant difference with a change in the catalysts. As revealed by the SEM images displayed in Fig. 10, the silica-supported cobalt nanospheres possessed a mean diameter of 200 nm, which maintained their morphology even after calcination at 150 °C. With a increase rise in the calcination temperature to about 550 °C, the integrity of the nanostructure remained intact. However, calcination at 650 °C resulted in the formation of an egg-yolk structure (comprised of bundles of nanocrystals with structure confined by supported silica channels). Amongst the catalysts, Co_3O_4-550 showed the highest activity and selectivity to generate the desired epoxide (Table 4).

The objective of achieving unprecedented selectivity for the oxidation of styrene and its derivatives was also fulfilled by Rajabi and co-workers, who developed iron oxide NPs and supported them on a mesoporous aluminosilicate matrix.[211] The catalyst was prepared by functionalizing SBA-15 with aminopropyl motifs to acquire NH_2-functionalized SBA-15 and the ensuing step involved the deposition of iron oxide NPs, which was done using iron(III) nitrate nonahydrate as the precursor. The desirable feature of this catalytic protocol is that with the use of only 0.5 mol% of the active catalyst, remarkable yields of the targeted aldehyde products (>90%) and an exceptionally high oxidant efficiency (>95%) could be obtained. The supported catalyst showed good proficiency in its recovery, reuse as well as stability, showing no metal leaching.

In the quest to design a new promising class of transition metal-free oxide-based catalysts for the epoxidation of alkenes, Lueangchaichaweng along and team developed gallium oxide nanoparticles, which were embedded and stabilized in a mesoporous silica matrix.[212] By fabricating the silica-supported gallium oxide NPs, they combined the intrinsic advantages of the high surface area to volume ratio of the nanoparticles and the defined pore size aspects of the mesoporous matrix material. Typically, the synthesis of the Ga_2O_3 NPs was conducted by the dissolution of gallium trichloride in a mixture of ethylene–glycol water, followed by the dropwise addition of NaOH, and

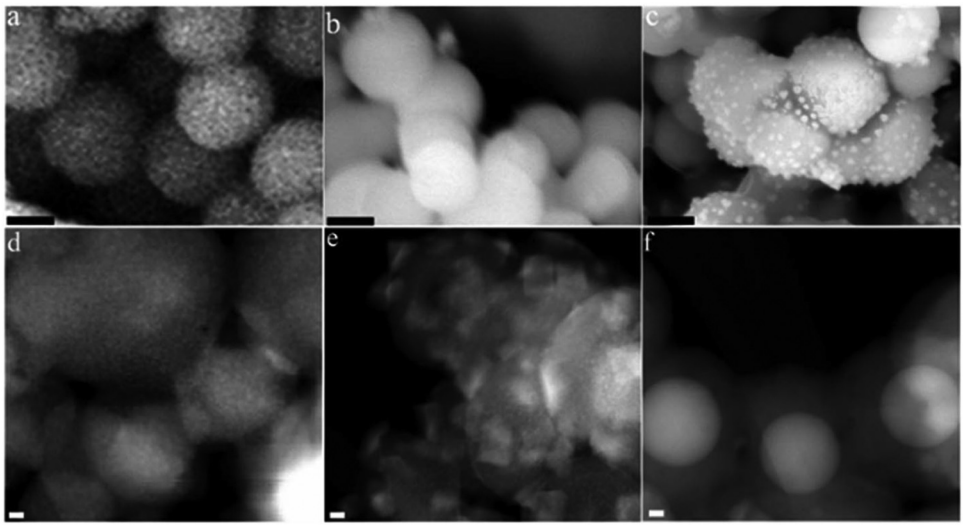

Fig. 10 SEM images of (a) cobalt nanospheres before calcination, (b) Co_3O_4-150, and (c) Co_3O_4-550. STEM images (d) Co_3O_4-150, (e) Co_3O_4-550 and (f) Co_3O_4-650. Reproduced with permission from ref. 210. Copyright 2016, The Royal Society of Chemistry.

Table 4 Selective oxidation of styrene on supported cobalt oxide catalysts[a]

Particle size calculated from XRD					Selectivity (%)				
Catalyst	[Co][b] (wt%)	Before reaction	After reaction	Conv. (%)	Styrene epoxide	Benzaldehyde	Other product	TOF[c]	BET ($m^2\ g^{-1}$)
Co_3O_4-150	9.1	N/A[d]>	N/A[d]	12	80	15	5	3.3	15
Co_3O_4-550	8.4	11	12	97	91	5	4	28.3	46
Co_3O_4-650	8.1	70	73	27	96	2	2	8.2	42

[a] Reaction conditions: catalyst weight = 30 mg. [b] Determined by ICP-AES. [c] mol (C_8H_8 converted) mol(Co)$^{-1}$ h^{-1}. [d] The peak is too weak to do the calculation from the X-ray line broadening.

after continuous stirring the contents were transferred to an autoclave. Thereafter, a series of mpGa_2O_3-*x* gallia/silica composites was prepared using a liquid-handling robotic workstation (programmed by Gemini software). For the preparation of the mesoporous silica-supported NPs, the templating solution was prepared *via* the addition of CTAB (a structure-directing reagent) to a mixture of water and ammonium hydroxide, followed by the stirring of the reaction contents in a closed bottle. In the following step, a suspension of Ga_2O_3 NPs in ethanol was prepared, which was subjected to ultrasonic irradiation for about 30 min, and subsequently stirred for some more time with the addition of tetraethyl orthosilicate (TEOS). The morphological analysis of the prepared material using TEM revealed that the Ga_2O_3 NPs possessed a narrow size distribution ranging between 1.5 to 3.0 nm (Fig. 11). Amongst the library of mesoporous composites synthesized, that containing 80% and 90% of gallium oxide nanoparticles rendered the best catalytic performance in terms of activity and selectivity (>99%) (Table 5).

Polyoxometalates (POMs), as a class of celebrated transition metal oxygen clusters, have also received wide acceptance in the field of catalysis, and particularly proven promising for the

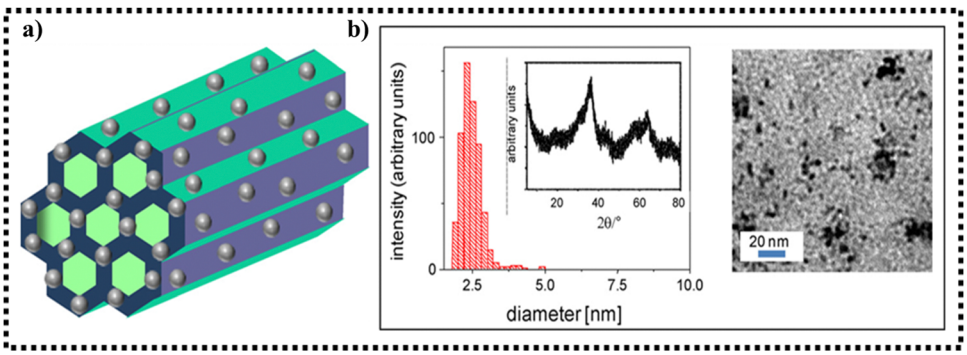

Fig. 11 (a) Mesoporous composites of gallium oxide nanoparticles and silica. (b) Characterisation of Ga_2O_3-NP by DLS (left), wide-angle XRD (insert) and TEM (right). Reproduced with permission from ref. 212. Copyright 2013, Elsevier B.V.

Table 5 Catalytic activity of $mpGa_2O_3$-80 in the epoxidation of different alkenes with aqueous H_2O_2

Entry	Alkene	Reaction time (h)	Temperature (°C)	Epoxide yield (%)	Epoxide selectivity (%)
1	Cyclooctene	4	80	25	>99
2	Cyclooctene	6	80	34	>99
3	Cyclohexene	6	70	10	90
4	1-Octene	6	80	10	91
5	Styrene	4	80	7	49
6	Styrene	6	80	10	50

H_2O_2-based epoxidation of olefins. However, the recovery of homogeneous POMs remains a challenge for scientists, thus witnessing an increase in the design of recoverable POMs, wherein a recoverable support matrix is chosen for the purpose of attaching the POMs. However, despite the attempts to engineer POMs through their immobilization on diverse support materials, and their subsequent use for the oxidation of alkenes, their low reaction rates, poor catalyst recovery ratio and leaching of the active catalytic species hinder their large-scale industrial applicability. Moreover, the epoxidation of bio-derived olefins, which form important vegetable oils using supported catalysts, has also been rarely attempted owing to the high viscosity and hydrophobicity associated with these type of olefins, which prevent the efficient mass transfer in the liquid–solid biphasic reaction medium. With the aim to overcome the shortcomings associated with supported POMs and considering the need to develop competent catalysts for the preparation of bio-derived olefins, the synthesis of an amphiphilic composite comprised of a magnetic core in addition to a dodecyl amine-modified polyoxometalate-paired poly-(ionic liquid) shell (Fe@PILPW-AM) was reported by Leng *et al.*[213] The steps involved in the synthesis of the catalyst are depicted in Scheme 20. This catalyst could catalyse the epoxidation of bioderived olefins in the presence of H_2O_2 with extraordinarily high conversion and selectivity. The high activity of Fe@PILPW-AM was attributed to its amphiphilic nature and the possible intramolecular charge transfer between the poly-anion (PILPW) and the amino group.

Oxidation of arenes

The production of high-value-added commodity chemicals at the industrial and laboratory scaled is a rapidly growing field of chemistry. Owing to the increasing demand for pharmaceuticals, perfumery, agrochemicals and clean technologies, the synthesis of resins, alcohols, esters and aldehydes is gaining considerable attention. Nevertheless, the direct synthesis of many of them is restricted due to the cumbersome work-up procedures, generation of by-products and use of toxic and expensive reagents. Thus, to overcome aforesaid issues and satisfy the economic and environmental requirements, the design and fabrication of recyclable, efficient, easily separable metal oxide-based heterogeneous catalysts has become one of the most active areas of research. In this regard, several efforts have been dedicated to catalysing the oxidation of arenes under mild conditions, which are summarized below.

Arab and team prepared Fe_3O_4 supported on nanoporous carbon (Fe_3O_4/CMK-3) *via* the impregnation route, which was subsequently used for the oxidation of benzene to phenol.[214] The superior activity and high selectivity of the developed catalyst were attributed to the generation of Fe_3O_4 on CMK-3 and uptake of excess hydroxyl radicals by CMK-3, respectively. Interestingly, the defect sites in CMK-3 were primarily responsible for the exceptional activity of the catalyst. The effect of different variables such as temperature, volume of H_2O_2, catalyst dosage and reaction time on the performance of the catalyst was scrutinized. In this direct hydroxylation process, 18% conversion with 92% phenol selectivity and 8.7 h^{-1} TOF was observed. The recyclability of the synthesized material was also analyzed, which indicated a slight decrease in its catalytic activity after completion of four runs.

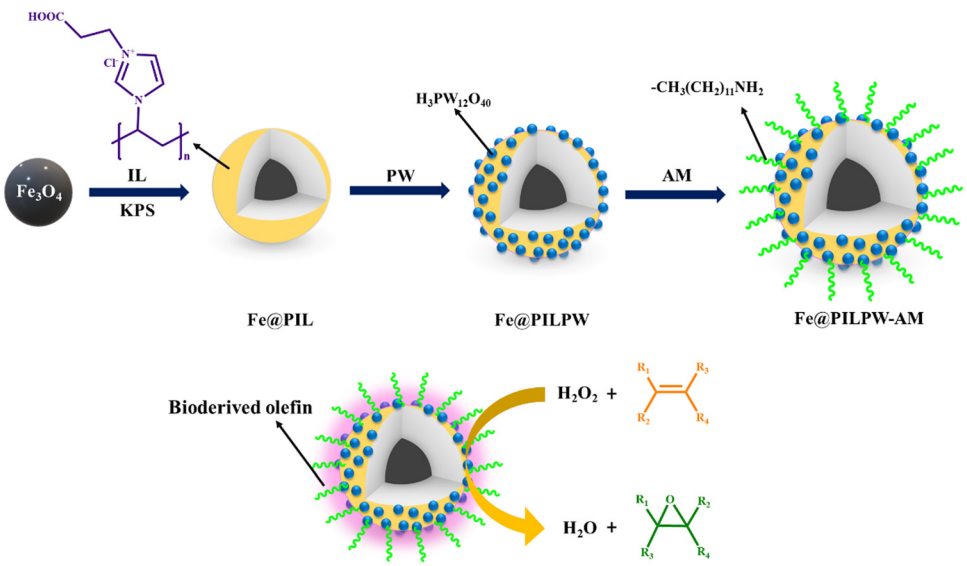

Scheme 20 Synthetic methodology for obtaining the Fe@PILPW-AM catalyst.

Inspired by the versatility of bimetallic metal oxides, Acharyya and coworkers reported a facile hydrothermal, green and economical viable protocol to develop $CuCr_2O_4$ spinel NPs with an average size of 20–50 nm and applied them in the one-pot hydroxylation of benzene.[215] The tetragonally distorted normal spinel structure and presence of copper in these NPs make them highly active for the selective oxidation of arenes. Investigations on temperature, reaction time, substrate to oxidant ratio, and solvent were carried out to ascertain the best outcomes. The reusability of the catalyst was also analyzed, which evinced that it could be recycled for more than 5 runs without any significant loss in its performance. These heterogeneous oxide NPs converted 72.5% benzene to the anticipated product with 94% selectivity at 80 °C and have potential to be explored for large-scale applications.

Moreover, considering the potential of three-dimensional (3D) nanoarchitectures in catalysis and extending their research work, this group designed raspberry-like $CuCr_2O_4$ spinel NPs *via* the hydrothermal route using cetyltrimethylammonium bromide (CTAB) as a cationic surfactant in a simple, low temperature and water-based pathway.[216] The evolution of the desired morphology involved two stages, in which initially the NPs were produced, and then they self-assembled. Their unique surface properties and other features were thoroughly characterized using different physicochemical techniques, which suggested that the spinel phase was comprised of nanoparticles with a size in the range of 20 to 50 nm (Fig. 12). In the presence of H_2O_2, these raspberry-shape structures demonstrated remarkable catalytic activity at 80 °C for the oxidation of benzene to phenol with 68.5% conversion and 95% phenol selectivity. Further, no leaching was observed for up to 10 successive cycles, confirming the true heterogeneous nature of this 3D material.

Proceeding on the same track, another methodology was described by Acharyya and team to generate spherical spinel $CuCr_2O_4$ NPs, wherein cetyl alcohol was employed as a soft template to form spinel structures.[217] Here, the cationic surfactant served as a growth promoter and modifier, which controlled the particle size of the copper chromite NPs. The diameter of the NPs was found to be in the range of 20 to 40 nm. The studies illustrated that these nanostructures not only catalyzed the selective hydroxylation of benzene but also of other aromatic alkanes. With 67% conversion and 94% phenol selectivity at 75 °C, benzene was converted into phenol. The catalyst could be reused for more than five consecutive runs owing to its good stability and recyclability, thus making it a promising candidate for industrial purposes.

Considering the benefits of mixed nanostructured metal oxides, Makgwane and Ray fabricated a highly efficient and magnetically responsive copper–iron oxide (Cu–Fe) catalyst and successfully utilized it for the hydroxylation of benzene to phenol under benign reaction conditions.[218] Their studies revealed that compared to the corresponding single nano metal oxide, the mixed binary catalyst displayed better activity and excellent performance. Various parameters such as solvent, reaction temperature, duration and amount of H_2O_2 were optimized to achieve the best results. It was also observed that the calcination temperature during the synthesis of the desired nanomaterial also a played a critical role in enhancing the activity of the catalyst. Calcination at 400 °C induced structural phase and redox transformations in the mixed CuFe catalyst, and consequently it efficaciously oxidized benzene to phenol with 44% conversion and 91% phenol selectivity in a sustainable manner.

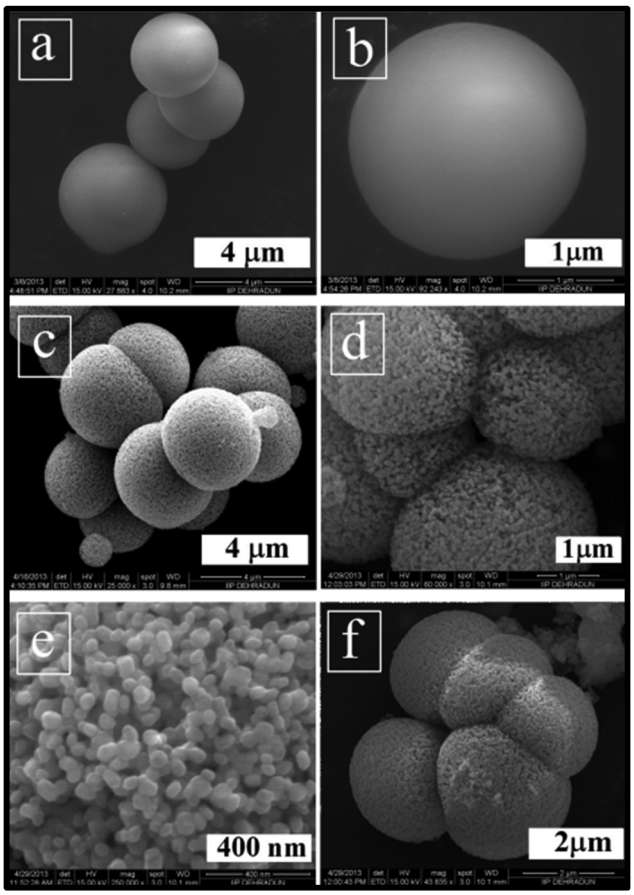

Fig. 12 SEM images of (a and b) uncalcined and (c–e) calcined $CuCr_2O_4$ raspberry-like fresh and (f) spent catalyst (after 10 recycles). Reproduced with permission from ref. 216. Copyright 2014, the American Chemical Society.

On similar grounds, a novel and cost-effective method was adopted to synthesize nano Ag/ZnO using $Zn(NO_3)_2{\cdot}6H_2O$, $AgNO_3$ and urea.[219] The loading of Ag on ZnO was calculated by inductively coupled plasma (ICP) spectroscopy. Experimental exploration revealed that the ZnO-supported sliver proficiently catalyzed the oxidation of arenes with the aid of H_2O_2 under solvent-free conditions. The Ag-doped ZnO catalyst actively participated in the reaction, facilitated the oxidation of benzylic C–H bonds and gave the products in good to excellent yields.

Considering the benefits associated with vanadium-based materials, which are commonly known for their highly efficient oxidation of inert hydrocarbons, Wanna *et al.* delineated the fabrication of vanadium nanorods (V_{nr}) by using VCl_3,

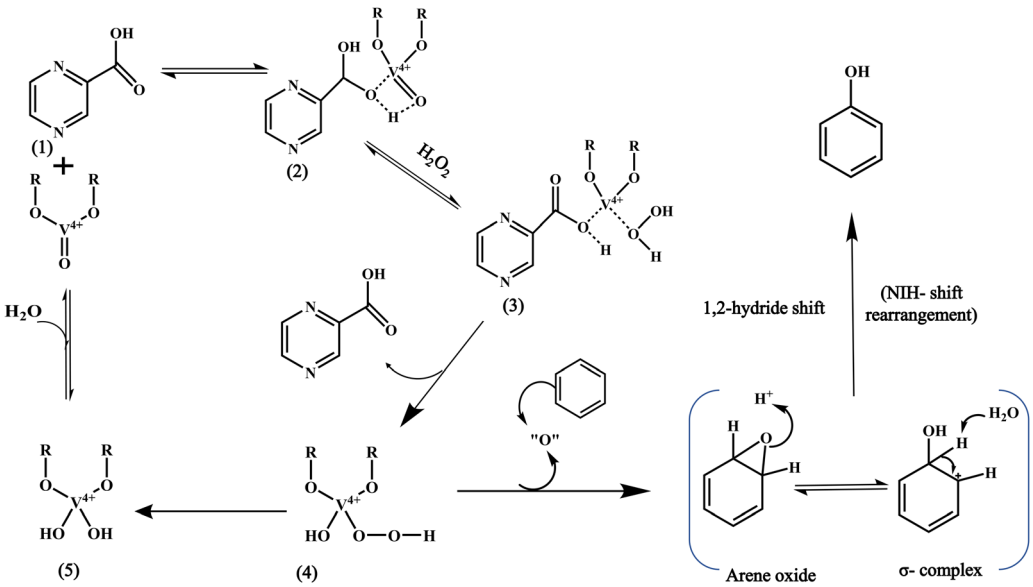

Scheme 21 Proposed reaction mechanism for the formation of vanadium–PCA complex in H_2O_2(aq)–CH_3CN system (R = bulk VO_x).

acetonitrile and 35% H_2O_2.[220] The synthesized V_{nr} were implemented for the selective oxidation of benzene to phenol in CH_3CN using H_2O_2 and pyrazine-2-carboxylic acid (PCA) as the oxidant and co-catalyst, respectively (Scheme 21). The mechanistic studies disclosed that PCA assisted in the oxidation process by ameliorating the catalytic activity of V_{nr} with 87–99% phenol selectivity. This procedure was also successfully extended for the oxidation of toluene and benzyl alcohols. Due to the heterogeneity, high efficacy and flexibility of V_{nr}, the developed approach was proven to be a better alternative to existing methods.

Recently, a novel recyclable catalyst was developed for the liquid-phase oxidation of ethyl substituted benzene to acetophenone, in which CuO NPs were impregnated on activated red mud (CuO_AARM).[221] The analytical studies disclosed that the CuO NPs were largely scattered on the support material and played a crucial role in the progress of the reaction. Insights into the mechanistic pathway exposed that the process was driven by the generation of hydroperoxyl radicals and followed pseudo-first-order kinetics (Scheme 22). The synergism between the active components of red mud and ultra-small CuO NPs facilitated the reaction with a conversion efficiency of

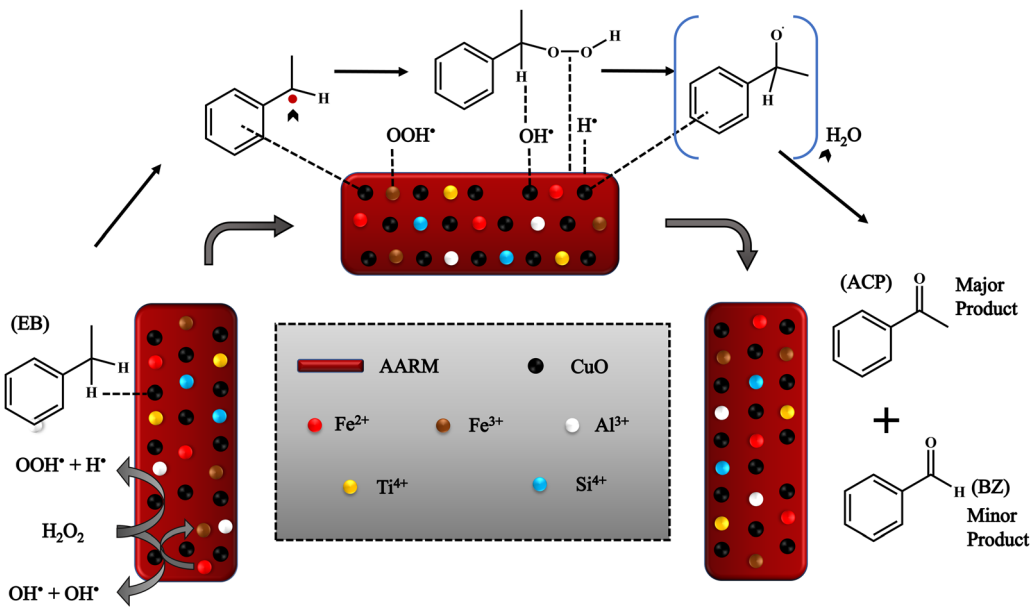

Scheme 22 Surface-catalysed oxidation of ethyl benzene to acetophenone, with mechanism showing the cooperative effects of the presence of various metals in the CuO AARM catalyst. Reproduced with permission from ref. 221. Copyright 2021, The Royal Society of Chemistry.

86% together with 74% selectivity. The hydrothermally synthesized heterogeneous catalyst exhibited good stability and reusability.

Conclusion

Over the past few decades, nanocatalysis has witnessed explosive growth, significantly contributing to shaping the sustainable future of modern society given that it provides a great array of opportunities such as lower energy consumption, economic viability, less environmental impact, industrial applications and sustainable development. The present review aimed to compile all the research work conducted on the utilization of surface-engineered metal oxide-based nanomaterials in expediting oxidation reactions, which is of paramount importance in manufacturing fine chemicals. The previous sections clearly demonstrated that nano-scale engineered metal oxide-based architectures have facilitated the large-scale production of an array of commodity products by speeding up a myriad of oxidative transformations. In fact, the use of hydrogen peroxide as an oxidant has also been proven to be a great asset in improvising industrially significant existing oxidative protocols for the greening of industrial manufacturing processes to tackle the significant environmental and economic issues.

To date, there is no review in the literature that presents a compilation of the vast and scattered literature of heterogeneous nanocatalysis based on different oxide nanostructures in a comprehensible manner. All the presented information will be fruitful for researchers, academicians and industrial personnel to conceptualize the idea of a new generation of catalytic materials for sustainable chemical processes. Hence, it can bridge the gap between different research groups focused on designing distinct metal oxide-based nanostructures across the globe by providing vast knowledge in a single reference.

Despite the fabulous advancements, there is still room for great improvements in several areas, which further necessitate extra efforts to cover the remaining gaps. The focus of the future research must be directed towards designing multifunctional materials, addressing the complexity of catalysts, understanding their structure–activity relationships and mechanistic aspects, developing computational approaches and exploring the catalytic effect of different morphologies. An existing challenge is also obtaining identical nanostructures, where despite the fact that a variety of methods has been explored and provide prospects of controlling the size and morphology of NPs, developing a reliable strategy for the modulation of their texture, composition and electronic structure is crucial for various catalytic applications, especially electrocatalytic reactions. Another issue that confronts scientists is understanding the dynamics of the catalytic nanostructures given that they have a propensity to undergo structural and compositional changes during the course of the reaction. Henceforth, a correlation between the static and dynamic structure of the active catalytic centers is important. Also, emphasis is required in understanding the mechanisms at the nanoscale, which can be facilitated by the use of sophisticated and advanced computational tools. Undeniably, fruitful collaborations between theoretical and experimental chemists involving molecular modeling studies and reaction intermediate studies can have impressive effects in this regard. Further, researchers need to devote efforts towards the utilization of greener synthetic strategies that employ continuous flow microwave reactors and other advanced reactors for obtaining supported catalysts on a large scale. This certainly calls for further investigation in testing the efficacy of reactors for the production of a wide variety of supported nanocatalysts possessing durable properties. A number of gaps remain to be resolved towards the development of green and sustainable catalytic processes, which can be achieved only through united efforts of chemists, material engineers and other relevant stakeholders.

It is envisaged that this review will not only give directions to the upcoming scientific generation to decide their future work-plans in this field and improve on-going research programs but also offers benchmark reference for upcoming scientific generation, industrialists and academicians to construct next-generation benign catalytic technologies ranging from scaling up to final commercialization.

Conflicts of interest

There are no conflicts to declare.

References

1 S. Mitchell, R. Qin, N. Zheng and J. Pérez-Ramírez, *Nat. Nanotechnol.*, 2021, **16**, 129–139.
2 K. Pushparaj, W.-C. Liu, A. Meyyazhagan, A. Orlacchio, M. Pappusamy, C. Vadivalagan, A. A. Robert, V. A. Arumugam, H. Kamyab and J. J. Klemeš, *Energy*, 2022, **240**, 122732.
3 M. Muzzio, J. Li, Z. Yin, I. M. Delahunty, J. Xie and S. Sun, *Nanoscale*, 2019, **11**, 18946–18967.
4 Y. Dai, Y. Wang, B. Liu and Y. Yang, *Small*, 2015, **11**, 268–289.
5 R. K. Sharma, S. Yadav, S. Dutta, H. B. Kale, I. R. Warkad, R. Zbořil, R. S. Varma and M. B. Gawande, *Chem. Soc. Rev.*, 2021, **50**, 11293–11380.
6 R. K. Sharma, S. Sharma, S. Dutta, R. Zboril and M. B. Gawande, *Green Chem.*, 2015, **17**, 3207–3230.
7 M. B. Gawande, Y. Monga, R. Zboril and R. K. Sharma, *Coord. Chem. Rev.*, 2015, **288**, 118–143.
8 R. K. Sharma and S. Sharma, *Dalton Trans.*, 2014, **43**, 1292–1304.
9 R. K. Sharma, S. Sharma and G. Gaba, *RSC Adv.*, 2014, **4**, 49198–49211.
10 C. Xu, Q. Li, Q. Zhang, K. Li, H. Yin and S. Zhou, *ACS Appl. Nano Mater.*, 2019, **2**, 5086–5095.
11 S. Sadjadi, M. Akbari, B. Léger, E. Monflier and M. M. Heravi, *ACS Sustainable Chem. Eng.*, 2019, **7**, 6720–6731.

12 S. Dey and G. C. Dhal, *Mater. Today Chem.*, 2020, **17**, 100282.
13 S. H. Khan and B. Pathak, *Environ. Nanotechnol., Monit. Manage.*, 2020, **13**, 100290.
14 J. Zhang, H. Wang, L. Wang, S. Ali, C. Wang, L. Wang, X. Meng, B. Li, D. S. Su and F.-S. Xiao, *J. Am. Chem. Soc.*, 2019, **141**, 2975–2983.
15 R. K. Sharma, S. Dutta, S. Sharma, R. Zboril, R. S. Varma and M. B. Gawande, *Green Chem.*, 2016, **18**, 3184–3209.
16 A. Akbari, M. Amini, A. Tarassoli, B. Eftekhari-Sis, N. Ghasemian and E. Jabbari, *Nano-Struc. Nano-Objects*, 2018, **14**, 19–48.
17 G. Zhao, F. Yang, Z. Chen, Q. Liu, Y. Ji, Y. Zhang, Z. Niu, J. Mao, X. Bao and P. Hu, *Nat. Commun.*, 2017, **8**, 1–8.
18 R. Medhi, M. D. Marquez and T. R. Lee, *ACS Appl. Nano Mater.*, 2020, **3**, 6156–6185.
19 D. Wang and D. Astruc, *Chem. Soc. Rev.*, 2017, **46**, 816–854.
20 Y. Ishii, S. Sakaguchi and T. Iwahama, *Adv. Synth. Catal.*, 2001, **343**, 393–427.
21 S. Wolfe and C. F. Ingold, *J. Am. Chem. Soc.*, 1983, **105**, 7755–7757.
22 J. Muzart, *Chem. Rev.*, 1992, **92**, 113–140.
23 M. Hu, W. Wu and H. Jiang, *ChemSusChem*, 2019, **12**, 2911–2935.
24 G. De Faveri, G. Ilyashenko and M. Watkinson, *Chem. Soc. Rev.*, 2011, **40**, 1722–1760.
25 R. Noyori, M. Aoki and K. Sato, *Chem. Commun.*, 2003, 1977–1986.
26 Q. Xing, Z. Hao, J. Hou, G. Li, Z. Gao, J. Gou, C. Li and B. Yu, *J. Org. Chem.*, 2021, **86**, 9563–9586.
27 D. Hâncu, J. Green and E. J. Beckman, *Acc. Chem. Res.*, 2002, **35**, 757–764.
28 W. Xiao, S. Yang, P. Zhang, P. Li, P. Wu, M. Li, N. Chen, K. Jie, C. Huang and N. Zhang, *Chem. Mater.*, 2018, **30**, 2924–2929.
29 P. A. C. Bedoya, P. M. Botta, P. G. Bercoff and M. A. Fanovich, *J. Alloys Compd.*, 2021, **860**, 157892.
30 T. Boningari, S. N. R. Inturi, V. I. Manousiouthakis and P. G. Smirniotis, *Ind. Eng. Chem. Res.*, 2018, **57**, 9054–9061.
31 G. D. Park, J. H. Kim and Y. C. Kang, *Nanoscale*, 2018, **10**, 13531–13538.
32 M. Verma, V. Kumar and A. Katoch, *Mater. Sci. Semicond. Process.*, 2018, **76**, 55–60.
33 N. Zamora-Romero, M. A. Camacho-Lopez, A. R. Vilchis-Nestor, V. H. Castrejon-Sanchez, G. Aguilar, S. Camacho-Lopez and M. Camacho-Lopez, *Mater. Chem. Phys.*, 2020, **240**, 122163.
34 P. Kupracz, E. Coy, K. Grochowska, J. Karczewski, J. Rysz and K. Siuzdak, *Appl. Surf. Sci.*, 2020, **530**, 147097.
35 C. Zheng, A. Gentils, J. Ribis, V. Borodin, L. Delauche and B. Arnal, *Nucl. Instrum. Methods Phys. Res. B: Beam Interact. Mater. At.*, 2017, **409**, 333–337.
36 S. Sankar, A. I. Inamdar, H. Im, S. Lee and D. Y. Kim, *Ceram. Int.*, 2018, **44**, 17514–17521.
37 E. Luévano-Hipólito and L. Torres-Martínez, *Mater. Sci. Eng. B*, 2017, **226**, 223–233.
38 J. Kim, V. T. Tran, S. Oh, C.-S. Kim, J. C. Hong, S. Kim, Y.-S. Joo, S. Mun, M.-H. Kim and J.-W. Jung, *ACS Appl. Mater. Interfaces*, 2018, **10**, 41935–41946.
39 S. Saddeler, U. Hagemann and S. Schulz, *Inorg. Chem.*, 2020, **59**, 10013–10024.
40 M. F. Khan, A. H. Ansari, M. Hameedullah, E. Ahmad, F. M. Husain, Q. Zia, U. Baig, M. R. Zaheer, M. M. Alam and A. M. Khan, *Sci. Rep.*, 2016, **6**, 1–12.
41 R. Yarbrough, K. Davis, S. Dawood and H. Rathnayake, *RSC Adv.*, 2020, **10**, 14134–14146.
42 R. Joshi, *Mater.*, 2018, **2**, 104–110.
43 K. V. Manukyan, Y.-S. Chen, S. Rouvimov, P. Li, X. Li, S. Dong, X. Liu, J. K. Furdyna, A. Orlov and G. H. Bernstein, *J. Phys. Chem. C*, 2014, **118**, 16264–16271.
44 J. Singh, V. Kumar, K.-H. Kim and M. Rawat, *Environ. Res.*, 2019, **177**, 108569.
45 A. Pugazhendhi, R. Prabhu, K. Muruganantham, R. Shanmuganathan and S. Natarajan, *J. Photochem. Photobiol., B*, 2019, **190**, 86–97.
46 A. Muthuvinothini and S. Stella, *Process Biochem.*, 2019, **77**, 48–56.
47 M. Parashar, V. K. Shukla and R. Singh, *J. Mater. Sci.: Mater. Electron.*, 2020, **31**, 3729–3749.
48 N. P. Herring, A. B. Panda, K. AbouZeid, S. H. Almahoudi, C. R. Olson, A. Patel and M. El-Shall, *Metal Oxide Nanomaterials for Chemical Sensors*, 2013, 245–284.
49 N. Pokhrel, P. K. Vabbina and N. Pala, *Ultrason. Sonochem.*, 2016, **29**, 104–128.
50 A. Nandagudi, S. H. Nagarajarao, M. S. Santosh, B. M. Basavaraja, S. J. Malode, R. J. Mascarenhas and N. P. Shetti, *Mater. Today Sustain.*, 2022, 100214.
51 A. K. Ganguli, A. Ganguly and S. Vaidya, *Chem. Soc. Rev.*, 2010, **39**, 474–485.
52 A. Kaur, B. Bajaj, A. Kaushik, A. Saini and D. Sud, *Mater. Sci. Eng. B*, 2022, **286**, 116005.
53 J. Jeevanandam, Y. S. Chan and M. K. Danquah, *ChemBioEng Rev.*, 2016, **3**, 55–67.
54 T. Tsuzuki, *Commun. Chem.*, 2021, **4**, 143.
55 V. Amendola, D. Amans, Y. Ishikawa, N. Koshizaki, S. Scirè, G. Compagnini, S. Reichenberger and S. Barcikowski, *Chem. – Eur. J.*, 2020, **26**, 9206–9242.
56 T. Bharat, S. Mondal, H. Gupta, P. Singh and A. Das, *Mater. Today: Proc.*, 2019, **11**, 767–775.
57 P. Colson, C. Henrist and R. Cloots, *J. Nanomater.*, 2013, **2013**, 21.
58 A. V. Rane, K. Kanny, V. Abitha and S. Thomas, *Synthesis of inorganic nanomaterials*, Elsevier, 2018, pp. 121–139.
59 S. Shi, M. Cao, X. He and H. Xie, *Cryst. Growth Des.*, 2007, **7**, 1893–1897.
60 Z. Bao, Y. Yuan, C. Leng, L. Li, K. Zhao and Z. Sun, *ACS Appl. Mater. Interfaces*, 2017, **9**, 16417–16425.
61 T. Guo, Y. Luo, Y. Zhang, Y.-H. Lin and C.-W. Nan, *Cryst. Growth Des.*, 2014, **14**, 2329–2334.
62 C. Jia, Y. Cheng, F. Bao, D. Chen and Y. Wang, *J. Cryst. Growth*, 2006, **294**, 353–357.
63 F. N. Sayed and V. Polshettiwar, *Sci. Rep.*, 2015, **5**, 1–14.

64 L. Huang, H. Wang, Z. Wang, A. Mitra, D. Zhao and Y. Yan, *Chem. Mater.*, 2002, **14**, 876–880.
65 J. Li, X. Liu, Q. Han, X. Yao and X. Wang, *J. Mater. Chem. A*, 2013, **1**, 1246–1253.
66 Y. Li and W. Shen, *Chem. Soc. Rev.*, 2014, **43**, 1543–1574.
67 X. Xie and W. Shen, *Nanoscale*, 2009, **1**, 50–60.
68 H.-X. Mai, L.-D. Sun, Y.-W. Zhang, R. Si, W. Feng, H.-P. Zhang, H.-C. Liu and C.-H. Yan, *J. Phys. Chem.*, 2005, **109**, 24380–24385.
69 Y. Zheng, Y. Cheng, Y. Wang, F. Bao, L. Zhou, X. Wei, Y. Zhang and Q. Zheng, *J. Phys. Chem. B*, 2006, **110**, 3093–3097.
70 B. M. Choudary, R. S. Mulukutla and K. J. Klabunde, *J. Am. Chem. Soc.*, 2003, **125**, 2020–2021.
71 S. Konar, H. Kalita, N. Puvvada, S. Tantubay, M. K. Mahto, S. Biswas and A. Pathak, *J. Catal.*, 2016, **336**, 11–22.
72 H. Tan, J. Wang, S. Yu and K. Zhou, *Environ. Sci. Technol.*, 2015, **49**, 8675–8682.
73 X.-Y. Lou, R. Boada, L. Simonelli and M. Valiente, *J. Colloid Interface Sci.*, 2022, **614**, 460–467.
74 N. Kitchamsetti, M. S. Ramteke, S. R. Rondiya, S. R. Mulani, M. S. Patil, R. W. Cross, N. Y. Dzade and R. S. Devan, *J. Alloys Compd.*, 2021, **855**, 157337.
75 Y. Li, M. Jiao, H. Zhao and M. Yang, *Sens. Actuators, B*, 2018, **264**, 285–295.
76 E. Comini, *Mater. Today Adv.*, 2020, **7**, 100099.
77 M. H. Raza, N. Kaur, E. Comini and N. Pinna, *ACS Appl. Mater. Interfaces*, 2020, **12**, 4594–4606.
78 A. Xia, W. Yu, J. Yi, G. Tan, H. Ren and C. Liu, *J. Electroanal. Chem.*, 2019, **839**, 25–31.
79 B. Abebe, E. A. Zereffa, A. Tadesse and H. Murthy, *Nanoscale Res. Lett.*, 2020, **15**, 1–19.
80 M. Sundrarajan, K. Bama, M. Bhavani, S. Jegatheeswaran, S. Ambika, A. Sangili, P. Nithya and R. Sumathi, *J. Photochem. Photobiol. B: Biology*, 2017, **171**, 117–124.
81 J. Rahimi, S. S. Mirmohammadi and A. Maleki, *Front. Chem. Sci. Eng.*, 2021, **15**, 1008–1020.
82 M. Z. Kassaee, H. Masrouri and F. Movahedi, *Appl. Catal. A: Gen.*, 2011, **395**, 28–33.
83 F.-C. Zheng, Q.-W. Chen, L. Hu, N. Yan and X.-K. Kong, *Dalton Trans.*, 2014, **43**, 1220–1227.
84 F. Zamani, S. M. Hosseini and S. Kianpour, *Solid State Sci.*, 2013, **26**, 139–143.
85 P. Singh, P. Yadav, A. Mishra and S. K. Awasthi, *ACS Omega*, 2020, **5**, 4223–4232.
86 J. He, S. Yang and A. Riisager, *Catal. Sci. Technol.*, 2018, **8**, 790–797.
87 R. Eisavi and K. Naseri, *RSC Adv.*, 2021, **11**, 13061–13076.
88 N. Ž. Knežević, B. G. Trewyn and V. S.-Y. Lin, *Chem. Commun.*, 2011, **47**, 2817–2819.
89 A. Maleki, Z. Hajizadeh and P. Salehi, *Sci. Rep.*, 2019, **9**, 1–8.
90 S. Yu, H. J. Yun, D. M. Lee and J. Yi, *J. Mater. Chem.*, 2012, **22**, 12629–12635.
91 H. Hagiwara, T. Nakamura, T. Hoshi and T. Suzuki, *Green Chem.*, 2011, **13**, 1133–1137.
92 R. Tandon, N. Tandon and S. M. Patil, *RSC Adv.*, 2021, **11**, 29333–29353.
93 X. Li, O. Niitsoo and A. Couzis, *J. Colloid Interface Sci.*, 2013, **394**, 26–35.
94 A. Zhu, H. Diao, Q. Rong and A. Cai, *J. Appl. Polym. Sci.*, 2010, **116**, 2866–2873.
95 N. Nakayama and T. Hayashi, *Polym. Degrad. Stab.*, 2007, **92**, 1255–1264.
96 S. Saire-Saire, E. C. Barbosa, D. Garcia, L. H. Andrade, S. Garcia-Segura, P. H. Camargo and H. Alarcon, *RSC Adv.*, 2019, **9**, 22116–22123.
97 Y.-m Kim, S. Farrah and R. H. Baney, *Int. J. Antimicrob. Agents*, 2007, **29**, 217–222.
98 S. P. Pujari, L. Scheres, A. T. Marcelis and H. Zuilhof, *Angew. Chem., Int. Ed.*, 2014, **53**, 6322–6356.
99 K. Sever, M. Sarikanat, Y. Seki, G. Erkan and Ü. H. Erdoğan, *J. Compos. Mater.*, 2010, **44**, 1913–1924.
100 H. Kim, K. Okubo, T. Fujii and K. Takemura, *J. Adhes. Sci. Technol.*, 2013, **27**, 1348–1358.
101 M. Abdelmouleh, S. Boufi, M. N. Belgacem, A. Dufresne and A. Gandini, *J. Appl. Polym. Sci.*, 2005, **98**, 974–984.
102 L. A. Pothan, J. George and S. Thomas, *Compos. Interfaces*, 2002, **9**, 335–353.
103 L. A. Pothan and S. Thomas, *Compos. Sci. Technol.*, 2003, **63**, 1231–1240.
104 L. A. Pothan, S. Thomas and G. Groeninckx, *Compos. Part A Appl. Sci.*, 2006, **37**, 1260–1269.
105 H. Shah, B. Srinivasulu and S. Shit, *Int. J. Sci. Eng. Technol.*, 2012, **1**, 86–90.
106 M. Joshy, L. Mathew and R. Joseph, *Int. J. Polym. Mater.*, 2008, **58**, 2–20.
107 P. Sreekumar, S. P. Thomas, J. Marc Saiter, K. Joseph, G. Unnikrishnan and S. Thomas, *Compos. A Appl. Sci. Manuf*, 2009, **40**, 1777–1784.
108 P. K. Kushwaha and R. Kumar, *Polym. Plast. Technol. Eng.*, 2009, **49**, 45–52.
109 M. A. Sawpan, K. L. Pickering and A. Fernyhough, *Compos. A Appl. Sci. Manuf.*, 2012, **43**, 519–526.
110 K. O. Reddy, M. Shukla, C. U. Maheswari and A. V. Rajulu, *J. Compos. Mater.*, 2012, **46**, 2987–2998.
111 T.-Y. Ma, X.-J. Zhang and Z.-Y. Yuan, *J. Phys. Chem. C*, 2009, **113**, 12854–12862.
112 X. Wei and X. Shi, *J. Phys. Chem. C*, 2014, **118**, 4213–4221.
113 Y.-P. Zhu, Y.-L. Liu, T.-Z. Ren and Z.-Y. Yuan, *Nanoscale*, 2014, **6**, 6627–6636.
114 K. Lv, J. Han, C.-T. Yang, C.-M. Cheng, Y.-M. Luo and X.-L. Wang, *Chem. Eng. J.*, 2016, **302**, 368–376.
115 V. Luca, J. J. Tejada, D. Vega, G. Arrachart and C. Rey, *Inorg. Chem.*, 2016, **55**, 7928–7943.
116 R. Silbernagel, C. H. Martin and A. Clearfield, *Inorg. Chem.*, 2016, **55**, 1651–1656.
117 R. Silbernagel, T. C. Shehee, C. H. Martin, D. T. Hobbs and A. Clearfield, *Chem. Mater.*, 2016, **28**, 2254–2259.
118 D. J. Miller, L. Sun, M. Walzak, N. Mclntyre, D. Chvedov and A. Rosenfeld, *Surf. Interface Anal.*, 2003, **35**, 463–476.

119 P. Taheri, J. Wielant, T. Hauffman, J. Flores, F. Hannour, J. De Wit, J. Mol and H. Terryn, *Electrochim. Acta*, 2011, **56**, 1904–1911.
120 T. Bauer, T. Schmaltz, T. Lenz, M. Halik, B. Meyer and T. Clark, *ACS Appl. Mater. Interfaces*, 2013, **5**, 6073–6080.
121 F. Cheng, E. Verrelli, F. A. Alharthi, S. Das, T. D. Anthopoulos, K. T. Lai, N. T. Kemp, M. O'Neill and S. M. Kelly, *RSC Adv.*, 2020, **10**, 25540–25546.
122 L. M. Bishop, J. C. Yeager, X. Chen, J. N. Wheeler, M. D. Torelli, M. C. Benson, S. D. Burke, J. A. Pedersen and R. J. Hamers, *Langmuir*, 2012, **28**, 1322–1329.
123 S. E. Denmark and N. S. Werner, *J. Am. Chem. Soc.*, 2008, **130**, 16382–16393.
124 S. M. Sieburth and W. Mu, *J. Org. Chem.*, 1993, **58**, 7584–7586.
125 A. Ulman, *Chem. Rev.*, 1996, **96**, 1533–1554.
126 A. Glaser, J. Foisner, H. Hoffmann and G. Friedbacher, *Langmuir*, 2004, **20**, 5599–5604.
127 P. H. Mutin, G. Guerrero and A. Vioux, *J. Mater. Chem.*, 2005, **15**, 3761–3768.
128 E. Hoque, J. DeRose, G. Kulik, P. Hoffmann, H. Mathieu and B. Bhushan, *J. Phys. Chem. B*, 2006, **110**, 10855–10861.
129 M. A. White, J. A. Johnson, J. T. Koberstein and N. J. Turro, *J. Am. Chem. Soc.*, 2006, **128**, 11356–11357.
130 L. Forget, F. Wilwers, J. Delhalle and Z. Mekhalif, *Appl. Surf. Sci.*, 2003, **205**, 44–55.
131 G. P. Holland, R. Sharma, J. O. Agola, S. Amin, V. C. Solomon, P. Singh, D. A. Buttry and J. L. Yarger, *Chem. Mater.*, 2007, **19**, 2519–2526.
132 G. Guerrero, P. Mutin and A. Vioux, *Chem. Mater.*, 2001, **13**, 4367–4373.
133 Q.-L. Zhang, L.-C. Du, Y.-X. Weng, L. Wang, H.-Y. Chen and J.-Q. Li, *J. Phys. Chem. B*, 2004, **108**, 15077–15083.
134 X. Jia, J. Ma, F. Xia, Y. Xu, J. Gao and J. Xu, *Nat. Commun.*, 2018, **9**, 1–7.
135 K. Wilson and J. H. Clark, *Pure Appl. Chem.*, 2000, **72**, 1313–1319.
136 C. Vogt and B. M. Weckhuysen, *Nat. Rev. Chem.*, 2022, **6**, 89–111.
137 P. Manjunathan, V. Prasanna and G. V. Shanbhag, *Sci. Rep.*, 2021, **11**, 15718.
138 L. Liu, W. He, Z. Fang, Z. Yang, K. Guo and Z. Wang, *Ind. Eng. Chem. Res.*, 2020, **59**, 19938–19951.
139 S. Mirfakhraei, M. Hekmati, F. H. Eshbala and H. Veisi, *New J. Chem.*, 2018, **42**, 1757–1761.
140 A. Ghorbani-Choghamarani, Z. Darvishnejad and B. Tahmasbi, *Inorg. Chim. Acta*, 2015, **435**, 223–231.
141 A. Zheng, S. Li, S.-B. Liu and F. Deng, *Acc. Chem. Res.*, 2016, **49**, 655–663.
142 P. M. Kouotou, H. Vieker, Z. Tian, P. T. Ngamou, A. El Kasmi, A. Beyer, A. Gölzhäuser and K. Kohse-Höinghaus, *Catal. Sci. Technol.*, 2014, **4**, 3359–3367.
143 T. Mallat and A. Baiker, *Chem. Rev.*, 2004, **104**, 3037–3058.
144 C. Parmeggiani, C. Matassini and F. Cardona, *Green Chem.*, 2017, **19**, 2030–2050.
145 D. Wang, P. Wang, S. Wang, Y.-H. Chen, H. Zhang and A. Lei, *Nat. Commun.*, 2019, **10**, 1–8.
146 S. E. Davis, M. S. Ide and R. J. Davis, *Green Chem.*, 2013, **15**, 17–45.
147 I. Tamiolakis, I. N. Lykakis, A. P. Katsoulidis, C. D. Malliakas and G. S. Armatas, *J. Mater. Chem.*, 2012, **22**, 6919–6927.
148 J. L. Sousa, I. C. Santos, M. M. Simões, J. A. Cavaleiro, H. I. Nogueira and A. M. Cavaleiro, *Catal. Commun.*, 2011, **12**, 459–463.
149 B. Karimi, F. B. Rostami, M. Khorasani, D. Elhamifar and H. Vali, *Tetrahedron*, 2014, **70**, 6114–6119.
150 P. Garcia-Albar, N. Lazaro, Z. A. ALOthman, A. A. Romero, R. Luque and A. Pineda, *Mol. Catal.*, 2021, **506**, 111537.
151 F. Rajabi, A. Pineda, S. Naserian, A. M. Balu, R. Luque and A. A. Romero, *Green Chem.*, 2013, **15**, 1232–1237.
152 R. K. Sharma, S. Yadav, S. Sharma, S. Dutta and A. Sharma, *ACS Omega*, 2018, **3**, 15100–15111.
153 S. Yadav, S. Sharma, S. Dutta, A. Sharma, A. Adholeya and R. K. Sharma, *Inorg. Chem.*, 2020, **59**, 8334–8344.
154 S. Yadav, R. Dixit, S. Sharma, S. Dutta, B. Arora, P. Rana, B. Kaushik, A. Adholeya, M. B. Gawande and R. K. Sharma, *Mater. Chem. Front.*, 2021, **5**, 7343–7355.
155 S. Yadav, R. Dixit, S. Sharma, S. Dutta, B. Arora, P. Rana, B. Kaushik, K. Solanki and R. K. Sharma, *New J. Chem.*, 2022, **46**, 10829–10843.
156 S. Yadav, R. Dixit, S. Sharma, S. Dutta, K. Solanki and R. K. Sharma, *Mater. Adv.*, 2021, **2**, 2153–2187.
157 C. Ragupathi, J. J. Vijaya, S. Narayanan, S. Jesudoss and L. J. Kennedy, *Ceram. Int.*, 2015, **41**, 2069–2080.
158 F. Shi, M. K. Tse, M.-M. Pohl, J. Radnik, A. Brückner, S. Zhang and M. Beller, *J. Mol. Catal. A*, 2008, **292**, 28–35.
159 F. Sadri, A. Ramazani, A. Massoudi, M. Khoobi, R. Tarasi, A. Shafiee, V. Azizkhani, L. Dolatyari and S. W. Joo, *Green Chem. Lett. Rev.*, 2014, **7**, 257–264.
160 P. B. Bhat and B. R. Bhat, *New J. Chem.*, 2015, **39**, 273–278.
161 P. B. Bhat and B. R. Bhat, *Appl. Nanosci.*, 2016, **6**, 425–435.
162 A. Pourjavadi, S. H. Hosseini, F. M. Moghaddam, B. K. Foroushani and C. Bennett, *Green Chem.*, 2013, **15**, 2913–2919.
163 A. Heidarnezhad and F. Zamani, *Catal. Commun.*, 2015, **60**, 105–109.
164 A. Maleki, R. Rahimi and S. Maleki, *Environ. Chem. Lett.*, 2016, **14**, 195–199.
165 A. Chakraborty, T. Chakraborty, M. I. Menendez and T. Chattopadhyay, *ACS Omega*, 2019, **4**, 11558–11565.
166 J. Ni, W.-J. Yu, L. He, H. Sun, Y. Cao, H.-Y. He and K.-N. Fan, *Green Chem.*, 2009, **11**, 756–759.
167 S. Verma and S. L. Jain, *Inorg. Chem. Front.*, 2014, **1**, 534–539.
168 P. N. Amaniampong, Q. T. Trinh, J. J. Varghese, R. Behling, S. Valange, S. H. Mushrif and F. Jérôme, *Green Chem.*, 2018, **20**, 2730–2741.
169 A. Naeimi, M. Honarmand and A. Sedri, *Ultrason. Sonochem.*, 2019, **50**, 331–338.
170 A. Naeimi, S. Abbasspour and S. A. Torabizadeh, *Artificial Cells, Nanomed. Biotechnol.*, 2020, **48**, 560–571.
171 M. Amini, Y. Mousazade, Z. Zand, M. Bagherzadeh and M. M. Najafpour, *Sci. Rep.*, 2021, **11**, 1–10.
172 R. Behling, G. Chatel and S. Valange, *Ultrason. Sonochem.*, 2017, **36**, 27–35.

173 S. Saha, S. B. Abd Hamid and T. H. Ali, *Appl. Surf. Sci.*, 2017, **394**, 205–218.
174 M. Heidari-Golafzani, M. Rabbani, R. Rahimi and A. Azad, *RSC Adv.*, 2015, **5**, 99640–99645.
175 Z. Zhang, Q. Zhu, J. Ding, X. Liu and W.-L. Dai, *Appl. Catal. A: Gen.*, 2014, **482**, 171–178.
176 F. Rajabi, S. Naserian, A. Primo and R. Luque, *Adv. Synth. Catal.*, 2011, **353**, 2060–2066.
177 A. Rostami and B. Atashkar, *J. Mol. Catal. A: Chem.*, 2015, **398**, 170–176.
178 Y. Kuwahara, T. Ando, H. Kango and H. Yamashita, *Chem. – Eur. J.*, 2017, **23**, 380–389.
179 W. Zhao, C. Yang, H. Sun, Z. Cheng and T. Chang, *New J. Chem.*, 2018, **42**, 19349–19352.
180 F. Rajabi, T. Kakeshpour and M. R. Saidi, *Catal. Commun.*, 2013, **40**, 13–17.
181 A. Sabet, E. Kolvari, N. koukabi, A. Fakhraee, M. Ramezanpour and G. Bahmannia, *J. Sulfur Chem.*, 2015, **36**, 300–307.
182 A. M. Kulkarni, U. V. Desai, K. S. Pandit, M. A. Kulkarni and P. P. Wadgaonkar, *RSC Adv.*, 2014, **4**, 36702–36707.
183 M. Nikoorazm, F. Ghorbani, A. Ghorbani-Choghamarani and Z. Erfani, *Phosphorus, Sulfur Silicon Relat. Elem.*, 2018, **193**, 552–561.
184 S. S. Acharyya, S. Ghosh and R. Bal, *ACS Sustainable Chem. Eng.*, 2014, **2**, 584–589.
185 S. Ghosh, S. S. Acharyya, T. Sasaki and R. Bal, *Green Chem.*, 2015, **17**, 1867–1876.
186 S. Han, Y. Cheng, S. Liu, C. Tao, A. Wang, W. Wei, H. Yu and Y. Wei, *Angew. Chem., Int. Ed.*, 2021, **133**, 6452–6455.
187 S. Fountoulaki, P. L. Gkizis, T. S. Symeonidis, E. Kaminioti, A. Karina, I. Tamiolakis, G. S. Armatas and I. N. Lykakis, *Adv. Synth. Catal.*, 2016, **358**, 1500–1508.
188 P. Veerakumar, S. Balakumar, M. Velayudham, K.-L. Lu and S. Rajagopal, *Catal. Sci. Technol.*, 2012, **2**, 1140–1145.
189 M. Kidwai and S. Bhardwaj, *Synth. Commun.*, 2011, **41**, 2655–2662.
190 G. Chu and C. Li, *Org. Biomol. Chem.*, 2010, **8**, 4716–4719.
191 V. Panwar, P. Kumar, A. Bansal, S. S. Ray and S. L. Jain, *Appl. Catal. A Gen.*, 2015, **498**, 25–31.
192 F. Vetr, Z. Moradi-Shoeili and S. Özkar, *Appl. Organomet. Chem.*, 2018, **32**, e4465.
193 P. R. Makgwane and S. Ray, *Catal. Commun.*, 2014, **54**, 118–123.
194 S. S. Acharyya, S. Ghosh and R. Bal, *Green Chem.*, 2015, **17**, 3490–3499.
195 R. Goyal, B. Sarkar, S. Sameer, A. Bag and A. Bordoloi, *ACS Appl. Nano Mater.*, 2019, **2**, 5989–5999.
196 N. M. Martins, A. J. Pombeiro and L. M. Martins, *Catal. Commun.*, 2019, **125**, 15–20.
197 C. M. Crombie, R. J. Lewis, D. Kovačič, D. J. Morgan, T. J. Slater, T. E. Davies, J. Edwards, M. S. Skjøth-Rasmussen and G. J. Hutchings, *Catal. Lett.*, 2021, **151**, 2762–2774.
198 H. Shoukat, A. A. Altaf, M. Hamayun, S. Ullah, S. Kausar, M. Hamza, S. Muhammad, A. Badshah, N. Rasool and M. Imran, *ACS Omega*, 2021, **6**, 19606–19615.
199 J. Tong, X. Cai, H. Wang and Q. Zhang, *Mater. Res. Bull.*, 2014, **55**, 205–211.
200 S. Rayati, D. Moradi and F. Nejabat, *New J. Chem.*, 2020, **44**, 19385–19392.
201 M. Afshari, M. Gorjizadeh, S. Nazari and M. Naseh, *J. Magn. Magn. Mater.*, 2014, **363**, 13–17.
202 A. Mavrogiorgou, M. Baikousi, V. Costas, E. Mouzourakis, Y. Deligiannakis, M. Karakassides and M. Louloudi, *J. Mol. Catal. A: Chem.*, 2016, **413**, 40–55.
203 M. Lashanizadegan, Z. Gorgannejad and M. Sarkheil, *Inorg. Chem. Commun.*, 2021, **125**, 108373.
204 M. S. S. Adam, A. M. Hafez and M. M. Khalaf, *J. Iran. Chem. Soc.*, 2020, **17**, 3237–3250.
205 M. M. Najafpour, F. Rahimi, M. Amini, S. Nayeri and M. Bagherzadeh, *Dalton Trans.*, 2012, **41**, 11026–11031.
206 M. M. Najafpour, M. Amini, D. J. Sedigh, F. Rahimi and M. Bagherzadeh, *RSC Adv.*, 2013, **3**, 24069–24074.
207 S. Ghosh, S. S. Acharyya, S. Adak, L. S. Konathala, T. Sasaki and R. Bal, *Green Chem.*, 2014, **16**, 2826–2834.
208 B. Huang, C. Fan, C. Pan, A. Zheng, X. Ma, Y. Li, J. Zhang and Y. Sun, *Powder Technol.*, 2017, **315**, 258–269.
209 B. Paul, S. K. Sharma, R. Khatun, S. Adak, G. Singh, V. Joshi, M. K. Poddar, A. Bordoloi, T. Sasaki and R. Bal, *Ind. Eng. Chem. Res.*, 2019, **58**, 18168–18177.
210 Z. Wang, X. Hou, J. Shen and T. Li, *RSC Adv.*, 2016, **6**, 89503–89509.
211 F. Rajabi, N. Karimi, M. R. Saidi, A. Primo, R. S. Varma and R. Luque, *Adv. Synth. Catal.*, 2012, **354**, 1707–1711.
212 W. Lueangchaichaweng, L. Li, Q.-Y. Wang, B.-L. Su, C. Aprile and P. P. Pescarmona, *Catal. Today*, 2013, **203**, 66–75.
213 Y. Leng, J. Zhao, P. Jiang and J. Wang, *ACS Appl. Mater. Interfaces*, 2014, **6**, 5947–5954.
214 A. Pezhman, A. Badiei, A. Koolivand and G. M. Ziarani, *Chin. J. Catal.*, 2011, **32**, 258–263.
215 S. S. Acharyya, S. Ghosh, S. Adak, T. Sasaki and R. Bal, *Catal. Sci. Technol.*, 2014, **4**, 4232–4241.
216 S. S. Acharyya, S. Ghosh and R. Bal, *ACS Appl. Mater. Interfaces*, 2014, **6**, 14451–14459.
217 S. S. Acharyya, S. Ghosh, N. Siddiqui, L. S. Konathala and R. Bal, *RSC Adv.*, 2015, **5**, 4838–4843.
218 P. R. Makgwane and S. S. Ray, *J. Mol. Catal. A: Chem.*, 2015, **398**, 149–157.
219 M. Hosseini-Sarvari, T. Ataee-Kachouei and F. Moeini, *RSC Adv.*, 2015, **5**, 9050–9056.
220 W. H. Wanna, D. Janmanchi, N. Thiyagarajan, R. Ramu, Y.-F. Tsai, C.-W. Pao and S. S.-F. Yu, *New J. Chem.*, 2019, **43**, 17819–17830.
221 S. Mishra, S. W. Sangma, R. Bal and R. K. Dey, *New J. Chem.*, 2021, **45**, 13070–13079.